

4.6 Fluid Flow in the Deep Crust

JJ Ague, Yale University, New Haven, CT, USA

© 2014 Elsevier Ltd. All rights reserved.

4.6.1	Introduction	203
4.6.2	Evidence for Deep-Crustal Fluids	204
4.6.3	Devolatilization	204
4.6.4	Porous Media and Fracture Flow	207
4.6.4.1	Pervasive Flow and Darcy's Law	207
4.6.4.2	Fluid Flux, Fluid Velocity, and Porosity	207
4.6.4.3	Fluid Pressure Gradients	208
4.6.4.4	Permeability	209
4.6.4.5	Dynamic Viscosity	209
4.6.4.6	Crack Flow	209
4.6.4.7	Porosity Waves	210
4.6.5	Overview of Fluid Chemistry	211
4.6.6	Chemical Transport and Reaction	213
4.6.6.1	Mass Fluxes	213
4.6.6.2	Reaction Rates	215
4.6.6.3	Transport and Reaction Within Crystals	217
4.6.6.4	Advection–Dispersion–Reaction Equation	219
4.6.7	Geochemical Fronts	219
4.6.8	Flow and Reaction Along Gradients in Temperature and Pressure	221
4.6.9	Examples of Mass and Heat Transfer	223
4.6.9.1	Regional Devolatilization and Directions of Fluid Motion	223
4.6.9.1.1	Shallow crustal levels	223
4.6.9.1.2	Deeper levels	224
4.6.9.2	Regional Fluid Fluxes	226
4.6.9.3	Channelized Flow	227
4.6.9.3.1	Fractures, veins, and shear zones	227
4.6.9.3.2	Lithologic contacts and layer-parallel flow	230
4.6.9.3.3	Flow channelization in subduction zones	230
4.6.9.4	Channelization and Fluid Fluxes at the Regional Scale	232
4.6.9.5	Mass Transport by Fluids	232
4.6.9.6	Heat Transport by Fluids	236
4.6.9.7	Timescales of Fluid Flow	237
4.6.9.8	Fluids in the Granulite Facies	238
4.6.10	Concluding Remarks	239
Acknowledgments		239
References		239

4.6.1 Introduction

The heating and burial of rock masses during mountain building drives chemical reactions that liberate volatile fluid species (Figure 1). These volatiles, including H₂O, CO₂, and CH₄, are much less dense and viscous than the surrounding rock and will, therefore, have a strong tendency to migrate along grain boundaries or fractures through the Earth's crust. Fluids released in the deep crust interact geochemically with their surroundings (Rye et al., 1976) as they ascend to shallow levels where they invade hydrothermal and groundwater systems and, ultimately, interact with the hydrosphere and atmosphere. This flux of fluid from actively metamorphosing mountain belts to the surface is a major contributor to planetary volatile cycling and is estimated to be currently in excess of $\sim 10^{17}$ kg per million years (based on Kerrick and Caldeira, 1998; Wallmann, 2001a,b).

The deep crust is composed largely of metamorphic rock (Rudnick and Fountain, 1995; Wedepohl, 1995). Fluids and magmas are the primary agents of chemical mass transport through the deep crust; fluid flow dominates at temperatures $< \sim 600$ °C and can be important at much higher temperatures as well – even in the granulite facies. As a consequence, an understanding of the fundamental controls exerted by metamorphic fluids on mass and heat transfer, mineral reactions, and rock rheology is critical for determining the geochemical and petrological evolution of the crust. Moreover, metamorphic fluids impact directly many problems of societal relevance, including ore deposit formation, global release of greenhouse gases, seismic hazards, and arc magma genesis and the associated volcanic hazards.

In this chapter, basic fluid flow, mass transfer, and reaction concepts will be examined first. This discussion is followed by

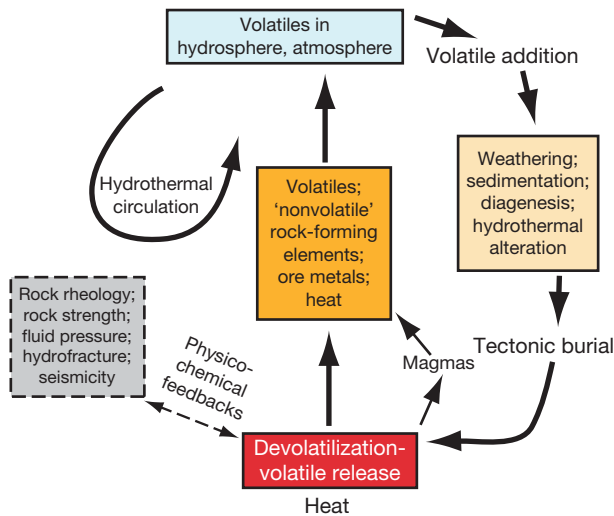


Figure 1 Diagram of crustal fluid cycling.

a review of selected natural examples of fluid transport during active metamorphism. The focus is on deeper levels of the lithosphere (>15 km depth), although many of the concepts discussed are general and also apply to shallower levels.

4.6.2 Evidence for Deep-Crustal Fluids

The body of evidence for deep-crustal fluids has grown substantially in the last several decades and includes the following: (1) high-density fluid inclusions that were trapped in metamorphic minerals that grew under deep-crustal conditions, (2) high-pressure metamorphic vein minerals characterized by habits diagnostic of growth into fluid-filled fractures with macroscopic apertures, (3) formation of veins and fractures under conditions where fluid pressure in cracks exceeded the sum of the minimum principal stress and the tensile strength of the rock, (4) general consistency between the mineral assemblages observed in exhumed natural settings and the phase assemblages developed during laboratory experiments done under high fluid pressures, (5) alteration of the chemical and isotopic compositions of rocks due to mass transfer driven by infiltrating fluids, (6) petrologic and isotopic evidence indicating volumetric fluid-rock ratios greater than one that exceed rock porosity and, thus, require infiltration of fluids, and (7) large time-integrated fluid fluxes based on petrologic and isotopic evidence from rocks and numerical models of orogenesis. Note that (5)–(7) require both the presence of fluids and considerable mass transport via a fluid phase.

A number of these topics are addressed in more detail in the succeeding text, and for additional perspectives, the reader is referred to Fyfe et al. (1978), Etheridge et al. (1983, 1984), Peacock (1983), Rumble (1989), Ferry (1994a,b), Person and Baumgartner (1995), Young (1995), Ferry and Gerdes (1998), Zack and John (2007), Yardley (2009), Connolly (2010), Putnis and Austrheim (2010), and Thompson (2010). Fluids have been demonstrated to be an integral part of prograde and retrograde metamorphism, but it is important to point out that they need not be present continuously throughout an orogenic episode (Thompson, 1983).

4.6.3 Devolatilization

The fact that rocks lose volatiles during metamorphic heating is a fundamental tenet of petrology (Fyfe et al., 1978; Shaw, 1956). Devolatilization is a ubiquitous source of fluid during mountain building, although other sources, including degassing magmas and the mantle, can also play important roles. Pseudosection phase diagrams (Connolly, 1990; de Capitani and Petrakakis, 2010; Powell et al., 1998) for representative aluminous pelite, hydrothermally altered mafic rock (spillite), and ultramafic rock are shown in Figure 2 to illustrate rock water contents as a function of pressure and temperature (P – T) conditions. Of course, different bulk compositions will yield different phase relations, but the general patterns depicted in the figures will be robust.

The diagrams illustrating the wt% water in solids (right panels in Figure 2) show the substantial water loss expected for prograde metamorphism. Metapelitic rocks, for example, will typically lose 2–4 wt% H_2O from low to high grade (Figure 2(a)). This general prediction corresponds well with field relations. Pattison (2006), for example, documented ~2.9 wt% volatile loss from metapelitic rocks between 550 and 625 °C ($\sim 4.5 \text{ mol l}^{-1}$); numerous similar examples can be found in the literature (e.g., Fyfe et al., 1978). The water loss corresponds to reactions that destroy hydrous phases, like muscovite, chlorite, and lawsonite, to produce less hydrous or nominally anhydrous ones, such as garnet, aluminosilicates, and pyroxene. The greenschist–amphibolite and blueschist–eclogite facies transitions correspond in a general way to the disappearance of chlorite (Figure 2(a)), although the reader is cautioned that the stability of chlorite and other phases is dependent on the bulk composition of the rock. As is well known, water will be retained to greater depths along subduction zone geotherms, as opposed to the P – T paths characteristic of continental collisions (Figure 2(a); Chapters 4.19 and 4.20).

It is generally held that most dehydration accompanies prograde heating, but if reaction dP/dT slopes are shallow relative to the P – T path, then some dehydration can even occur during cooling and exhumation. For example, the schematic collisional path in Figure 2(a) passes from the 3 wt% to the 2.5 wt% field during exhumation. Vry et al. (2009) provide evidence for volatile loss during exhumation of the Alpine Schist, New Zealand.

The diagram for metamorphosed spillite indicates loss of 2–4 wt% water during heating to amphibolite facies conditions (Figure 2(b)). By contrast, substantial water is retained in the high-pressure, low-temperature part of the blueschist facies to pressures of 2 GPa and beyond (Chapters 4.19 and 4.20). Steep drops in water content down to 2–3 wt% in the eclogite facies and the higher- T part of the blueschist facies are due largely to lawsonite breakdown.

The water content contours for an example of partially serpentinized harzburgite differ substantially from the other rock types (Figure 2(c)). Here, even larger amounts of water are lost (up to ~10 wt%), and the major episodes of water loss take place over relatively narrow temperature intervals. The first of these (at lower T) corresponds to the destruction of brucite and some of the antigorite (a serpentine-group mineral); it involves loss of ~2 wt% H_2O in the greenschist and blueschist facies. The second occurs at higher T in the

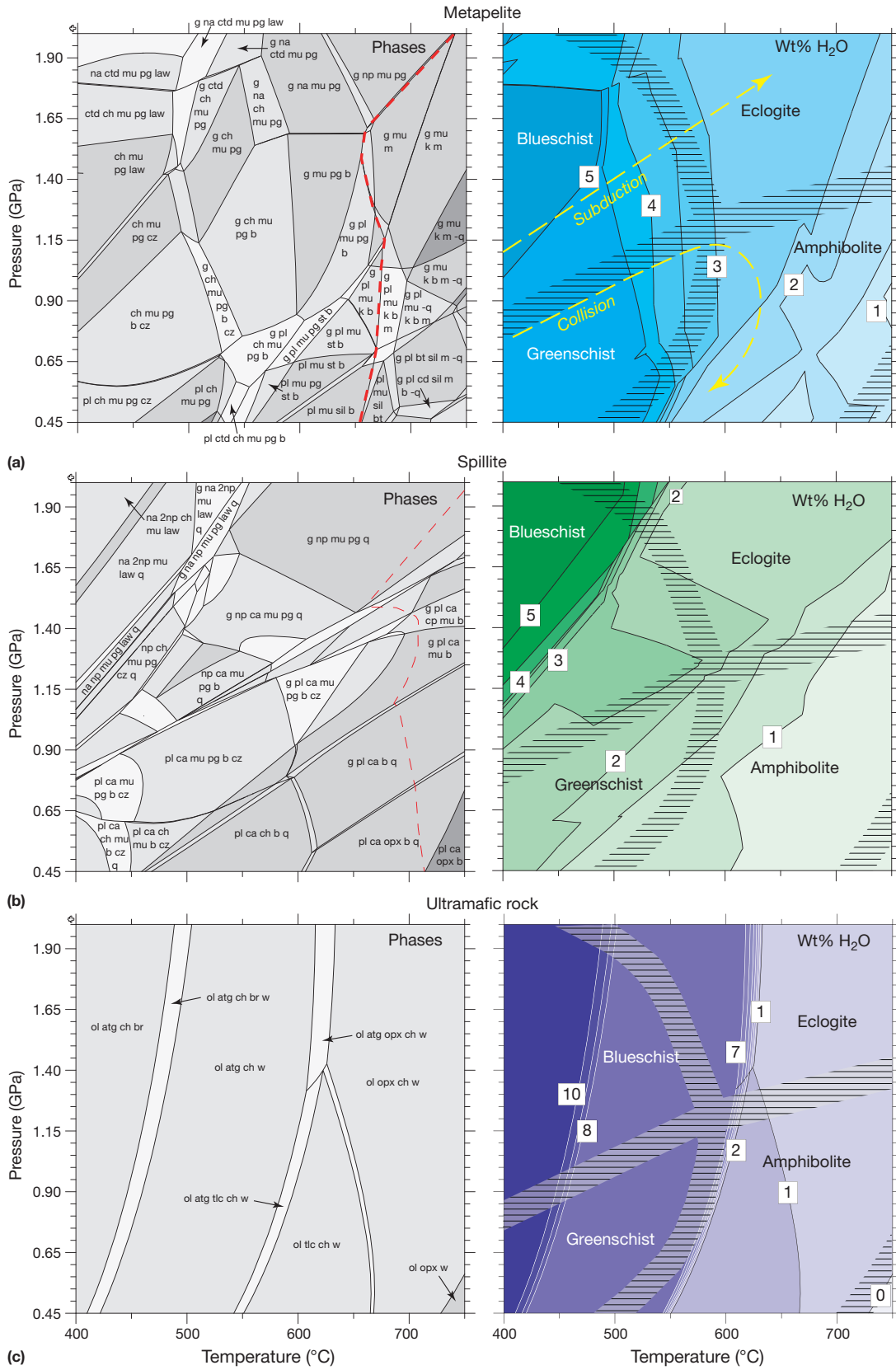


Figure 2 (Continued)

amphibolite or eclogite facies, corresponds to the destruction of antigorite, and releases 5–6 wt% H₂O over a *T* interval of only ~10–20 °C. The reactions take place over narrow temperature intervals, as there is relatively little solid solution in the phases involved owing to the bulk composition, which is dominated by MgO, SiO₂, and H₂O. The intervals would be somewhat wider if iron–magnesium solid solution in antigorite and brucite could be accounted for, but the effects are expected to be minor, as these phases are dominated by magnesium (iron–magnesium–aluminum solution is accounted for in the other solids). The release of large amounts of water over small temperature ranges has important implications for rock rheology, as discussed further in the succeeding text.

The diagrams depict water loss due to dehydration, but other volatiles, particularly CO₂, are also critical components of metamorphic fluids. Devolatilization reaction progress in C-bearing systems is a strong function of fluid composition and reaction history; thus, it is not possible to depict simply on diagrams like Figure 2. Field studies, however, document the large quantities of volatiles that are lost. For example, Ferry (1992) and Léger and Ferry (1993) studied infiltration-driven devolatilization of impure carbonate rocks intercalated with metaclastic rocks in the Waits River Formation, Vermont, United States, which underwent broadly Barrovian-style metamorphism during the Acadian orogeny. Ague (2003) studied similar rocks in the Wepawaug Schist, Connecticut, United States, and highly reacted zones along flow conduits.

In both field settings, volatile loss was extensive; on average, ~15 kg volatiles were lost from typical amphibolite facies rocks (diopside zone) relative to 100 kg of low-grade protolith (Figure 3). More than 95% of this volatile mass was CO₂. The low-grade protolith rocks contain considerable calcite, ankerite, albite, muscovite, and quartz. These combined to yield a rich spectrum of devolatilization reactions that operated during heating and produced minerals like biotite, calcic amphibole, and diopside with increasing grade. Volatile losses were even larger – about 25 wt% – in highly altered, amphibolite facies calc-silicate rocks situated along fluid conduits, such as lithologic contacts and quartz veins (Figure 3; Ague,

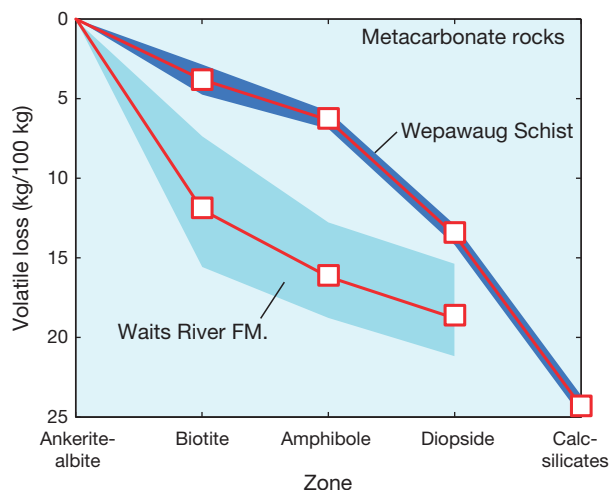


Figure 3 Loss of CO₂ and H₂O from impure carbonate rocks during regional metamorphism; Waits River Formation, Vermont (Ferry, 1992; Léger and Ferry, 1993) and the Wepawaug Schist, Connecticut (Ague, 2003). Prograde reaction progress increases to the right. Kilograms lost relative to 100 kg of average low-grade (Ankerite–Albite zone) precursors. Mean values shown, together with their 1 σ standard errors (shaded fields around lines). CO₂ comprises over 95% of the lost mass. Calculations for Wepawaug are described in Ague (2003). Calculations for the Waits River used the aluminum geochemical reference frame of Ferry (1992) and Léger and Ferry (1993); loss on ignition as a proxy for volatile content; and eqns [21.99]–[21.100] in Philpotts and Ague (2009).

2003). As metacarbonate rocks comprise 20–50% of the western part of the Waits River Formation, 50–80% of the eastern part, and about 10% of the Wepawaug Schist, the production of CO₂ clearly played a significant role in the overall deep-crustal (25–35 km) volatile budget.

Other kinds of devolatilization systematics are, of course, possible. Many rocks will contain hydrous minerals and carbonate minerals, such that substantial amounts of both CO₂ and H₂O are liberated from the same lithology. Ferry (1994a,b) found that carbonate-bearing metasandstones and

Figure 2 Representative pseudosections (left panels) and corresponding contours of wt% water in solids (right panels) for (a) pelite, (b) hydrothermally altered basalt, and (c) ultramafic rock. Facies boundaries after Spear FS (1993) *Metamorphic Phase Equilibria and Pressure–Temperature–Time Paths*. Washington, DC: Mineralogical Society of America and Philpotts AR and Ague JJ (2009) *Principles of Igneous and Metamorphic Petrology*, 2nd edn. Cambridge: Cambridge University Press. Calculated using Theriak–Domino software and thermodynamic dataset tcd55c2d (de Capitani and Petrakakis, 2010); dataset based on Holland and Powell (1998) and includes recent updates. Tick marks on *P*-axis are 0.05 GPa. (a) Aluminous metapelite TN205 (Nagel et al., 2002). Note schematic subduction zone and collisional *P*–*T* paths (yellow dashed lines) on wt% water diagram. KNaCaFMASH system. Provisional ideal mixing model used for glaucophane–ferroglaucophane solid solution. All mineral assemblages coexist with water and quartz, except those marked –q that lack quartz. Beginning of water-saturated partial melting denoted with dashed red line. (b) Hydrothermally altered mafic rock (spillite), sample SF-2100, California. Rock composition reproduced from Coleman RG and Lee DE (1963) Glaucophane-bearing metamorphic rock types of the Cazadero area, California. *Journal of Petrology* 4: 260–301. KNaCaFMASH system. Provisional ideal mixing models used for sodic amphibole (glaucophane–ferroglaucophane) and calcic amphibole (tremolite–ferrotremolite–pargasite) solid solutions. All assemblages coexist with water. Beginning of water-saturated partial melting denoted with thin dashed red line, but melt phase relations not shown due to current uncertainties in mineral–melt equilibria for metabasaltic systems. (c) Partially serpentinized harzburgite, sample 65-R-10, California. Rock composition reproduced from Himmelberg GR and Coleman RG (1968) Chemistry of primary minerals and rocks from the Red Mountain–Del Puerto ultramafic mass, California. *United States Geological Survey Professional Paper 600-C*, C18–C26. FMASH system; small amounts of Ca and Fe³⁺ not considered. Phase abbreviations for all plots: atg, antigorite; b, biotite; br, brucite; ca, calcic amphibole; cd, cordierite; ch, chlorite; cp, calcic clinopyroxene; ctd, chloritoid; cz, clinozoisite; g, garnet; k, kyanite; law, lawsonite; m, melt; mu, muscovite (contains substantial phengite component at high pressures); na, Na amphibole; np, Na pyroxene; opx, orthopyroxene; pg, paragonite; pl, plagioclase; q, quartz; sil, sillimanite; st, staurolite; tlc, talc; w, water.

metapelites of the Waits River Formation lost, on average, 4.25 mol total fluid (several wt% $\text{CO}_2 + \text{H}_2\text{O}$) per liter rock over the comparatively small temperature interval of 475–550 °C. Relatively pure marbles and quartzites will generate little fluid during heating, but these rock types are not dominant in most metasedimentary sequences (although there are of course exceptions, such as the thick marbles of Naxos, Greece). Intrusive and extrusive igneous rocks may have a wide range of volatile contents, depending on bulk composition, crystallization history, and the extent of postmagmatic hydrothermal alteration. Strongly altered rocks, like spillites, will act as volatile sources during heating, whereas less hydrous igneous protoliths may act as fluid sinks, particularly if infiltration and the accompanying hydration and/or carbonation reactions occur at low metamorphic grades. Hydration and carbonation reactions typically produce increases in solid volume. Traditionally, this has been thought to close off porosity and, thus, limit infiltration. However, recent work suggests that it is possible that volume production by such reactions could generate enough stress to fracture rocks, creating new pathways for fluid flow (Jamtveit et al., 2008; Kelemen and Matter, 2008).

4.6.4 Porous Media and Fracture Flow

Fluid flow through rocks is commonly referred to as being *pervasive* or *channelized*, although some overlap exists in the definitions of these terms. Fluid migration around individual mineral grains through an interconnected porosity is known as *pervasive* or *porous media* flow (Figure 4). *Channelized* or *focused* flow implies preferential fluid motion in one or more high-permeability conduits (Figure 5). These include highly permeable layers, lithologic contacts, fracture sets, or individual fractures. Note that flow in a permeable layer could still be *pervasive* at the grain scale within the layer, whereas flow in a fracture is much more strongly localized to the open space between the crack walls. Some metamorphic systems involve both channelized and pervasive flow components (e.g., Oliver, 1996; Rumble et al., 1991).

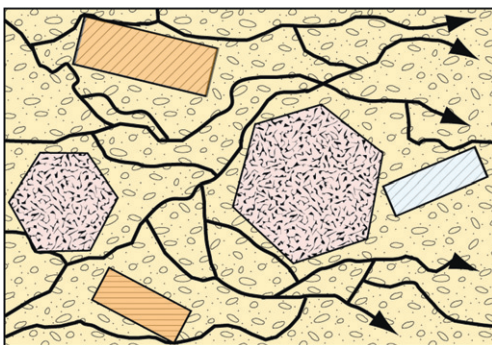


Figure 4 Schematic representation of metamorphic porphyroblasts and matrix illustrating concept of pervasive, grain-scale flow. Flow paths around grains denoted by black arrows.

4.6.4.1 Pervasive Flow and Darcy's Law

Pervasive fluid flow through a porous, permeable medium is described by Darcy's law, written here for three dimensions (e.g., Bear, 1972):

$$\begin{aligned} \vec{q}_D &= \begin{pmatrix} q_x \\ q_y \\ q_z \end{pmatrix} = -\frac{\tilde{k}}{\mu} \cdot \begin{pmatrix} \left(\frac{\partial P_f}{\partial x} \right) \\ \left(\frac{\partial P_f}{\partial y} \right) \\ \left(\frac{\partial P_f}{\partial z} \right) \end{pmatrix} + \rho_f g \begin{pmatrix} \left(\frac{\partial Z}{\partial x} \right) \\ \left(\frac{\partial Z}{\partial y} \right) \\ \left(\frac{\partial Z}{\partial z} \right) \end{pmatrix} \\ &= -\frac{\tilde{k}}{\mu} \cdot (\nabla P_f + \rho_f g \nabla Z) \end{aligned} \quad [1]$$

in which x , y , and z are Cartesian spatial coordinates; \vec{q}_D is the fluid flux vector or Darcy flux (q_x , q_y , and q_z are the components of the flux in the x , y , and z directions, respectively); \tilde{k} is the intrinsic permeability tensor; μ is the dynamic viscosity of the fluid; P_f is fluid pressure; ρ_f is fluid density; g is the acceleration of gravity expressed as a constant (9.81 ms^{-2}); and Z is a vertical reference coordinate axis that increases upward (Table 1). Darcy's law is valid only when the flow is laminar, not turbulent (Bear, 1972, pp. 125–129). Note that fluid flux is a vector, having both magnitude and direction. Clearly, the flux is increased by increasing permeability, increasing fluid pressure gradients, and/or decreasing the fluid viscosity. These key geologic variables are examined in the following paragraphs.

4.6.4.2 Fluid Flux, Fluid Velocity, and Porosity

\vec{q}_D is sometimes referred to as the *Darcy velocity*, but it is really a flux expressed in terms of volume of fluid passing over unit

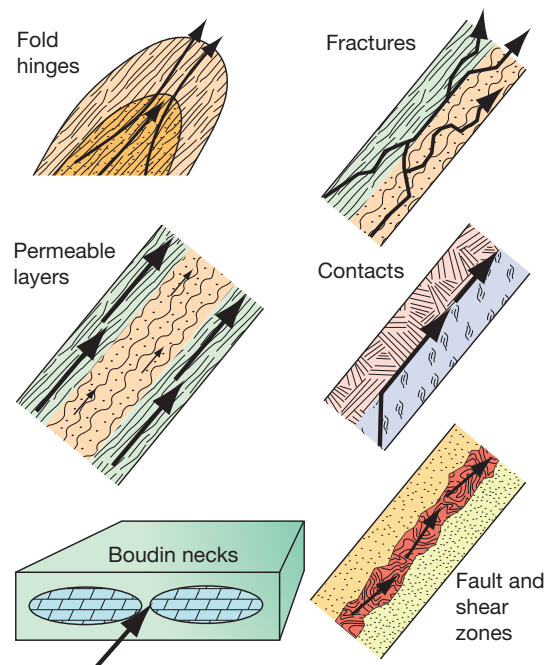


Figure 5 Examples of channelized flow.

Table 1 General symbols and symbols for fluid and heat flow

Symbol	Definition and SI units
x, y, z	Subscripts denoting x -, y -, z -axes
Z	Vertical reference coordinate
x'	Coordinate which is parallel to, and increases in, the direction of flow
$2b$	Distance between fracture walls (m)
B	Thermal Peclet number
$C_{p,f}$	Heat capacity of fluid ($\text{J kg}^{-1} \text{K}^{-1}$)
f_m	Mass fluid released per unit mass solid ($\text{kg (fluid) kg}^{-1}$ (solid))
f_{mv}	Mass fluid released per unit volume rock (kg (fluid) m^{-3} (rock))
g	Acceleration of gravity (m s^{-2})
$K_{T,r}$	Thermal conductivity of rock ($\text{J m}^{-1} \text{s}^{-1} \text{K}^{-1}$)
\bar{k}	Permeability tensor (m^2)
k	Permeability (constant) (m^2)
k_f	Permeability due to fractures (m^2)
L_c	Length of crustal column (m)
η_{fr}	Frequency of fractures (fractures m^{-1})
P	Pressure
P_f	Fluid pressure
\vec{q}_D	Darcy flux vector ($\text{m}^3 \text{m}^{-2} \text{s}^{-1}$)
q_{fr}	Fluid flux through fractured rock ($\text{m}^3 \text{m}^{-2} \text{s}^{-1}$)
q_{TI}	Time-integrated fluid flux ($\text{m}^3 \text{m}^{-2}$)
t	Time (s)
Δt	Total time of fluid–rock interaction (s)
T	Temperature
\vec{v}	Pore velocity vector (m s^{-1})
μ	Dynamic viscosity of fluid (Pa s)
ρ_f	Fluid density (kg m^{-3})
ρ_r	Rock density (kg m^{-3})
ρ_s	Solid density (kg m^{-3})
ϕ	Porosity (m^3 (fluid) m^{-3} (rock))
ω	Constant for porosity–permeability law (m^2)

surface area per unit time. The true average pore fluid velocity is found by dividing the flux by the amount of interconnected porosity, ϕ , through which the fluid flows. Porosity for a fully saturated porous medium is the fluid volume in pores per unit volume rock (volume rock = volume solids + volume pore space; ϕ is expressed as a fraction and is assumed here to represent interconnected pores). Thus,

$$\frac{\vec{q}_D}{\phi} = \vec{v} = \begin{pmatrix} v_x \\ v_y \\ v_z \end{pmatrix} \quad [2]$$

in which \vec{v} is the pore fluid velocity vector. The theoretical estimates of syn-metamorphic porosity of Connolly (1997) are $\sim 10^{-3}$ – 10^{-4} , and Hiraga et al. (2001) found similar values based on direct observation of relic pores preserved in schist. Theoretical analysis of isotopic profiles across lithologic contacts suggest values in the range 10^{-4} – 10^{-6} (Bickle and Baker, 1990) and 10^{-3} – 10^{-6} (Skelton, 2011; Skelton et al., 2000), comparable to grain-scale porosity measurements made on metamorphic rock samples (Norton and Knapp, 1977). Because grain-scale porosities are likely to be small during metamorphism, the magnitude of the pore velocity will be much larger than that of the Darcy flux. For example, if $q_x = 10^{-3} \text{ m}^3_{\text{(fluid)}} \text{ m}^{-2}_{\text{(rock)}} \text{ year}^{-1}$ and $\phi = 10^{-3}$, then the pore velocity, v_x , is 1 m year^{-1} . If

the total porosity includes some *dead end* pores that are not interconnected and do not transmit fluid, then ϕ in eqn [2] must be reduced by multiplying it by the fraction of interconnected pore space.

Porosity evolves as a result of deformation and fluid–rock reactions. Four general pathways of porosity evolution are commonly recognized. First, deformation can collapse porosity and drive fluids out or produce cracking at the grain scale or larger to create porosity. The low-porosity values estimated by Bickle and Baker (1990) for nearly pure marbles may reflect the relative ease with which calcite can deform plastically (e.g., Rutter, 1995) and choke off porosity. Second, increases in fluid pressure will tend to expand pore spaces and increase porosity, whereas decreases in pressure will do the opposite (Walder and Nur, 1984). Third, the mineral products of prograde reaction are typically denser and occupy less volume than reactants, so increases in porosity may accompany fluid infiltration and devolatilization if fluid pressure is sufficient to keep the pore space from collapsing (e.g., Ague et al., 1998; Balashov and Yardley, 1998; Rumble and Spear, 1983; Zhang et al., 2000). The coupled metamorphic–rheological models of Connolly (1997) suggest that devolatilization reactions generate pulses of fluid that travel upward in the form of porosity waves, leaving trails of interconnected pore space in their wake (Section 4.6.4.7). Finally, infiltrating metasomatic fluids will destroy porosity if they precipitate new minerals in the pore spaces or create porosity if they dissolve existing minerals (Balashov and Yardley, 1998; Bolton et al., 1999). In addition to the four processes mentioned earlier, Nakamura and Watson (2001) have shown experimentally that interfacial energy-driven infiltration of water or NaCl-bearing aqueous solution into quartzite can create high-porosity zones that propagate through rock much like traveling waves. Nakamura and Watson (2001) suggest that this mechanism may contribute significantly to fluid fluxes in high-grade metamorphism.

4.6.4.3 Fluid Pressure Gradients

Fluid motion occurs in a direction of decreasing pressure. In Darcy's law, the driving pressure gradient is given by $(\nabla P_f + \rho_f g \nabla Z)$. The $\rho_f g \nabla Z$ term is necessitated by gravity. Pressure increases downward in a column of motionless fluid according to the hydrostatic gradient ($= -\rho_f g$), yet there is no flow. To drive flow upward, the total pressure gradient must exceed the hydrostatic gradient. For convenience, the z -axis of the coordinate system is commonly oriented vertically so that it coincides exactly with the vertical reference Z -axis. Then, $\partial Z/\partial x$ and $\partial Z/\partial y$ are 0, and $\partial Z/\partial z$ is 1. For example, the net pressure gradient driving the vertical component of flow would be given by the difference between the total pressure gradient, $\partial P_f/\partial z$, and $-\rho_f g$, thus yielding $\partial P_f/\partial z - (-\rho_f g)$ or, equivalently, $\partial P_f/\partial z + \rho_f g$.

Brittle deformation involves fracturing on the scale of individual mineral grains or larger, whereas ductile (plastic) deformation occurs without fracturing (e.g., Passchier and Trouw, 1996). In the shallow crust, rocks are in the brittle regime, have substantial strength, and can support open pore networks over kilometer-scale distances. Fluid pressure gradients are close to the hydrostatic gradient, and free convection cells may develop if permeability and thermal gradients are large enough, as is

often the case around cooling intrusions (Norton and Dutrow, 2001; Norton and Knight, 1977). Furthermore, groundwater can circulate down into sedimentary basins to depths of several kilometers by gravity-driven (or topography-driven) flow involving fluid input into high-elevation parts of foreland basins, subhorizontal flow for tens or even hundreds of kilometers, and discharge into lower-elevation areas (Garven and Freeze, 1984a, 1984b).

The transition between hydrostatic and deeper regimes is thought to occur at around 10 km (e.g., Manning and Ingebritsen, 1999), but is not precisely constrained and may be considerably deeper. At deeper levels, where plastic deformation becomes more important, rocks are considerably weaker and tend to collapse around fluid-filled pores, producing larger pressure gradients that may approach lithostatic ($dP/dZ = -\rho_r g$; ρ_r is rock density). Thus, for vertical, upward flow under the lithostatic gradient, the pressure gradient term in Darcy's law is the difference between the lithostatic and hydrostatic gradients ($-\rho_r g + \rho_f g \approx -1.7 \times 10^4$ to -2.0×10^4 Pa $m^{-1} \approx -0.17$ to -0.2 bar m^{-1}). In general, deep-crustal fluid pressure regimes that drive flow are thought to be closer to lithostatic than hydrostatic (e.g., Hanson, 1997), but much uncertainty remains. For example, the subhorizontal flow constrained by nearly flat-lying lithologic layering inferred on petrologic grounds for regional metamorphism in northern New England by Ferry (1992, 1994a) could have been driven by very small gradients – even smaller than the hydrostat ($< -10^4$ Pa m^{-1}).

4.6.4.4 Permeability

The intrinsic permeability is a property of the porous medium only and is a quantitative measure of how readily a fluid can flow through the medium. Permeability varies over a remarkable 16 orders of magnitude in the Earth's crust, from values as high as 10^{-7} m² in gravels to 10^{-23} m² in some shales and crystalline igneous and metamorphic rocks (e.g., Brace, 1980; Connolly, 1997; Freeze and Cherry, 1979; Manning and Ingebritsen, 1999). In the general case, \tilde{k} is a second-rank tensor because permeability varies with direction. Metamorphic foliations defined by inequidimensional minerals, particularly sheet silicates, are a primary source of anisotropy (e.g., Zhang et al., 2001). The measurements of Huenges et al. (1997) reveal mean permeability parallel to foliation as much as ~ 10 times greater than perpendicular to it, consistent with field-based studies that suggest fluid fluxes are greatest parallel to layering and foliation (e.g., Baker, 1990; Cartwright et al., 1995; Ferry, 1987, 1994a,b; Ganor et al., 1989; Oliver et al., 1990; Rumble and Spear, 1983; Rye et al., 1976; Williams et al., 1996). Oriented fracture sets are another source of anisotropy. If, on the other hand, the medium is isotropic and can transmit fluid equally well in all directions, then \tilde{k} reduces to a constant (k). Permeability also varies from one layer to the next and even within individual layers, regardless of the degree of anisotropy, producing permeability contrasts that can exceed two orders of magnitude (Baumgartner and Ferry, 1991; Baumgartner et al., 1997; Oliver, 1996). Comparisons of inferred metamorphic fluid fluxes suggest that metapelitic rocks are often more permeable than metapsammities or very pure calcite marbles (e.g., Chamberlain and Conrad, 1991; Oliver et al., 1998; Rye et al., 1976; Skelton et al., 1995).

Following the approach of Baumgartner and Ferry (1991), Manning and Ingebritsen (1999) estimated a mean k of $10^{-18.5 \pm 1}$ m² for rocks deeper than ~ 12 km undergoing active metamorphism and combined this result with permeability data for shallower geothermal systems to yield the depth-permeability relation: $\log k \approx -3.2 \log(\text{depth in km}) - 14$. Permeability likely exceeds these predicted values during transient events that increase porosity and permeability, such as earthquake faulting, and falls below these values in quiescent rocks undergoing little metamorphism or deformation (Ingebritsen and Manning, 2010). Although considerable uncertainty remains regarding crustal depth-permeability relationships (Connolly, 2010), available estimates strongly suggest that significant permeability is possible even at the base of the continental crust during orogenesis.

In general, permeability increases as the amount of interconnected pore space increases, resulting in strong coupling between porosity and permeability. Thus, because porosity is time-dependent, permeability is as well. A number of porosity-permeability relationships, such as the Kozeny-Carman equation, have been proposed; these commonly include a strong (often cubic) dependence of permeability on porosity (e.g., Bear, 1972, p. 166; Bickle and Baker, 1990; Bolton et al., 1999; David et al., 1994; Walder and Nur, 1984; Wong and Zhu, 1999; and references therein). For example, Connolly (1997) described deep-crustal permeability using $k = \omega \varphi^3$ in which the constant $\omega = 10^{-13}$ m². While calculated porosity-permeability relationships are still subject to major uncertainties of order of magnitude scale or larger, it is clear that porosity-permeability feedbacks can control spatial patterns of flow. For example, increases in porosity due to infiltration and devolatilization reaction can increase permeability, causing more flow to focus into the reacting area (e.g., Balashov and Yardley, 1998; Spiegelman and Kelemen, 2003), whereas precipitation of minerals that occlude the porosity can decrease permeability and divert flow away (e.g., Lyubetskaya and Ague, 2009).

4.6.4.5 Dynamic Viscosity

The dynamic viscosity is the viscosity of a moving fluid; it depends on T , P , and fluid composition. Values for pure H₂O, CO₂, and, by extension, H₂O–CO₂ mixtures are similar and vary relatively little compared to properties like porosity and permeability; a representative value for the middle and lower crust is $\sim 1.5 \times 10^{-4}$ Pa s (see Walther and Orville, 1982). However, the effects on viscosities of solute species, as well as very high pressures (1–2 GPa), remain to be fully explored.

4.6.4.6 Crack Flow

The deformational behavior of rocks, whether brittle or ductile, depends mainly on temperature, fluid pressure, rock pressure, mineralogy, grain size, and strain rate. Temperature is one of the main controls on deformation behavior. For example, for slow strain rates, common minerals, like quartz, are brittle at $T < \sim 300$ °C, but ductile deformation involving dislocation glide and creep becomes increasingly important at higher T . The transition from dominantly brittle to dominantly ductile behavior is thought to occur at depths corresponding to temperatures of ~ 300 °C – usually around ~ 15 km for typical

crustal geotherms (e.g., Scholz, 1990; Sibson, 1983; Yeats et al., 1997). These depths are consistent with measured and inferred near-hydrostatic fluid pressure gradients in much of the shallow crust.

Nonetheless, brittle behavior is not restricted to shallow levels. If the fluid pressure exceeds the sum of the tensile strength of the rock and the least principal stress, then hydrofracturing, transient fluid release, and associated drops in fluid pressure will occur (e.g., Etheridge, 1983; Hubbert and Willis, 1957; Yardley, 1986). The maximum tensile strength of most rocks is only ~ 0.01 GPa (~ 100 bars), so even modest fluid overpressures will cause hydrofracturing. Elevated pore fluid pressures generated by metamorphic devolatilization reactions (e.g., Ague et al., 1998), as well as by deformation and collapse of pore space (e.g., Cox, 2007; Sibson, 1992; Sibson et al., 1975; Walder and Nur, 1984; Wong et al., 1997), can lead to rock weakening and hydrofracture. With time, the porosity and permeability created by a hydrofracturing event are reduced as cracks are sealed and pores collapse. If permeability reaches low enough levels ($< \sim 10^{-20}$ m²), then fluid pressure can once again build up and ultimately produce another hydrofracturing event. The episodes of fracturing and healing preserved in veins attest to this cyclic behavior (Fisher and Brantley, 1992; Kirschner et al., 1993; Oliver and Bons, 2001; Ramsay, 1980; Rye and Bradbury, 1988). Oxygen isotope disequilibrium suggests transient timescales of fluid–rock interaction as short as 10^3 – 10^5 years in and around some veins (Section 4.6.9.7; Palin, 1992; van Haren et al., 1996; Young and Rumble, 1993). At very shallow crustal levels, hydrofracturing may be less common if relatively high rock permeabilities prevent fluid pressures from building up.

Rocks that are ductile at low strain rates can undergo brittle deformation at larger strain rates. For example, earthquakes release massive amounts of energy in seconds or minutes during fault slippage and are capable of producing regionally extensive brittle deformation. Data from several recent, damaging earthquakes, including the Northridge and Loma Prieta events in California and the Kobe event in Japan, demonstrate that rupture and brittle deformation occur well below 10–13 km (e.g., Davis and Namson, 1994; Lees and Lindley, 1994; Priestley et al., 2008; Zhao et al., 1996). For the Northridge event, the main shock occurred at 17–18 km, and some aftershocks extended to ~ 25 km. In fact, from April 1980 to February 1994, nearly 1100 seismic events were recorded in the 20–35 km depth range in the Los Angeles, California area alone (Ague, 1995). If rapid devolatilization and hydrofracturing occur within seismically active areas, then the rock failure may trigger earthquakes that recur on human timescales (e.g., Ague et al., 1998). The fluid-filled earthquake hypocenters that have been inferred on the basis of seismic evidence for both the Loma Prieta (Lees and Lindley, 1994) and Kobe (Zhao et al., 1996) events strongly suggest links between the presence of fluids and seismicity.

The evidence mentioned earlier establishes that fracturing and seismic behavior can extend well into the mid to lower crust. Veins preserve a valuable record of this brittle deformation; they are fractures into which mineral mass has been deposited. The most common vein-forming minerals are quartz, calcite, and the feldspars, but a huge variety of other minerals are also observed. Fractures tend to focus flow because they are zones of elevated permeability. Fracture flow is

commonly approximated using the well-known expression from fluid mechanics for laminar flow between two parallel plates (e.g., White, 1979). For a set of parallel fractures, the flux is approximated by (e.g., Norton and Knapp, 1977)

$$q_{fr} = -\frac{(2b)^3 n_{fr}}{12\mu} \left(\frac{dP_f}{dx'} + \rho_f g \frac{dZ}{dx'} \right) \quad [3]$$

in which q_{fr} is the fluid flux through the fractures in the rock mass, the coordinate x' is parallel to, and increases in, the direction of flow, $2b$ is the distance between the fracture walls (or crack aperture), and n_{fr} is the frequency of the fractures. Equation [3] has been shown experimentally to be applicable to real fractures, even those with rough walls and many points of contact (asperities), if $2b$ is taken as the average crack aperture. By comparison with eqn [1], it is clear that the $(2b)^3 n_{fr}/12$ grouping is directly analogous to the permeability in Darcy's law. Consequently, the fracture permeability, k_{fr} , of a rock mass can be estimated if the average number and aperture of fractures are known (e.g., Norton and Knapp, 1977):

$$k_{fr} = \frac{(2b)^3 n_{fr}}{12} \quad [4]$$

Metamorphic fracture apertures range from the micrometer scales (Etheridge et al., 1984; Ramsay, 1980) to millimeter or centimeter scales (Ague, 1995).

Even small amounts of fracturing can affect markedly the permeability. If an unfractured rock with low permeability, say 10^{-23} m², is deformed to produce, on average, just one 10^{-5} m aperture fracture per meter of rock ($n_{fr} = 10^{-5}$ m⁻¹), then eqn [4] gives $k_{fr} \sim 8 \times 10^{-17}$ m² – over seven orders of magnitude greater than 10^{-23} m². The permeability systematics of crystalline rocks suggest a scale dependence; laboratory measurements made on unfractured rock cores generally yield the smallest values, whereas regional field tests indicate the largest (Brace, 1984). At least some of this discrepancy is probably due to natural fractures that increase considerably the permeability of the field test sites (Manning and Ingebritsen, 1999).

4.6.4.7 Porosity Waves

Transient relationships between porosity, permeability, and fluid flow are well illustrated by the concept of porosity waves. Solitary waves of porosity were independently predicted to form in fluid-saturated, compacting porous media by Scott and Stevenson (1984) and Richter and McKenzie (1984). Connolly and coworkers extended the theory to dewatering metamorphic systems (e.g., Connolly, 1997; Connolly and Podladchikov, 1998). Periodic wave behavior is also predicted under appropriate geologic circumstances.

Consider a layer undergoing devolatilization in low-permeability rock. As most devolatilization reactions will decrease solid volume, the porosity and, thus, permeability in the reacting zone will tend to increase. As reviewed by Connolly (2010), this will lead to elevated pressures near the top of the reacting zone and diminished pressures near the base. Given the low strength of rocks, the lower-pressure zone at the base will tend to compact and reduce porosity. Fluids in the upper part, by contrast, will be under elevated pressures and be squeezed upward via dilational deformation of the rock matrix. This coupled

expansion and collapse is predicted to produce a zone of elevated porosity that migrates upward and that can ultimately detach itself from the region undergoing active dewatering. In multiple dimensions, such instabilities are predicted to take elongated, tubelike forms (Connolly and Podladchikov, 2007).

Solitary porosity wave behavior has been experimentally verified for flow through a single nonporous conduit (Olson and Christensen, 1986; Scott et al., 1986). Bouihol et al. (2011) presented field evidence for porosity waves that channelize melt. However, to the author's knowledge, fluid (as opposed to melt) flow by porosity waves has not been verified for a deformable porous medium either by experiments or by field observations of metamorphic rocks, although some tantalizing field relations have been observed (e.g., John et al., 2012; Podladchikov et al., 2009). Melt formation, segregation, and ascent can involve very large changes in porosity (e.g., Aharonov et al., 1995), but fluid

flow need not. As a consequence, the geological fingerprint of porosity wave fluid transport recorded in rocks may be very cryptic. Nonetheless, the more general processes of porosity collapse and compaction undoubtedly play important roles during devolatilization. A major challenge going forward is to assess the nature and extent of fluid propagation by porosity waves in the lithosphere.

4.6.5 Overview of Fluid Chemistry

Metamorphic fluids are chemically diverse and are able to transport *molecular* species, like H_2O , CO_2 , CH_4 , and H_2S , and solutes, including $\text{H}_4\text{SiO}_4^\circ$, Na^+ , NaCl° , and many others (Figure 6). This section provides a brief review of some common fluid constituents.

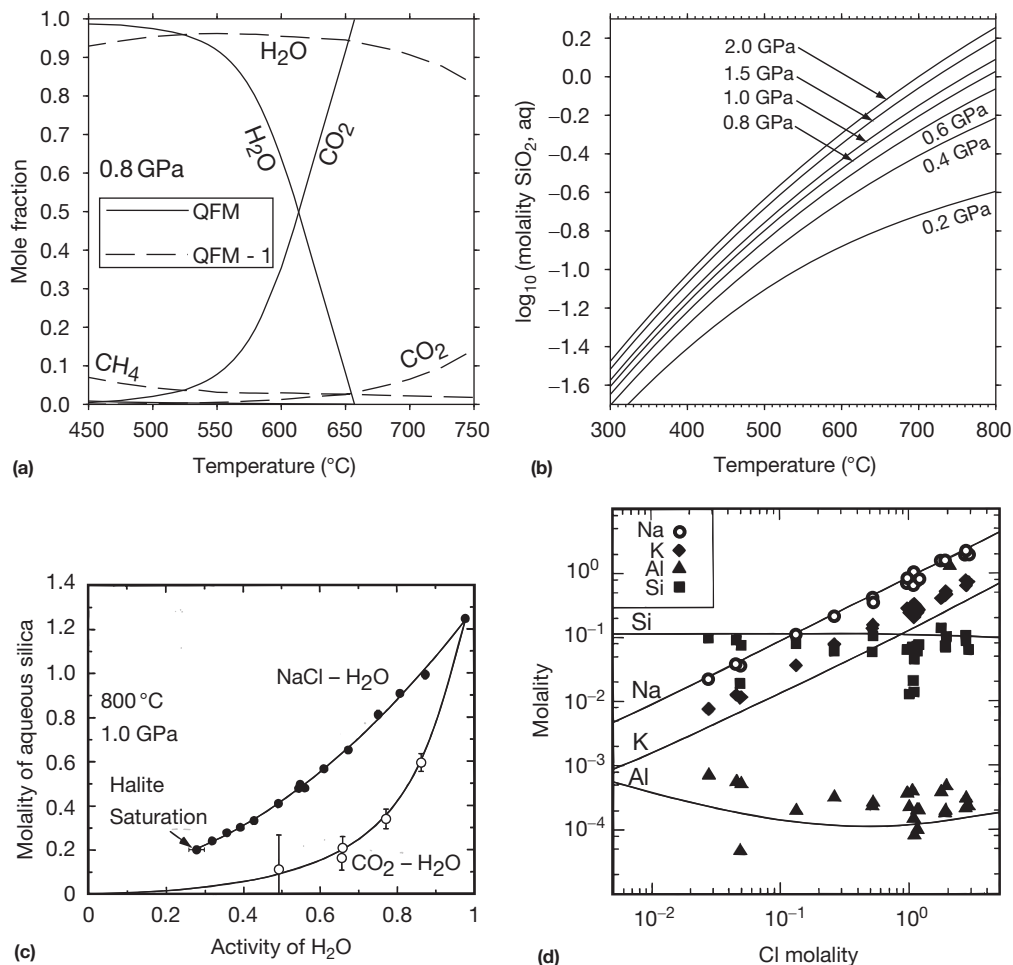


Figure 6 Examples of metamorphic fluid compositions. (a) Species in C–O–H fluids at 0.8 GPa and oxygen fugacities equivalent to the quartz–fayalite–magnetite buffer (QFM) and one \log_{10} unit below QFM (QFM-1). Computed following Ague et al. (2001). Graphite is unstable above ~ 660 °C for QFM. (b) Quartz solubility computed using the expression of Manning (1994). (c) Effect of NaCl and CO_2 on quartz solubility. Reproduced from Newton RC and Manning CE (2000) Quartz solubility in H_2O –NaCl and H_2O – CO_2 solutions at deep crust–upper mantle pressures and temperatures: 2–15 kbar and 500–900 °C. *Geochimica et Cosmochimica Acta* 64: 2993–3005. Experimental data for H_2O –NaCl fluids (filled symbols) and H_2O – CO_2 fluids (open symbols) shown. (d) Fluid composition coexisting with quartz, microcline, albite, and andalusite as a function of total Cl molality at 0.2 GPa and 600 °C (after Figure 6(d) in Hauzenberger CA, Baumgartner LP, and Pak TM (2001) Experimental study on the solubility of the ‘model’-pelite mineral assemblage albite + K-feldspar + andalusite + quartz in supercritical chloride-rich aqueous solutions at 0.2 GPa and 600 °C. *Geochimica et Cosmochimica Acta* 65: 4493–4507). Symbols: experimental data; lines: theoretical calculations. Note that total molalities of potassium and sodium increase with increasing chlorine content, unlike silicon and aluminum, which do not form significant chloride complexes.

Deep-crustal H₂O is released mostly by prograde devolatilization of sheet silicates and amphiboles and, in some cases, by degassing magmas, whereas CO₂ is released mostly by devolatilization of carbonate minerals. Because H₂O and CO₂ are such fundamental constituents of crustal fluids, considerable attention has been focused on their physicochemical properties. Thermodynamic treatment is complicated because both pure H₂O and pure CO₂ deviate strongly from ideal gas behavior and because mixing of H₂O and CO₂ is also nonideal (e.g., Aranovich and Newton, 1999; Blencoe et al., 1999; Ferry and Baumgartner, 1987; Kerrick and Jacobs, 1981; Schmidt and Bodnar, 2000; Shi and Saxena, 1992). The fugacity and activity coefficient expressions of Kerrick and Jacobs (1981) for pure H₂O, pure CO₂, and H₂O–CO₂ mixtures have been widely used and are accurate for $P \leq \sim 1$ GPa. Similar results for pure H₂O and pure CO₂ are obtained using Haar et al. (1984) and Mäder and Berman (1991), respectively. Expressions valid for pure species to pressures well in excess of 1 GPa include those of Holland and Powell (1991, 1998), Shi and Saxena (1992), and Sterner and Pitzer (1994). Aranovich and Newton (1999) provide activity–composition relations for H₂O–CO₂ mixtures valid between ~ 600 – 1000 °C and 0.6–1.4 GPa.

H₂O and CO₂ are extremely important, but deep-crustal fluids contain many other constituents. For example, at low enough oxygen fugacities in the presence of reactive graphite, CH₄ can be significant (e.g., French, 1966; Skippen and Marshall, 1991; Connolly, 1995; Figure 6(a)). Furthermore, progressive heating promotes desulfidation of pyrite to produce pyrrhotite and liberate S (e.g., Carpenter, 1974; Mohr and Newton, 1983). Thermodynamic treatments of geologically important species, including CH₄, CO, H₂, S₂, H₂S, and COS, can be found in, for example, Holland and Powell (2003), Jacobs and Kerrick (1981) and Shi and Saxena (1992).

Rock-forming and ore-forming metals are key components of aqueous, chloride-bearing metamorphic fluids. Salinity varies from near zero to as much as several molal in typical metamorphic environments (e.g., Crawford and Hollister, 1986; Hollister and Crawford, 1981; Roedder, 1984; Smith and Yardley, 1999; Yardley, 1997) and can reach extreme levels in granulites (Crawford and Hollister, 1986; Markl et al., 1998). Standard state thermodynamic properties for many aqueous species of interest can be calculated to ~ 1000 °C and ~ 0.5 GPa using the internally consistent methods and data sets of Pokrovskii and Helgeson (1995), Shock et al. (1997), and Sverjensky et al. (1997). These data have also been extrapolated to somewhat higher pressures with reasonable results (e.g., Dipple and Ferry, 1992a). Holland and Powell (1998) advanced an alternative method and data set for calculating standard state properties relevant for the deep crust. Dolejš and Manning (2010) presented a model for mineral dissolution based on the thermodynamic and volumetric properties of the aqueous solvent; it is applicable up to 1100 °C and 2.0 GPa. The extended Debye–Hückel equation is commonly used to estimate the activities of charged species, although it cannot be applied to highly concentrated brines (Sverjensky, 1987). Activity coefficients for neutral species are assumed to be in unity or, in some cases, are modeled using the Setchénow equation (e.g., Sverjensky, 1987; Xie and Walther, 1993). The activity of H₂O remains close to unity if the salt content is low (Sverjensky, 1987) but decreases markedly in

concentrated brines (Aranovich and Newton, 1996, 1997). An important area of future research is the experimental and theoretical investigation of activity–composition relations for aqueous species in fluids that contain considerable CO₂, CH₄, and H₂S.

Experimental, fluid inclusion, and field-based evidence indicates the following four generalized groupings of elemental abundances for fluids in typical quartz-bearing rocks at moderate pressures (~ 0.5 GPa): (1) Cl, Na, K, and Si; (2) Ca, Fe, and Mg; (3) Al; and (4) high-field-strength elements (HFSE), like zirconium, titanium, and rare earth elements (REE). Abundances are generally highest in the first group and lowest in the last. The concentrations of silicon, potassium, and sodium are relatively large in crustal fluids that coexist with quartz, feldspars, and/or micas. Aqueous silica concentrations in equilibrium with quartz increase markedly with T and P (Anderson and Burnham, 1965; Kennedy, 1950; Weill and Fyfe, 1964). Manning (1994) performed experiments at high P and T and combined the results with those of the previous studies to obtain an expression for silica molality applicable to ~ 900 °C and at least 2 GPa (Figure 6(b)). At deep-crustal conditions, quartz solubility decreases as the NaCl content of the fluid increases, and drops very sharply with the addition of CO₂; thus, if immiscible brine–CO₂ fluids exist in the deep crust, then silica will partition strongly into the brine (Figure 6(c); Newton and Manning, 2000a, 2000b; Walther and Orville, 1983). The effective solubility of albite also increases with P and T and decreases with increasing NaCl, although it should be noted that its dissolution is incongruent (Shmulovich et al., 2001). The behavior of aqueous silica, which is present mainly as the neutral H₄SiO₄⁰ complex, differs from that of sodium and potassium, which are present mostly as the charged species Na⁺ and K⁺ and the neutral chloride complexes NaCl⁰ and KCl⁰. Consequently, the total concentrations of sodium and potassium generally increase as the total concentration of chlorine increases in typical mica-bearing quartzofeldspathic rocks (Figure 6(d); e.g., Hauzenberger et al., 2001).

Calcium, magnesium, and iron are also present mostly as charged species or chlorine complexes and can reach relatively high concentrations in some fluids, particularly those coexisting with metaultramafic and calcium silicate-bearing metacarbonate rocks (e.g., Dipple and Ferry, 1992a; Ferry and Dipple, 1991; Vidale, 1969). A study of the incongruent dissolution of diopside shows that its effective solubility increases with increasing NaCl content, owing mostly to complexing of calcium and magnesium with chlorine in solution (Shmulovich et al., 2001). The retrograde solubility of calcite at low P and T is well known, but surprisingly, much remains to be learned about calcite behavior in the deep crust. The results of Dolejš and Manning (2010), however, indicate that calcite solubility in H₂O is considerable – for example, ~ 1100 ppm at 600 °C and 1 GPa.

The concentration of aluminum is traditionally regarded as small in aqueous fluids (Figure 6(d)). However, complexing with alkalis and/or halides (Diakonov et al., 1996; Tagirov and Schott, 2001; Walther, 2001) and polymerization with aqueous silica and/or alkalis (Manning, 2006, 2007; Manning et al., 2010; Salvi et al., 1998; Wohlers and Manning, 2009) increases the concentration of aluminum in aqueous solutions, particularly at the high- P – T conditions relevant for the deep crust. For example, total aluminum concentrations at 700 °C and

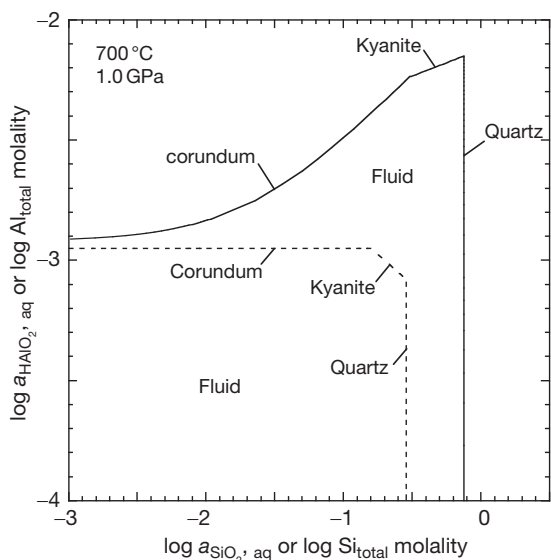


Figure 7 Mineral stabilities in the $\text{Al}_2\text{O}_3\text{-SiO}_2\text{-H}_2\text{O}$ system at 700°C and 1.0 GPa . Dashed lines depict mineral stabilities in terms of fluid concentrations (molality) calculated for the dominant species (aqueous HAlO_2 and SiO_2) in the absence of polymerization. Solid lines show enhanced total concentrations resulting from Si polymerization and Al-Si complexing in the fluid phase. Reproduced from Manning CE (2007) Solubility of corundum + kyanite in H_2O at 700°C and 10 kbar : Evidence for Al-Si complexing at high pressure and temperature. *Geofluids* 7: 258–269. With permission from John Wiley & Sons.

1.0 GPa reach 5.8×10^{-3} molal in equilibrium with quartz and kyanite (Manning, 2007; Figure 7). These concentrations are still relatively small compared to constituents, like aqueous silica, but are apparently sufficient for calc-silicate formation (Ague, 2003) and for the formation of aluminosilicates and other aluminum-rich phases in syn-metamorphic veins (e.g., Ague, 2011; Austrheim, 1990; Bucholz and Ague, 2010; Kerrick, 1990; Whitney and Dilek, 2000; Widmer and Thompson, 2001). In addition, polymerization can increase the concentration of dissolved silica beyond that predicted for $\text{H}_4\text{SiO}_4^\circ$ alone (Figure 7). Furthermore, the role of pH is important; both acidic (e.g., Kerrick, 1990; McLelland et al., 2002; Nabelek, 1997) and higher pH solutions (Wohlert and Manning, 2009) may increase the solubilities of aluminous minerals and aid aluminum transport.

The experimentally determined solubilities of rutile and zircon in quartz-saturated $\text{H}_2\text{O-CO}_2$ fluids are small; the titanium and zirconium are probably present mostly as $\text{Ti}(\text{OH})_4^\circ$ and $\text{Zr}(\text{OH})_4^\circ$ complexes (Ayers and Watson, 1991, 1993). However, titanium concentrations increase in the presence of dissolved sodium-aluminum silicates in an H_2O -rich fluid phase, suggesting that complexing with dissolved silicate material enhances rutile solubility and transport (Antignano and Manning, 2008a; Audétat and Keppler, 2005). Nonetheless, titanium concentrations in aqueous fluids with or without dissolved sodium-aluminum silicates are low; for example, Antignano and Manning (2008a) find $\sim 150\text{ ppm}$ at 1.0 GPa and 800°C in $\text{H}_2\text{O-NaAlSi}_3\text{O}_8$ fluid with 10 wt\% dissolved silicate material. With respect to zircon, a number of field-based studies indicate very limited zircon solubility (e.g., Breeding et al. 2004a; Carson et al., 2002; Fu et al., 2010;

Steyrer and Sturm, 2002). Zircon dissolves incongruently to form baddeleyite in quartz-undersaturated H_2O at high P and T , but the amount of zirconium in solution remains small (Ayers and Watson, 1991). Despite the low measured solubilities of rutile and zircon and likely low concentrations of HFSE in fluids (e.g., Becker et al., 1999), field evidence suggests that titanium and zirconium can be mobilized, particularly in some deep-crustal and subduction zone fluids (Section 4.6.9.5; e.g., Bröcker and Enders, 2001; Heaman et al., 2002; John et al., 2008; Philippot and Selverstone, 1991; Rubatto and Hermann, 2003; Sorensen and Grossman, 1989; Wilke et al., 2012).

REE can be transported by crustal fluids, but much remains to be learned about the processes and fluid chemistry involved (e.g., Grauch, 1989). The REE hosts monazite and apatite have relatively low solubilities in H_2O (Antignano and Manning, 2008b; Ayers and Watson, 1991). Fluorapatite solubility increases with P , T , and fluid NaCl content (Antignano and Manning, 2008b).

Fluorine, phosphorus, yttrium, or other agents might complex HFSE, thus enhancing their transport in crustal fluids; radiation damage in zircon might increase its solubility, and titanite and ilmenite might be more soluble than rutile, but much experimental and field work is needed to assess these possibilities (e.g., Ague, 2003; Ayers and Watson, 1991; Gieré, 1990, 1993; Gieré and Williams, 1992; Jiang et al., 2005; Ohr et al., 1994; Pan and Fleet, 1996; Whitney and Olmsted, 1998).

A number of laboratory- and field-based studies indicate that fluids and silicate melts can be completely miscible under appropriate conditions. For example, Bureau and Keppler (1999) observed experimentally complete miscibility between silicate melt and hydrous fluid for a variety of melt compositions and concluded that complete miscibility is possible in all but the shallowest parts of the upper mantle. Their results imply that amphibole breakdown in subduction zones should produce the mobile, hydrous fluids necessary for arc magma genesis, whereas breakdown of lawsonite or phengite deeper in subduction zones should produce much less mobile, silicate-rich fluids (see Chapters 4.19 and 4.20). While the results of Bureau and Keppler (1999) apply to relatively high-pressure settings, Thomas et al. (2000) showed that melt-fluid miscibility is possible even in low pressure ($\sim 0.1\text{ GPa}$) pegmatite environments if the system is rich in fluorine, boron, and phosphorous. The recognition of significant miscibility opens up a host of new research avenues for melt-hydrous fluid systems, including their compositions, phase relations, physical and transport properties, and impact on the chemical evolution of the crust and mantle.

4.6.6 Chemical Transport and Reaction

4.6.6.1 Mass Fluxes

The processes of advection, diffusion, and mechanical dispersion transport chemical species in fluids. For a porous medium, the flux, \vec{F}_i , of species i in the x , y , and z coordinate directions ($\text{mol m}^{-2}_{(\text{rock})} \text{s}^{-1}$) can be written:

$$\vec{F}_i = \vec{v}\phi C_i - D_{i,f}\bar{\tau}\phi\nabla C_i - \vec{D}_{\text{MD}}\phi\nabla C_i \quad [5]$$

in which C_i is the concentration of i in $\text{mol m}^{-3}_{(\text{fluid})}$, $D_{i,f}$ is the diffusion coefficient for i through a free fluid, $\bar{\tau}$ is the tortuosity

tensor, and \tilde{D}_{MD} is the mechanical dispersion tensor (Table 2). The first, second, and third terms on the right hand side describe fluxes due to fluid flow (advection), diffusion (Fick's first law), and mechanical dispersion, respectively. Transport through the solids is assumed negligible relative to the other processes (but see Section 4.6.6.3). Diffusion and mechanical dispersion are known collectively as *hydrodynamic dispersion* and are discussed in the succeeding text.

Values of $D_{i,f}$ for aqueous species under metamorphic conditions are typically on the order of $10^{-8} \text{ m}^2 \text{ s}^{-1}$ (Oelkers and Helgeson, 1988). Taking $\sqrt{D_{i,f}t}$ as a characteristic length scale for diffusion in a free fluid yields $\sim 0.6 \text{ m}$ for 1 year of diffusion to $\sim 600 \text{ m}$ for 1 My! In rocks, however, diffusive fluxes are

limited by porosity and tortuosity (eqn [5]). The pathways for diffusion between grains through an interconnected porosity are not straight, but are instead complex and *tortuous*. Consequently, diffusion through rock is *slower* than that through a free fluid; the tortuosity tensor is introduced to describe this behavior. Tortuosity is expressed as a tensor because it can vary with direction. Tortuosity systematics for metamorphic rocks are largely unknown, but it seems likely that pathways will be less tortuous parallel to penetrative fabrics than perpendicular to them. Ague (1997a) found that diffusion adjacent to a cross-cutting quartz vein occurred more readily in metapelitic layers than metapsammitic ones; the difference may reflect less tortuosity parallel to micaceous fabrics in the metapelites relative to the metapsammites. In theory, tortuosity can vary between 1 (perfectly *straight* pathways) and near 0. Values measured in porous media range from about 0.3 to 0.6 (Bear, 1972, p. 111), consistent with measurements of diffusion through pores in granodiorite (Fisher and Elliott, 1973), but much remains to be learned regarding tortuosity during active metamorphism.

Length scales of coupled diffusion and reaction can be considerable. Diffusion of mass across contacts between metapelitic and metacarbonate rocks can drive reactions that produce calc-silicate reaction zones on the centimeter to meter scale (e.g., Ague, 2002; Brady, 1977; Thompson, 1975; Vidale, 1969; Vidale and Hewitt, 1973). Bickle et al. (1997) estimated an $\sim 5\text{--}10 \text{ m}$ length scale for the diffusional component of oxygen isotope exchange across a lithologic contact. Characteristic length scales for reactive strontium diffusion across the lithologic contacts studied by Bickle et al. (1997) and Baxter and DePaolo (2000) are ~ 2 and $\sim 0.7 \text{ m}$, respectively. Numerical models suggest $\sim 1\text{--}10 \text{ m}$ length scales may be relevant for the exchange of H_2O and CO_2 between adjacent layers, particularly if the product $\phi\tau > \sim 5 \times 10^{-5}$ (Ague, 2000, 2002; Ague and Rye, 1999). Field tests confirm volatile mass exchange over such length scales in the deep crust (Ague, 2003; Ferry, 2008; Penniston-Dorland and Ferry, 2006). Extremely fluid-mobile elements, such as lithium, can have diffusional transport distances as large as $\sim 30 \text{ m}$ (Liu et al., 2010; Teng et al., 2006).

Diffusion transports mass down concentration gradients (from regions of high concentration to low concentration) according to eqn [5], although it is actually driven by gradients in chemical potential (e.g., Shewmon, 1969). The concentration gradient-based approach turns out to be accurate for most tracers. It is generally used for species at higher concentrations as well, but complications, including the dependence of diffusion coefficients on fluid composition and diffusion up concentration gradients, can arise as the diffusing species interact subject to their chemical potential gradients and mass and charge balance constraints. The papers of Graf et al. (1983) and Liang et al. (1996) illustrate some of the problems that need to be solved in future studies of complex diffusional behavior during metamorphism.

Mechanical dispersion of transported species occurs during fluid flow, increases as flow velocity increases, and arises because (1) fluid in adjacent porous pathways will be moving at slightly different velocities and (2) the tortuous nature of the flow paths causes mixing. Because of its dissipative nature, mechanical dispersion is generally modeled using a mathematical form identical to that for diffusion, although the processes underlying diffusion and mechanical dispersion are very

Table 2 Symbols for chemical mass transfer and reaction rates

Symbol	Definition and SI units
i	Subscript denoting fluid species i
m	Subscript denoting reaction m
θ	Subscript denoting solid phase θ
$\bar{A}_{i,m}$	Surface area of rate-limiting mineral i in reaction m ($\text{m}^2 \text{ m}^{-3}$)
A_θ	Reactive surface area of θ ($\text{m}^2 \text{ m}^{-3}$)
a_i	Activity of species i
C_i	Concentration of i in fluid (mol m^{-3})
C_i^{Solid}	Concentration of i in solid (mol m^{-3})
$\tilde{D}_{HD,i}$	Hydrodynamic dispersion tensor ($\text{m}^2 \text{ s}^{-1}$)
$D_{HD,i}$	Hydrodynamic dispersion coefficient ($\text{m}^2 \text{ s}^{-1}$)
$D_{i,f}$	Diffusion coefficient for i in fluid ($\text{m}^2 \text{ s}^{-1}$)
\tilde{D}_{MD}	Mechanical dispersion tensor ($\text{m}^2 \text{ s}^{-1}$)
E_a	Activation energy (J mol^{-1})
\vec{F}_i	Flux vector for species i ($\text{mol m}^{-2} \text{ s}^{-1}$)
ΔG	Gibbs free energy change for reaction (J mol^{-1})
K_v	Equilibrium fluid/solid partition coefficient by volume ($\text{mol m}^{-3} \text{ Fluid} / (\text{mol m}^{-3} \text{ Solid})$)
K_θ	Equilibrium constant (dissolution reaction for phase θ)
L	Characteristic length scale (m)
L_{GF}	Distance of geochemical front propagation (m)
N_m	Reaction order for reaction m
n_i	Moles i produced/consumed per unit volume rock (mol m^{-3})
\dot{n}	Nucleation rate
p, M, N	Constants for rate expressions
P_e	Peclet number
Q_θ	Ion activity product
R	Gas constant ($\text{J mol}^{-1} \text{ K}^{-1}$)
$R_{i,m}$	Consumption/production rate of i ($\text{mol m}^{-3} \text{ s}^{-1}$)
r_θ	Dissolution/precipitation rate for θ ($\text{mol m}^{-3} \text{ s}^{-1}$)
s	Sign
T°	Kinetic reference temperature (K)
T_{eq}	Equilibrium temperature (K)
\bar{V}_f	Molar volume of fluid ($\text{m}^3 \text{ mol}^{-1}$)
\bar{V}_{Qtz}	Molar volume of quartz ($\text{m}^3 \text{ mol}^{-1}$)
X_i	Mole fraction of i in fluid
X_{eq}	Equilibrium mole fraction in fluid
α_L	Longitudinal dispersivity (m)
α_T	Transverse dispersivity (m)
κ	Rate constant (s^{-1})
κ_m	Intrinsic rate constant for reaction m ($\text{mol m}^{-2} \text{ s}^{-1}$ (J mol^{-1}) $^{-1}$)
κ_θ	Intrinsic dissolution/precipitation rate constant for phase θ ($\text{mol m}^{-2} \text{ s}^{-1}$)
$\nu_{i,m}$	Stoichiometric coefficient for i in reaction m
$\tilde{\tau}$	Tortuosity tensor
τ	Tortuosity (constant)

different. Mechanical dispersion is a function of both the intrinsic properties of the porous medium and the fluid velocity and is described using a directional framework even for homogeneous, isotropic media because dispersion in the direction of flow (longitudinal) tends to be greater than that perpendicular to flow (transverse). For example, assume that flow occurs with velocity v_x parallel to the x coordinate direction. Then,

$$\tilde{D}_{MD} = \begin{pmatrix} \alpha_L |v_x| & 0 & 0 \\ 0 & \alpha_T |v_x| & 0 \\ 0 & 0 & \alpha_T |v_x| \end{pmatrix} \quad [6]$$

can be used, where α_L and α_T are the coefficients of longitudinal and transverse dispersivity, respectively (Bear, 1972). The $\alpha_T |v_x|$ term describes mechanical dispersion parallel to x , whereas the $\alpha_T |v_x|$ terms describe it parallel to y and z . Longitudinal dispersivity can vary over several orders of magnitude in natural geologic materials (Garven and Freeze, 1984b). It is another variable that is not well known for metamorphism, but by analogy with low-permeability rocks, like shales, values between near 0 and ~ 10 m appear reasonable (Ague, 2000). The transverse dispersivity is expected to be as much as two orders of magnitude smaller (Garven and Freeze, 1984b). When diffusion and mechanical dispersion act together, length scales of mass transfer can be considerable; Ferry (2008) documents cross layer transport of H_2O-CO_2 over distances > 70 m. Note that if the medium is anisotropic, then significant complexities are introduced into the tensor representation of mechanical dispersion (Bear, 1972).

4.6.6.2 Reaction Rates

The fluid infiltration histories of fossil metamorphic flow systems are recorded when the fluid reacts with the rock. If there was no reaction during flow, then fluxes could be large but the rock would not preserve evidence of the flow. Furthermore, the presence or absence of water is a critical factor in determining element mobility and, hence, rates of crustal reaction (e.g., Carlson, 2010). In a classic example, Austrheim (1987, 1990) documents dry, Precambrian granulite facies rocks that were metastable in the lower crust until infiltrated by hydrous fluids during Caledonian orogenesis. The infiltration occurred along shear zones, veins, and other permeable zones, converting anhydrous granulite facies assemblages to eclogite facies ones containing a variety of mineral assemblages, including omphacite, garnet, kyanite, phengite, paragonite, clinozoisite, and calcic amphibole (Figure 8). This example shows that the granulite facies rocks would have not recorded their passage through the eclogite facies without the reaction rate enhancement provided by fluids (and deformation).

The rates of chemical reactions link the timescales of mineralogical and fluid composition changes to those of mass and heat transfer (see Chapter 4.7). The rate of precipitation or dissolution is dependent on the rate that ions can be attached to or removed from the mineral surface and the rate at which ions can be transported to and from the surroundings to the mineral surface. A complete description of all these processes in multicomponent systems is generally not possible with current rate data, so the usual approach is to cast the rates in terms of the slowest or rate-limiting step (Figure 9; e.g., Berner, 1980). When the rate of attachment or removal of ions at



Figure 8 Phengite–kyanite–quartz vein and marginal reaction zones (selvages) cutting gabbroic anorthosite (light), Holsnøy, Bergen Arcs, Norway. Eclogite facies reaction zones (dark) on either side of the vein formed when fluid that flowed along the vein infiltrated into the host anorthosite under eclogite facies conditions. The anorthosite that was not infiltrated remained metastable under high-pressure conditions and did not react to form eclogite facies mineral assemblages. Reproduced from Austrheim H (1990) The granulite–eclogite facies transition: A comparison of experimental work and a natural occurrence in the Bergen Arcs, western Norway. *Lithos* 25: 163–169. With permission from Elsevier.

precipitating or dissolving areas of the mineral is slow relative to transport rates through the solution surrounding the grain, the rate is said to be *surface controlled*. The opposite case of fast attachment or removal relative to transport is called *transport controlled* or sometimes *diffusion controlled*. Consider a quartz crystal bathed in fluid. For surface-controlled rates, the concentration of aqueous silica species at the surface of the mineral is identical to that in the surrounding bulk solution. Note that these concentrations need not be at equilibrium values. On the other hand, for transport control by diffusion, the concentrations of aqueous silica species at the surface of the quartz are at equilibrium values, but concentration gradients exist between the solution composition at the surface and the composition in the surroundings. Either surface or transport control can be dominant, depending upon the nature of the reaction–transport system (e.g., Sanchez-Navas, 1999); a number of studies suggest dominance of surface control in many common fluid–rock settings (e.g., Steefel and Lasaga, 1994), but a more complex behavior is also possible (Dohmen and Chakraborty, 2003).

A wide array of experimental studies indicate that rates of mineral dissolution and precipitation in aqueous solution are controlled primarily by reactive surface area, rate constants, activities of catalyzing/inhibiting agents, and departures of Gibbs energy from equilibrium. The relationships between these factors can be described by the following generalized rate law, which is consistent with the transition state theory (see Steefel and Lasaga, 1994; and references therein):

$$\text{Rate} = A_\theta \kappa_\theta f(a_i) f(\Delta G) \quad [7]$$

in which A_θ is the reactive surface area of mineral θ in units of area mineral per unit volume rock; κ_θ is an intrinsic rate constant in units of moles mineral per unit area per time; $f(a_i)$ is a function of the activities of aqueous species i in

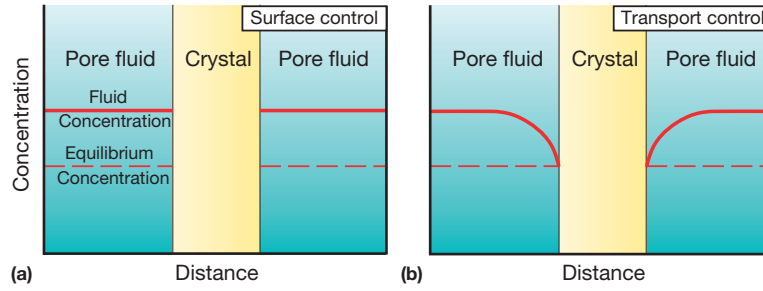


Figure 9 Illustration of rate-limiting steps and reaction kinetics. (a) Surface control. For example, the pore fluid phase could be supersaturated in quartz, but no significant concentration gradients in the fluid exist around a quartz crystal due to rapid transport relative to reaction rate as quartz precipitates. (b) Transport control. Here, concentration gradients exist around the crystal as a result of slow transport relative to reaction. Concentration at crystal–fluid interface is governed by local fluid–rock equilibrium.

solution, which act to either catalyze or inhibit reaction; and $f(\Delta G)$ is some function of the free energy of the system. A more specific form of eqn [7] that is generally applicable to surface-controlled reactions among common minerals is

$$r_{\theta} = sA_{\theta}\kappa_{\theta} \left(\prod_i a_i^p \right) \left| \left(\frac{Q_{\theta}}{K_{\theta}} \right)^M - 1 \right|^N \quad [8]$$

in which r_{θ} is the dissolution or precipitation rate for θ in moles per unit volume rock per unit time; p is an experimentally determined constant; M and N are two positive numbers also generally determined by experiment; Q_{θ} is the ion activity product; K_{θ} is the equilibrium constant for the reaction (Q_{θ} and K_{θ} are equal at equilibrium); and s is, by convention, negative if the solution is undersaturated with respect to θ and positive if supersaturated (Steeffel and Lasaga, 1994). If M and N are both one, then the rate law is said to be *linear*; otherwise, it is *non-linear*. The intrinsic dissolution or precipitation rate constant κ_{θ} is strongly T -dependent and is usually expressed as an Arrhenius-type equation (e.g., Oxtoby et al., 1999):

$$\kappa_{\theta} = \kappa_{\theta}^{\circ} \exp \left(\frac{-E_a}{R} \left[\frac{1}{T} - \frac{1}{T^{\circ}} \right] \right) \quad [9]$$

in which E_a is the activation energy and T° is the reference temperature (often 298.15 K). With this kinetic behavior, reaction rates will increase by a factor of ~ 10 km^{-1} for a geothermal gradient of 30 $^{\circ}\text{C km}^{-1}$ (holding all other rate terms constant). Consequently, departures from local equilibrium are expected to diminish as T increases. E_a values appear to be limited to the range ~ 40 – 90 kJ mol^{-1} for common silicate and carbonate minerals, averaging around ~ 60 kJ mol^{-1} . The dissolution or precipitation reaction that the rate expression [9] is keyed into is usually written for 1 mol of mineral, for example, for K-feldspar, one could write $\text{KAlSi}_3\text{O}_8 + 4\text{H}^+ = \text{K}^+ + \text{Al}^{3+} + 3\text{SiO}_{2,\text{aq}} + 2\text{H}_2\text{O}$. Dissolution proceeds from right to left and precipitation from left to right; at equilibrium, both rates are equal. The rates of reaction among the species in solution are commonly assumed to be instantaneous (e.g., Helgeson, 1979; Sverjensky, 1987).

The overall rate of a fluid–rock reaction can also be modeled rather than computing the dissolution and precipitation of each solid separately. For example, one could write an overall reaction between solids and fluids, such as muscovite + quartz = sillimanite + K-feldspar + H_2O (Schramke et al., 1987). The model for overall reactions in metamorphic

rocks advanced by Lasaga and Rye (1993) includes all the basic pieces of eqn [7] except the catalysis/inhibitor term (Agué, 1998):

$$R_{i,m} = \left(\frac{1}{\phi} \right) s \kappa_m v_{i,m} \bar{A}_{l,m} |\Delta G_m|^{N_m} \quad [10]$$

in which $R_{i,m}$ is the rate in moles of i per unit volume fluid per unit time for reaction m ; κ_m is the intrinsic reaction rate constant; $v_{i,m}$ is the stoichiometric coefficient for i ; $\bar{A}_{l,m}$ is the surface area of the rate-limiting mineral l per volume rock in reaction m ; $|\Delta G_m|$ is the absolute value of the Gibbs free energy change of reaction m at the T and P of interest; N_m is the reaction order; and s is, by convention, $+1$ if ΔG_m is negative and -1 otherwise. If $N_m = 1$, then the rate law is *linear*; otherwise, it is *nonlinear*. Lüttge et al. (2004), for example, apply kinetic theory and discuss intrinsic rate constants relevant for metamorphism of siliceous dolomites. Note that eqn [10] gives the production/consumption rate for moles of a fluid species i , whereas eqn [8] is written for moles of solid. The net production/consumption rate for i is obtained by summing over the rate expressions for all reactions m .

In general, the rate-limiting surface area, $\bar{A}_{l,m}$, in the overall rate eqn [10] is determined by the mineral with the slowest surface reaction kinetics and the lowest surface area in contact with fluid. $\bar{A}_{l,m}$ is thus a function of critical rock physical properties, including the rock porosity structure and the size, shape, and abundance of mineral grains. Much progress has been made by estimating mineral surface areas using simple geometric shapes, like spheres or cubes, that grow or shrink during reaction (Bolton et al., 1999; Steeffel and van Cappellen, 1990). However, the amount of reactive surface area remains as one of the major uncertainties in modeling reaction rates.

A simpler but useful expression has been widely used in geochemistry to model reaction rates:

$$R_i = \kappa (C_i^{\text{eq}} - C_i)^N \quad [11]$$

The reaction rate is proportional to the difference in concentration between the fluid in contact with the mineral assemblage at a particular place in the system (C_i) and the fluid composition that would be in equilibrium with the mineral assemblage (C_i^{eq}). Thus, the net rate is 0 when fluid and rock are at chemical equilibrium ($C_i = C_i^{\text{eq}}$). The rate constant κ actually combines several key rate variables and, for linear

rates ($N=1$), can be cast in terms of the product of the intrinsic reaction rate constant, a reactive surface area term, and the derivative of the ΔG of reaction with respect to concentration (Lasaga and Rye, 1993).

In real rocks, dissolution, precipitation, and devolatilization reactions proceed only if there is some departure from local fluid–rock equilibrium, a condition known as *overstepping*. Models of fluid–rock reaction that use the local equilibrium approximation assume that reaction rates are so fast as to be essentially instantaneous. However, for some reactions, such as those with small intrinsic rate constants and small reactive surface areas, the rate of reaction near equilibrium is slow. Consequently, the T , P , and/or fluid composition must depart significantly from equilibrium before ΔG (the *driving force* for reaction) is large enough to produce significant rates. The magnitude of the overstepping is likely to be larger if the reaction rate law is nonlinear (eqns [8]–[11]).

Overall rate expressions, like eqn [10], assume reactants and products are present and reacting, with the degree of overstepping being controlled by the rate at which the transformation of reactants into products occurs. Equilibrium is also overstepped if product solids fail to nucleate (e.g., Jamtveit and Anderson, 1992; Pattison and Tinkham, 2009; Putnis and Holland, 1986; Rubie, 1998; Waters and Lovegrove, 2002; Wilbur and Ague, 2006). Classical theory holds that when a new phase nucleates, extra energy is necessary to form the grain boundary between the new phase and the phases from which it is growing (e.g., Shewmon, 1969). At equilibrium, this extra energy is unavailable and no growth of reaction products occurs. Overstepping of the equilibrium condition, however, provides the energy necessary to nucleate and grow reaction products and decrease the overall free energy of the system. For the cases of T and fluid composition (X) overstepping, the nucleation rate \dot{n} is proportional to (Ridley and Thompson, 1986):

$$\dot{n} \propto \exp(T - T_{\text{eq}})^2 \quad [12]$$

and

$$\dot{n} \propto \exp(X - X_{\text{eq}})^2 \quad [13]$$

in which T_{eq} and X_{eq} are equilibrium temperature and fluid composition, respectively. Thus, once the products do nucleate in an overstepped reaction, it is likely that they will do so rapidly, given the exponential and power terms in these expressions. It appears that some phases, particularly garnet solid solutions, continue to nucleate well after the exponential stage, albeit at considerably reduced rates (e.g., Carlson, 1989).

The rates of metamorphic reactions and the magnitude of departures from local chemical equilibrium are important and controversial issues in the Earth sciences today. Fluid fluxes, P – T time evolution, and reaction histories estimated assuming local equilibrium models would clearly be in error if the actual processes operated far from equilibrium. Some examples of chemical disequilibrium, such as sluggish phase transformations among the Al_2SiO_5 polymorphs and selective retrograde reaction along pathways of fluid infiltration, have been well documented (e.g., Giorgetti et al., 2000; Kerrick, 1990). Other concrete examples of chemical disequilibrium for prograde metamorphic devolatilization reactions and fluid flow are

still relatively rare, but the number is steadily increasing as theoretical, textural, isotopic, and field studies focus on the problem (e.g., Baxter and DePaolo, 2000, 2002ab; Chernoff and Carlson, 1997; Jamtveit, 1992; Lüttge et al., 2004; Müller et al., 2004; Pattison and Tinkham, 2009; Pattison et al., 2011; Putnis and Holland, 1986; Waters and Lovegrove, 2002; Wilbur and Ague, 2006). It is common to observe variable grain sizes for a given mineral in a metamorphic rock. Such textures are inconsistent with equilibrium (Thompson, 1987), but it is unclear if they indicate large energetic departures from equilibrium. Laboratory evidence strongly suggests that the degree of prograde T overstepping due to nucleation problems may be on the order of 10–100 K and 1–10 kJ, with the smallest values for devolatilization reactions and the largest for reactions with small entropy changes such as solid–solid reactions (Ridley and Thompson, 1986). P oversteps may be 0.1 GPa or more (Ernst and Banno, 1991; Ridley and Thompson, 1986). When multiple product phases must nucleate, oversteps are likely to be large and may exceed ~ 0.7 GPa (Rubie, 1998). If devolatilization reactions are overstepped significantly in T , then the subsequent rapid reaction that occurs upon nucleation and mineral growth may generate large fluid pressures sufficient to drive hydrofracture and fluid flow (e.g., Ague et al., 1998; Walther, 1996) over short time-scales of 10– 10^3 years (Ague et al., 1998).

Theoretical calculations suggest that slow rates may cause significant reaction overstepping in metacarbonate rocks, consistent with observed oxygen and carbon isotopic disequilibrium in some contact aureoles (Lüttge et al., 2004; Müller et al., 2004). A particularly insidious problem here is that sequences of mineral assemblages produced in the field relatively far from equilibrium can mimic local equilibrium sequences (Lüttge et al., 2004).

Baxter and DePaolo (2000, 2002a,b) measured mineral chemistry and strontium isotope systematics for garnet and whole rock across a lithologic contact near Simplon Pass, Switzerland, and concluded that rates of reaction during cooling from ~ 610 to ~ 500 °C were extremely small, amounting to roughly 10^{-7} g solid reacted per gram of rock per year. The slow reaction rates may reflect, in part, the cooling regime of retrograde metamorphism when fluids are not abundant, but Baxter and DePaolo (2000) also argue that prograde rates could not have been fast either. One provocative implication is that the chemical systematics of minerals that participate in such slow reactions may be unable to track changes in fluid chemistry, P , and T (Baxter and DePaolo, 2002b). In summary, mounting field, laboratory, and theoretical evidence indicates that chemical kinetics may be an important control on metamorphic processes, so it is prudent to examine the assumption of equilibrium before using it.

4.6.6.3 Transport and Reaction Within Crystals

Thus far, mass transport and reaction around grains through fluid-filled pore spaces and cracks, but not within the grains themselves are considered. At low to moderate metamorphic grades, intracrystalline (within grain) diffusion is commonly assumed to be slow enough, relative to fluid-mediated transport and reaction, that it can be neglected. Nonetheless, in cases of slow fluid transport, diffusive transfer into and out of

grains could have a more significant impact on fluid geochemistry, particularly at high-temperature conditions where diffusion rates are enhanced. Although intracrystalline diffusion effects may be limited, a growing body of evidence indicates that mass transport to and from crystals by coupled dissolution and precipitation (referred to here as CDP) can operate rapidly enough to influence the chemical and isotopic compositions of crystals and migrating fluids over a wide range of crustal conditions (Dumond et al., 2008; Harlov et al., 2005; Labotka et al., 2004; O'Neill and Taylor, 1967; Putnis, 2002; Putnis and John, 2010).

CDP requires that a disequilibrium fluid comes into contact with crystal surfaces (Figure 10). Chemical reaction involving recrystallization then replaces the existing mineral with a new one in equilibrium with the fluid. This *reaction interface* then propagates into the crystal. As it does, it leaves behind a zone of fluid-filled, micro- or nanoscale porosity in the replaced mineral; these zones have been clearly documented in experimental studies and some field studies (Putnis and Austrheim, 2010; Putnis and John, 2010). Reactants are transported into, and products out of, such porous zones, facilitating the inward movement of the replacement front. The transport could be by diffusion, advection, or some combination. Porosity may be generated if the overall replacement reaction has a negative

volume change and/or if the rate of dissolution is faster than the rate of precipitation. A key point is that because transport is dominantly through a fluid-filled porous network in the replaced crystal, rates of mineral change are orders of magnitude faster than they would be if controlled by solid-state intracrystalline diffusion alone. Another key point is that the replacement fronts are extremely sharp, much sharper than normally expected for intracrystalline diffusion (Figure 11).

When parent and product minerals share some common crystallographic relationships, nucleation of the product is likely to be epitaxial (Putnis, 2002). This can result in pseudomorphic replacement. Experimental examples of albite replaced by K-feldspar, and replacement reactions involving apatite are shown in Figure 11(a) and 11(b). In cases where there is less lattice matching, reaction products will normally be polycrystalline and lack epitaxial relationships (Figure 11(c)).

CDP processes have major implications for interpretation of fluid–rock reactions in the geologic record (see Putnis and John, 2010). One is that the parent and product phases are probably not in chemical equilibrium with each other. Consequently, it is hazardous to use equilibria involving parent–product compositions to estimate pressures, temperatures, or fluid compositions. The most likely equilibrium is between the interfacial fluid and the product phase (Putnis and John, 2010). Another

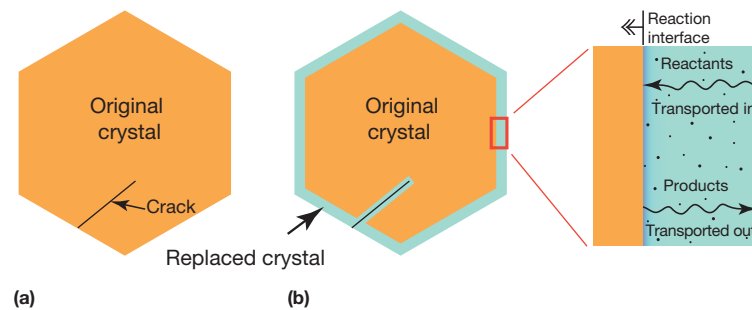


Figure 10 Schematic illustration of coupled dissolution–precipitation (CDP). (a) Original parent crystal. (b) Original crystal partially replaced on rims and along crack. Reaction interfaces propagate inward as reactants are transported in, and products out, through a network of fluid-filled micro- or nanopores in the replaced crystal.

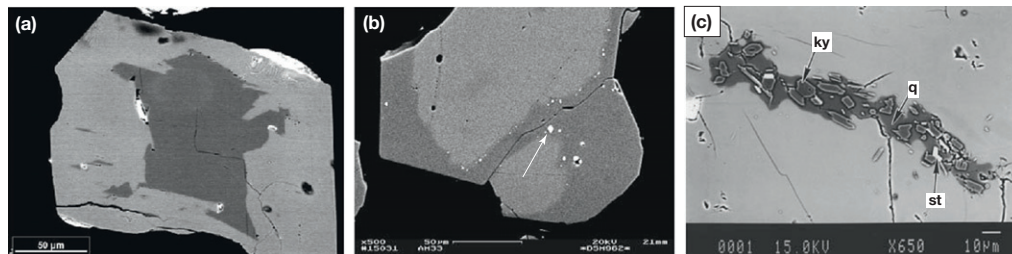


Figure 11 Backscattered-electron (BSE) images of CDP. (a) Experimental replacement of albite (dark) by potassium feldspar rim (light). Albite core is what remains of original pure albite crystal. Reproduced from Niedermeier DRD, Putnis A, Geisler T, Golla-Schindler U, and Putnis CV (2009) The mechanism of cation and oxygen isotope exchange in alkali feldspars under hydrothermal conditions. *Contributions to Mineralogy and Petrology* 157: 65–76. (b) Experimental reaction of fluorapatite with HCl fluid. Original crystal material is light gray; darker regions on rims and along cracks have undergone CDP and are depleted in (yttrium + rare earth elements (REE) + silicon + sodium + sulfur + chlorine). Bright grains are monazite formed during reaction (arrow). Reproduced from Harlov DE, Wirth W, and Förster H-J (2005) An experimental study of dissolution–reprecipitation in fluorapatite: Fluid infiltration and the formation of monazite. *Contributions to Mineralogy and Petrology* 150: 268–286. (c) Plagioclase (light gray) replaced by quartz, kyanite, and minor staurolite along crack. Infiltrating fluids removed calcium and sodium and precipitated quartz; kyanite formed from the aluminum left over after plagioclase breakdown. Reproduced from Ague JJ (1994b) Mass transfer during Barrovian metamorphism of pelites, south-central Connecticut. II: Channelized fluid flow and the growth of staurolite and kyanite. *American Journal of Science* 294: 1061–1134. With permission from Yale University.

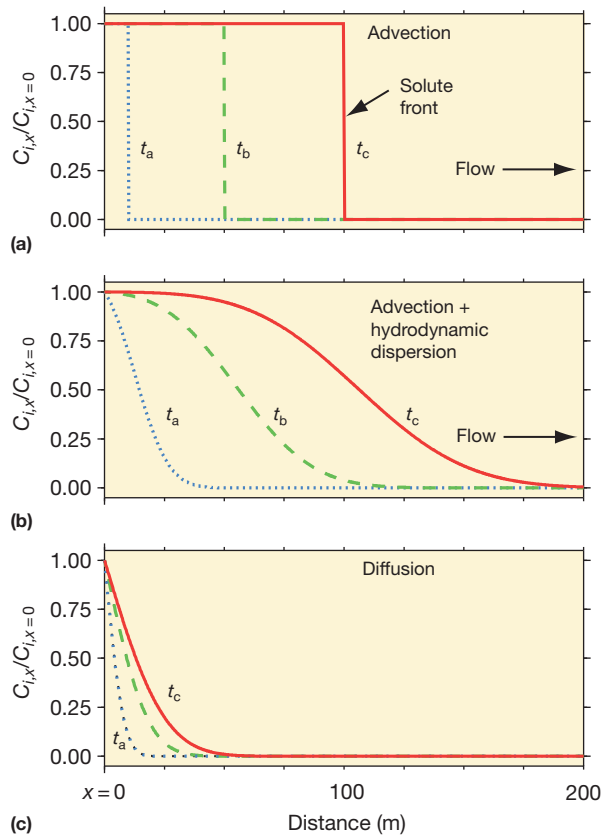


Figure 12 Fluid composition as a function of distance for three different model times ($t_a=100$ years; $t_b=500$ years; $t_c=1000$ years) computed using eqn [17]. No chemical reaction. $v_x=0.1$ m year^{-1} ; $D_{i,t}=10^{-8}$ m s^{-2} ; $\tau=0.6$; $\alpha_L=5$ m. (a) Propagation of solute front by advection. (b) Combined advection and hydrodynamic dispersion. Note front broadening with increasing time and distance. (c) Transport by diffusion.

L , whereas advection dominates for large L , say, on the scale of a mountain belt. The dissipative effects of hydrodynamic dispersion probably operate over length scales of $<\sim 100$ m (Bickle, 1992; Bickle and McKenzie, 1987).

The concept of steady state differs markedly from that of equilibrium. If, for example, the fluid composition is at steady state in a reacting flow system, then the fluid composition is not changing with time. The system is not at equilibrium, however, since equilibrium would require that no transport and no reaction were occurring. Instead, at steady state, the transport and reaction processes can be thought of as being in balance, such that the fluid composition remains constant. Transient changes in porosity, fluid velocity, and other geologic factors make it unlikely that natural systems ever reach perfect steady states, although the steady approximation has proven useful for constraining average time-integrated fluid fluxes and general processes of fluid–rock interaction.

Importantly, the concentration of i in the solid is not at steady state even if the fluid composition is (Figure 13). Consider a schematic example. A rock comprising corundum and kyanite in equilibrium with an aqueous pore fluid reacts with a fluid input at $x=0$ that is in equilibrium with quartz and kyanite. At moderate metamorphic temperatures and

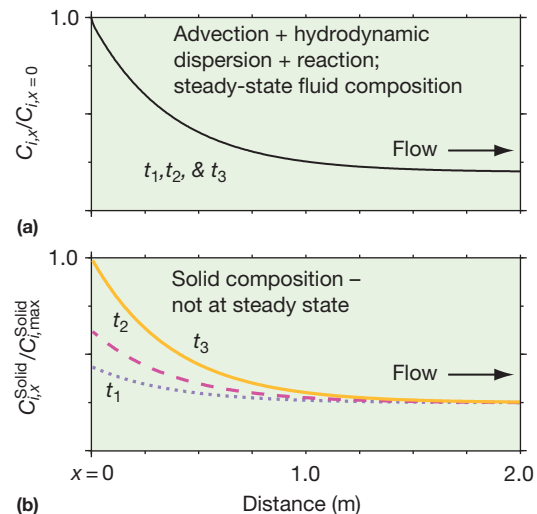


Figure 13 Steady and unsteady states for advection + hydrodynamic dispersion + reaction for three different model times ($t_1 < t_2 < t_3$; these do not correspond to times in Figure 12). $v_x=0.1$ m year^{-1} ; $D_{i,t}=10^{-8}$ m s^{-2} ; $\tau=0.6$; $\alpha_L=5$ m. Rate constant $\kappa=5$ year^{-1} used for illustration purposes and does not necessarily correspond to any specific reaction. $C_{i,max}^{Solid}$ is the maximum concentration of i possible for solid. Equations [15] and [16] solved using numerical methods described in Ague (1998). y -axis scaling is arbitrary. (a) Steady-state fluid composition. Note fluid composition does not change with time. (b) Solid compositions corresponding to times t_1 , t_2 , and t_3 . Concentration of i in solid increases with time due to its removal from fluid; thus, solid composition is not at steady state.

pressures, dissolved aqueous silica will be the dominant species in solution. The input fluid has a larger activity of aqueous silica, so as it enters the flow region, silica is consumed as corundum breaks down by reactions such as $\text{SiO}_{2(aq)} + \text{corundum} = \text{kyanite}$. Reaction is removing i (aqueous silica) from the fluid, so the concentration of SiO_2 in the bulk solid continually increases (e.g., Figure 13(b)). The fluid composition, however, is at steady state because the amount of i consumed at any given point is replenished by the amount transported to that point by advection and hydrodynamic dispersion (Figure 13(a)). These relations illustrate that one or more processes in a system may be in steady state, but others need not be. The boundary between the reacted and unreacted regions in the rock is known as a *reaction front* or a *geochemical front*. Eventually, all the corundum at the point of fluid input would be converted to kyanite, and the reaction and solute fronts would then begin to propagate out in the direction of flow (e.g., Figure 14). As a consequence, fossil geochemical fronts can provide valuable clues regarding the direction of fluid flow (e.g., Abart and Pozzorini, 2000; Baker and Spiegelman, 1995; Bickle, 1992; Bickle and Baker, 1990; Rye et al., 1976; Skelton et al., 1995). Note that when both fronts are moving, neither fluid nor rock compositions are steady state. For advection-dominated systems with small porosity ($<\sim 0.01$), the time-integrated fluid flux is approximated by (Ague, 1998)

$$q_{\text{T1}} \approx L_{\text{CF}} \frac{n_i}{C_i^{\text{eq}} - C_{i,x=0}^{\text{input}}} \quad [18]$$

in which L_{CF} is the distance of geochemical front propagation in the rock. For example, $C_{i,x=0}^{\text{input}}$ is the concentration of i (silica)

in the input fluid, whereas n_i is the number of moles of i produced (+) or consumed (-) per unit volume rock (mol m^{-3}). Of course, this highly reduced example neglects many factors, including the speciation of the multicomponent fluid and reaction mechanisms. In many cases, these complexities are not tractable with analytical solutions and require numerical modeling (e.g., Ague, 1998, 2000; Ague and Rye, 1999; Bolton et al., 1999; Cook et al., 1997; Nabelek, 2009).

The shapes of the fronts depend strongly on the reaction rate (Figure 15). If rates are fast, then i is consumed rapidly and the solute front dies away close to the boundary where reactive fluid is input. By contrast, fronts broaden considerably as the rate decreases. Front broadening can occur even if hydrodynamic dispersion is absent and can be significant at >100 m length scales (Bickle, 1992). Dimensionless Damköhler numbers are often used to assess the relative roles of transport and reaction. For the case of advective transport, the Damköhler number is $\kappa L/v_{\text{av}}$ and for transport by diffusion, it is $\kappa L^2/D_{i,f}$ (Boucher and Alves, 1959). In either case, solute and

geochemical fronts sharpen as the Damköhler number increases. If the rate of reaction is very fast (nearly instantaneous) relative to the rate of transport, then fluid and rock are essentially in chemical equilibrium at any given point along the flow path (the local equilibrium condition).

A somewhat different form of the reaction rate term in eqns [11] and [15] has been widely used for modeling transport of tracers, particularly isotopic tracers (e.g., Bickle, 1992; Bickle et al., 1997; Blattner and Lassey, 1989; DePaolo and Getty, 1996; Lassey and Blattner, 1988; Oagata, 1964):

$$\text{Rate} = \kappa \frac{1 - \phi}{\phi} \left(C_i^{\text{Solid}} - \frac{C_i}{K_v} \right) \quad [19]$$

in which K_v is the equilibrium fluid/solid partition coefficient by volume for species i and κ has been interpreted as the rate constant for fluid-rock exchange (Bickle, 1992) or for dissolution and precipitation of mineral material (DePaolo and Getty, 1996). Here, as the bulk composition of the solid changes, so too does the composition of the fluid in equilibrium with the solid. For advective transport, tracer exchange according to eqn [19], and constant porosity and fluid velocity, the time-integrated fluid flux (q_{TI}) is approximated by L_{CF}/K_v (Bickle, 1992). The q_{TI} expression for transport by advection with coupled local fluid-rock equilibrium exchange \pm hydrodynamic dispersion has exactly the same form (e.g., Bickle, 1992; Dipple and Ferry, 1992b). For example, if an oxygen isotopic front has propagated 1000 m and the K_v for oxygen is 0.6, then the q_{TI} estimate is $\sim 1700 \text{ m}^3_{\text{(fluid)}} \text{m}^{-2}_{\text{(rock)}}$. Fronts for tracers with smaller K_v would propagate smaller distances for the same flux, and *vice versa*. Interpretations become more complicated if K_v changes with T or the individual mineral grains become isotopically zoned during reaction (e.g., Abart and Sperber, 1997; Bowman et al., 1994; Ferry et al., 2010; Graham et al., 1998; Lewis et al., 1998). Radioactive decay is not considered in eqn [19] and must be handled with an additional term (DePaolo and Getty, 1996).

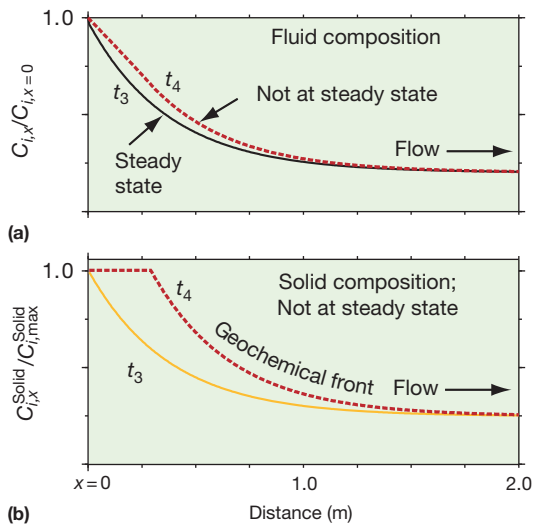


Figure 14 Front propagation for two different model times ($t_3 < t_4$). Time t_3 corresponds to time t_3 in Figure 13. At t_3 , fluid composition (a) is at steady state, but solid composition (b) is not (see Figure 13). At t_4 , both solute and geochemical fronts are propagating, and neither fluid nor rock compositions are in steady-state. See Figure 13 for calculation details.

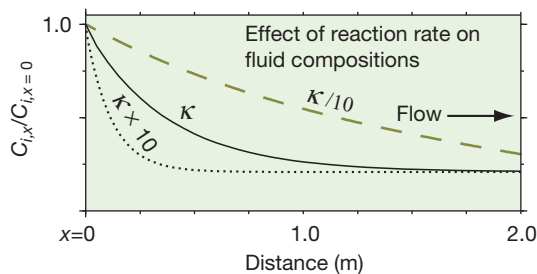


Figure 15 Effect of reaction rate. Solid line computed for reaction rate constant $\kappa = 5 \text{ year}^{-1}$, dotted line for $\kappa = 50 \text{ year}^{-1}$, and dashed line for $\kappa = 0.5 \text{ year}^{-1}$. Note that front sharpens as reaction rate increases. See Figure 13 for calculation details.

4.6.8 Flow and Reaction Along Gradients in Temperature and Pressure

In the examples thus far, fluid that is out of equilibrium with a rock mass of interest infiltrates across some type of lithologic boundary, drives reaction, and forms geochemical fronts. Reaction will also occur if fluid flows along gradients in T and P because fluid compositions coexisting with minerals change as T and P change. A classic example is the precipitation of quartz in fractures to form veins (Ferry and Dipple, 1991; Fyfe et al., 1978; Walther and Orville, 1982; Yardley, 1986). Precipitation occurs because the concentration of aqueous silica coexisting with quartz must decrease as T and P decrease along a flow path (Figure 6(b)). Imagine silica-saturated fluid ascending and cooling through a cubic control volume 1 m on a side. Fluid enters the bottom face of the cube and exits through the top. The concentration of aqueous silica at the inlet is higher than that at the outlet, since quartz is precipitating from the fluid within the control volume. Assume that this drop in concentration is $5 \times 10^{-2} \text{ mol m}^{-3}$ for a typical geothermal gradient (more will be said about this in the

succeeding text). The corresponding concentration gradient ($5 \times 10^{-2} \text{ mol m}^{-3} \text{ m}^{-1}$) is small, so fluxes due to hydrodynamic dispersion can be neglected. The amount of quartz needed to fill the control volume is equivalent to the molar volume of quartz ($\sim 4.4 \times 10^4 \text{ mol m}^{-3}$). The time-integrated fluid flux can then be estimated by reinterpreting eqn [18] slightly:

$$q_{\Pi} \approx (1 \text{ m}) \frac{4.4 \times 10^4 \text{ mol m}^{-3}}{5 \times 10^{-2} \text{ mol m}^{-3}} \approx 9 \times 10^5 \text{ m}^3 \text{ m}^{-2} \quad [20]$$

Ferry and Dipple (1991) derived a more formal one-dimensional, local equilibrium, steady-state expression based on eqn [14] that neglects hydrodynamic dispersion and explicitly accounts for changes in concentration along the flow path due to T and P :

$$q_{\Pi} = \frac{-1/\bar{V}_{\text{Qtz}}}{\left(\frac{\partial C_{\text{SiO}_2, \text{aq}}}{\partial T} \frac{\partial T}{\partial x'} + \frac{\partial C_{\text{SiO}_2, \text{aq}}}{\partial P} \frac{\partial P}{\partial x'} \right)} \quad [21]$$

in which \bar{V}_{Qtz} is the molar volume of quartz and the coordinate direction x' increases in, and is parallel to, the direction of flow. The $\partial C_{\text{SiO}_2, \text{aq}}/\partial T$ and $\partial C_{\text{SiO}_2, \text{aq}}/\partial P$ terms can be calculated using the known solubility of quartz (Figure 6(b)), whereas estimation of $\partial T/\partial x'$ and $\partial P/\partial x'$ requires some knowledge of thermal and baric gradients in the direction of flow. Since quartz solubility varies more strongly with T than with P along typical geotherms (Figure 6(b)), the $\partial C_{\text{SiO}_2, \text{aq}}/\partial T$ term generally dominates $\partial C_{\text{SiO}_2, \text{aq}}/\partial P$. The calculations do not account for kinetic effects. Nonetheless, in quartz-saturated rock sequences at metamorphic temperatures, concentration gradients in kinetically limited systems will still tend to approach local equilibrium gradients, even if the absolute concentration values depart from equilibrium (Ague, 1998). Equation [21] is inadequate, however, for shallow hydrothermal systems with high flow rates at relatively low T (Bolton et al., 1999).

Enormous fluxes on the order of $10^6 \text{ m}^3 \text{ m}^{-2}$ imply that a column of fluid $\sim 1000 \text{ km}$ long flowed across each square meter of vein cross section! A similar flux would be required to dissolve large amounts of quartz out of a rock, but here, the fluid would have to flow in a direction of increasing T ('up- T flow; Feehan and Brandon, 1999; Selverstone et al., 1991). The fluxes are large because changes in aqueous silica concentration along typical crustal geotherms are small. However, concentration gradients could be much steeper if quartz solubility drops due to decreases in water activity (Figure 6(c); Newton and Manning, 2000a; Walther and Orville, 1983). For example, local decreases in water activity due to increased fluid CO_2 content near marbles could dramatically lower quartz solubility and, thus, produce quartz veins with a much lower flux than predicted by eqn [21]. In addition, quartz veins can form by diffusion-dominated processes that require little or no fluid flow (Section 4.6.9.3.1, in the succeeding text).

The advective treatment for quartz veins can be extended to other types of metasomatic reactions. For example, alkali metasomatism is possible if a large amount of fluid flow occurs along gradients in T and P (e.g., Ague, 1994b, 1997a; Dipple and Ferry, 1992a; Orville, 1962). Total concentrations of potassium increase and sodium decrease with increasing T for chlorine-bearing fluids in typical quartzofeldspathic and micaeous rocks (Figure 16; P effects are smaller). Consequently,

up- T fluid flow will tend to destroy micas and/or potassium feldspar so as to remove potassium from the rock and, at the same time, produce a sodium-bearing phase, like plagioclase, and add sodium (*Na metasomatism*). Down- T flow will do the opposite, favoring the growth of potassium-rich phases and destroying sodium-rich ones (*K metasomatism*).

The expression describing the steady-state advection and reaction is similar to eqn [21] (Dipple and Ferry, 1992a):

$$q_{\Pi} = \frac{n_{\text{Na}}}{\left(\frac{\partial C_{\text{Na}, \text{aq}}}{\partial T} \frac{\partial T}{\partial x'} + \frac{\partial C_{\text{Na}, \text{aq}}}{\partial P} \frac{\partial P}{\partial x'} \right)} \quad [22]$$

in which n_{Na} is the total moles of sodium produced (+) or consumed (-) per unit volume of rock. An analogous expression can be written for potassium. As shown in Figure 16, the concentrations of sodium and potassium increase and $\partial C_{\text{Na}, \text{aq}}/\partial T$ changes as the total amount of chlorine in the fluid increases. Thus, chlorine molality must be known in order to evaluate the denominator of the expression. Furthermore, an unaltered starting rock or *protolith* composition is needed so that sodium gains or losses due to alteration can be quantified to provide an estimate for the numerator. These metasomatic gains and losses are evaluated using mass balance methods (e.g., Ague, 1994a; Grant, 1986; Gresens, 1967; Philpotts and Ague, 2009). For typical total chlorine molalities of ~ 1 molal and reasonable estimates for T and P gradients in the direction of flow, the time-integrated fluxes needed to cause alkali metasomatism are $\sim 10^4 \text{ m}^3 \text{ m}^{-2}$ (Ague, 1997a; Dipple and Ferry, 1992a; Ferry and Dipple, 1991). These fluxes are substantially smaller than those required to make quartz veins by advective flow (eqn [20]). Of course, metasomatism involving other elements that are transported effectively in chlorine-bearing fluids, including calcium, magnesium, and iron, can also be treated using eqn [22]. Metal leaching due to reaction with H^+ or HCl^{\ominus} (*hydrogen metasomatism*) is generally possible only if fluxes are well in excess of $10^4 \text{ m}^3 \text{ m}^{-2}$ due to the small concentrations of hydrogen species in typical fluids (e.g., $\text{HCl}^{\ominus} + \text{albite} = 0.5 \text{ kyanite} + 2.5 \text{ quartz} + \text{NaCl}^{\ominus} + 0.5\text{H}_2\text{O}$; see Ague, 1994b; Yardley, 1986).

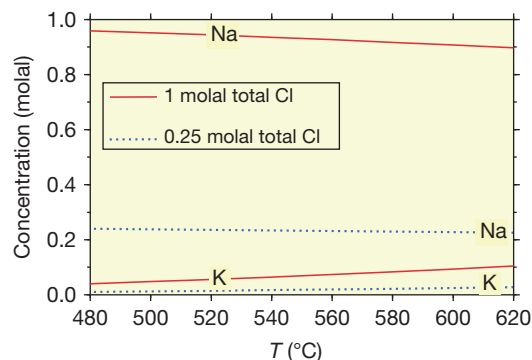


Figure 16 Total concentrations of sodium and potassium species in aqueous solution coexisting with quartz, albite, muscovite, and kyanite for total chlorine concentrations of 1 molal (solid lines) and 0.25 molal (dotted lines). Computed following Ague (1997a) along a geothermal gradient of $20^{\circ}\text{C km}^{-1}$. Note that total concentration of sodium decreases with increasing temperature, whereas the concentration of potassium increases. These trends become more pronounced as the total chlorine concentration in the fluid increases.

Reactions involving H₂O–CO₂ fluids in metacarbonate rocks (*mixed volatile reactions*) are invaluable for assessing fluid fluxes and mass transfer processes. Common prograde reactions release CO₂, so fluids in closed or nearly closed systems should get richer in CO₂ during heating (Greenwood, 1975). In many metasedimentary sequences, however, reactions proceeded at relatively low X_{CO_2} , implying that H₂O was also being added to the rocks (e.g., New England, United States; see Ague, 2002; Baumgartner and Ferry, 1991; Ferry, 1992, 1994a, 1994b; Hewitt, 1973). Input of external H₂O-bearing fluids, such as those derived from dehydrating schists or degassing magmas, can drive many prograde reactions (Figure 17(a); Ague and Rye, 1999; Hewitt, 1973). This type of infiltration has been treated quantitatively for advection-dominated systems (e.g., Ague and Rye, 1999; Dipple and Ferry, 1992b; Evans and Bickle, 1999; Ferry, 1996) and for systems in which hydrodynamic dispersion is important (Ague, 2000, 2002; Ague and Rye, 1999).

Prograde reaction and CO₂ release can also occur, however, if fluids flow along gradients in T and P , as pointed out by Baumgartner and Ferry (1991). For a simple H₂O–CO₂ fluid, the analog of eqns [21] and [22] for mixed volatile reactions can be written as (Baumgartner and Ferry, 1991; Ferry, 1992, 1994a,b; Léger and Ferry, 1993)

$$q_{\text{fl}} = \frac{\bar{V}_f (n_i - X_i (n_{\text{CO}_2} + n_{\text{H}_2\text{O}}))}{\left(\frac{\partial X_i}{\partial T} \frac{\partial T}{\partial x'} + \frac{\partial X_i}{\partial P} \frac{\partial P}{\partial x'} \right)} \quad [23]$$

in which \bar{V}_f is the molar volume of the fluid, i is either CO₂ or H₂O, and n_i is the total moles of i produced (+) or consumed (–) per unit volume rock. The expression can be evaluated given the estimates for P , T , fluid composition, total volatile production/consumption, and gradients in T and P along the flow path. Volatile production/consumption is typically quantified using reaction progress methods (Brimhall, 1979; Ferry, 1983). For many common reactions proceeding under water-rich conditions, eqn [23] requires that prograde reaction and CO₂ release be driven by up- T fluid flow (Baumgartner and

Ferry, 1991). For this case, fluid should become progressively more CO₂-rich along regional up- T flow paths; down- T fluid flow, by contrast, would tend to drive retrogression and remove CO₂ from the fluid (Figure 17(b)). Fluid salt content will also influence reaction progress along flow paths (e.g., Ferry and Gottschalk, 2009; Heinrich et al., 2004).

4.6.9 Examples of Mass and Heat Transfer

Bickle and McKenzie (1987) identified three broad crustal mass and heat transport regimes. In the first, fluid flow is limited, and chemical transport by diffusion and heat transport by conduction prevail. In the second, fluid fluxes are large enough so that advection of mass by fluid flow dominates diffusive transport. However, because conduction is relatively efficient, heat conduction through the rock still dominates heat advection by the fluid. Many deep-crustal systems are inferred to have formed in this regime (e.g., Manning and Ingebritsen, 1999). In the third regime, fluxes are very large, and both chemical and heat transport are predominantly by fluid flow. In addition to these three categories, hybrid modes of transport are possible. For example, regional-scale fluid flow along fractures can be coupled to local-scale diffusion to and from the wall rock adjacent to the fractures. The mass and heat transfer literature is vast and cannot be reviewed fully here; thus, the following sections explore some selected examples that illustrate a representative spectrum of processes.

4.6.9.1 Regional Devolatilization and Directions of Fluid Motion

4.6.9.1.1 Shallow crustal levels

The processes of metamorphic volatile release and the directions of fluid motion are basic questions in deep-crustal petrology (Figure 18). Recirculation of fluid by convection

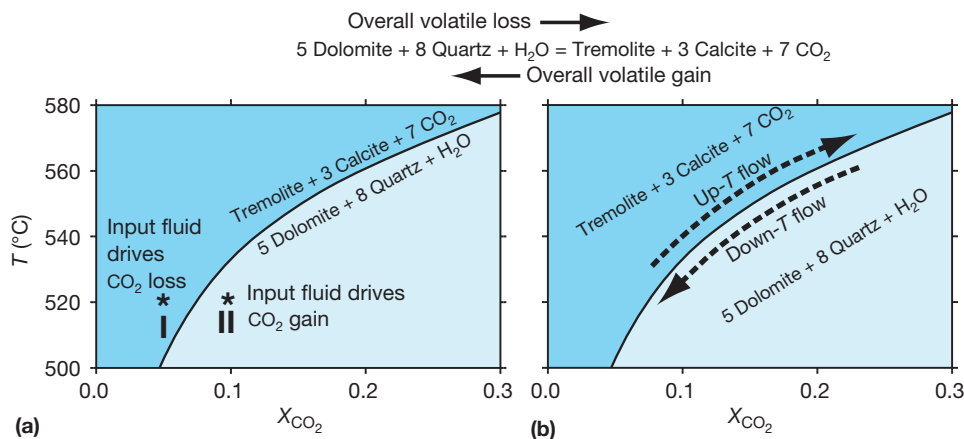


Figure 17 Two ways to drive CO₂ loss or gain for a common mineral assemblage in metacarbonate rocks (0.7 GPa). (a) Fluid composition I is more water-rich than the equilibrium fluid composition (solid line) at 520 °C and is in the stability field of the reaction products tremolite and calcite. Input of this fluid into a metacarbonate layer would thus drive prograde reaction and CO₂ loss. Input of fluid II would drive retrograde CO₂ gain. Fluid could be input by, for example, direct flow through a metacarbonate layer or diffusion/mechanical dispersion across lithologic contacts or vein margins. (b) Fluid flowing in a direction of increasing temperature (up- T flow) at or near local equilibrium with the assemblage dolomite + quartz + tremolite + calcite must get progressively richer in CO₂; it does so by driving prograde reaction and CO₂ release from the rock. Down- T flow would drive retrograde CO₂ gain. Computed following Ague (2000b).

(*multipass* flow; e.g., Etheridge et al., 1983) is widely recognized in shallow hydrothermal systems (Norton and Taylor, 1979). However, the conventional wisdom is that permeability is too small at deeper levels to allow the downward penetration of fluid necessary for convection (e.g., England and Thompson, 1984; Hanson, 1997; Manning and Ingebritsen, 1999; Walther and Orville, 1982). Nonetheless, studies of active mountain belts in New Zealand and Pakistan have shown that shallow fluids can penetrate to at least midcrustal levels near the brittle-ductile transition (e.g., Koons and Craw, 1991; Poage et al., 2000; Templeton et al., 1998). For example, fluid inclusion and stable isotopic systematics in Nanga Parbat, Pakistan, led Poage et al. (2000) to conclude that meteoric fluids penetrate downward to depths of ~10 km, where they mix with CO₂-rich fluids of metamorphic origin in the rapidly uplifting core of the mountain belt. Overall fluid fluxes, however, are inferred to be small, except in fault zones. Wickham and Taylor (1990) concluded that massive penetration of marine fluid to depths of at least 10–12 km resulted in widespread homogenization of stable isotope ratios in the Hercynian basement of the Pyrenees. Convection is also one possible explanation for midcrustal thermal anomalies preserved within the rock record in New Hampshire (Chamberlain and Rumble, 1989; Section 4.6.9.6).

The Mt. Isa Inlier, north Queensland, Australia, contains some of the largest metasomatic provinces exposed on the planet. Here, a complex and long-lived Paleo- to Mesoproterozoic metamorphic and fluid flow history produced widespread scapolitization, albitization (Na–Ca metasomatism), and ore deposition (e.g., Oliver et al., 1990, 2008; Rubenach, 2005; Rubenach and Lewthwaite, 2002). Although mass transfer affected the rock mass regionally at length scales on the order of 10–100 km, much of the most intense metasomatic activity occurred in and around shear zones, fractures, boudins, and breccia zones. Magmatic fluids, regional devolatilization, inflow from shallower crustal levels, and high-Cl, high-S fluids sourced from metamorphosed evaporite-bearing dolomitic rocks were all likely important at various times in the region's evolution.

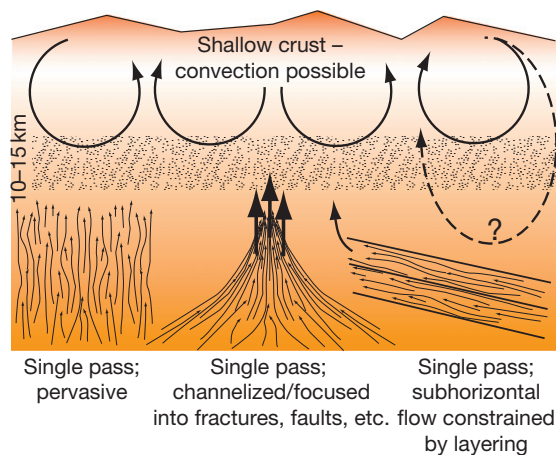


Figure 18 Schematic cross section through the crust illustrating some possible modes of regional fluid flow. Contains some elements modified from Figure 9 in Etheridge MA, Wall VJ, and Vernon RH (1983) The role of the fluid phase during regional metamorphism and deformation. *Journal of Metamorphic Geology* 1: 205–226.

The Mt. Isa rocks underwent fluid–rock reactions in the upper crust (<~0.4 GPa), considerably shallower than most of the other examples discussed in this chapter. Hydrologic processes at these levels likely differ considerably from those in the deeper crust. For example, Oliver et al. (1990) posit that dilatancy (or seismic) pumping during deformation was able to circulate fluids repeatedly through the Mary Kathleen Fold Belt at crustal levels around the hydrostatic–lithostatic fluid pressure transition (see Cox and Etheridge, 1989; Sibson et al., 1975). In this scenario, fractures and other kinds of pore space are created by rising tectonic shear stresses in zones of active deformation, producing low-pressure zones into which fluid flows. Under appropriate circumstances, this process can drive flow downward or sideways. The fluid inflow causes fluid pressures to rise, weakening the rock, and ultimately leading to failure (in many cases seismogenic). Collapse of pore space following deformation then drives fluid rapidly upward. In this way, circulation takes place and large fluid fluxes are generated due to repeated deformational–fluid flow cycles. The absence of Mt. Isa-type regional metasomatism in deeper rocks is important evidence that this kind of fluid circulation is probably limited to upper-crustal metamorphic environments.

4.6.9.1.2 Deeper levels

Fluid fluxes and flow directions at deeper-crustal levels continue to be the focus of vigorous research. The *single pass* flow model holds that fluids generated during devolatilization move upward toward the surface (e.g., Walther and Orville, 1982). Modeling of simple systems, such as fluid flow during thermal relaxation and exhumation of tectonically thickened crust, indicates a strong upward component of flow (Figure 19). Substantial prograde devolatilization occurs in the lower thrust plate; these upward-migrating fluids can produce retrogression in the base of the upper plate, which undergoes a period of cooling after thrust emplacement. The simple models shown in Figure 19 do not include the important effects of compaction (Connolly, 1997, 2010). In general, compaction will tend to reinforce the upward component of flow. Notably, large-scale convective circulation is not predicted at middle and lower crustal levels. In the simple model shown, this is due largely to the fact that devolatilization increases fluid pressures, driving fluid upward and out of the system. Moreover, when retrograde hydration in the base of the upper plate occurs, it can act to *pull* fluid upward. Downward motion associated with topographically driven flow is predicted at shallow crustal levels where permeability is higher (Figure 19(b); Garven and Freeze, 1984a, 1984b). Small downward fluxes at shallower levels may also be caused by retrograde hydration that draws fluid downward (Lyubetskaya and Ague, 2009) and may help explain the downward flow observed in the crystalline basement in Central Europe (Stober and Bucher, 2004) and the Transcaucasus region (Yakovlev, 1993).

Of course, flow can also have significant nonvertical components, particularly in the presence of permeability anisotropy, barriers to flow, conduits for flow, fluid sinks, and other heterogeneities (cf. Connolly, 2010; Hanson, 1997; Lyubetskaya and Ague, 2009). For example, permeability anisotropy due to layering and foliations can be considerable. Fluids can be constrained to follow flat-lying flow paths if layering is subhorizontal, given

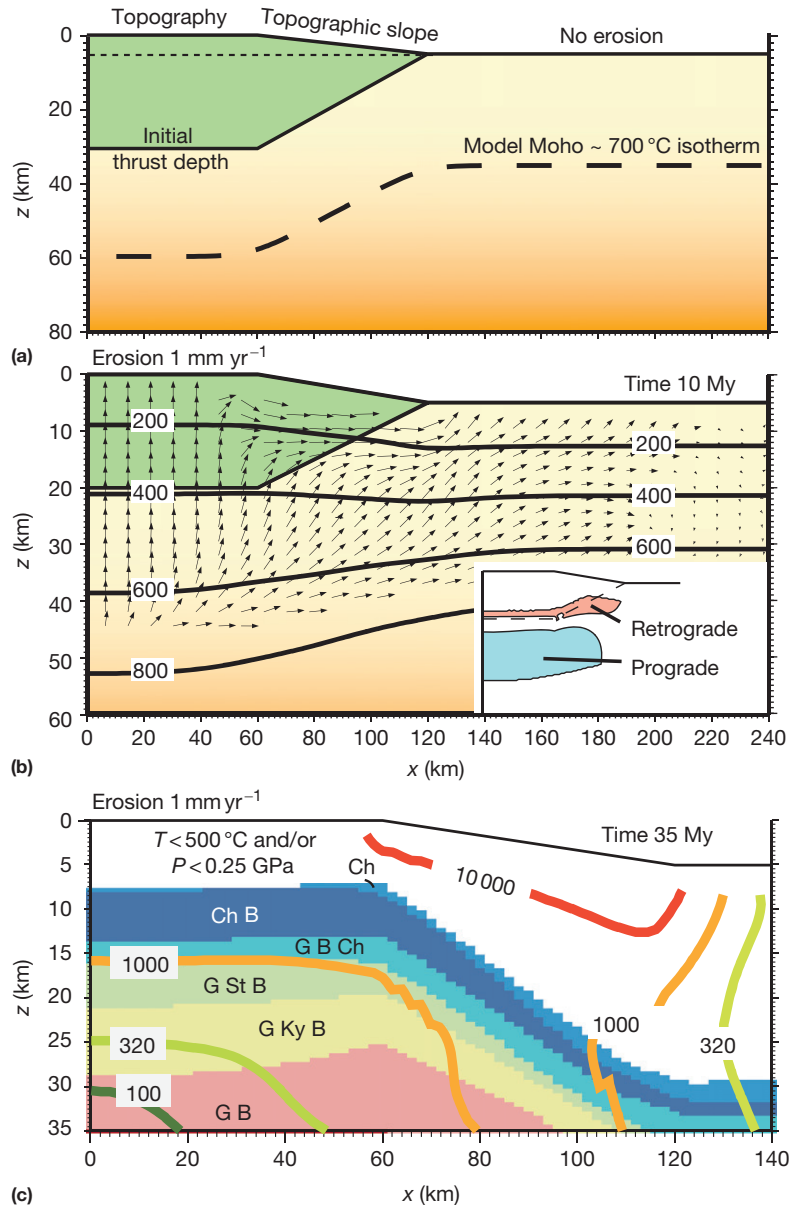


Figure 19 Two-dimensional fluid and heat flow in a model collisional orogen comprising metapelitic crust. (a) Model geometry. Upper thrust plate shown in green. Steady-state topography preserved during erosion of upper plate; no erosion past $x = 120$ km. (b) Fluid flow vectors and 200–800 °C isotherms after 10 Ma of model time, erosion rate = 1 mm year^{-1} . Inset shows major areas of retrograde hydration and prograde dehydration. Arrow lengths scaled to flux magnitudes. Modified from Lyubetskaya T and Ague JJ (2009) Modeling the magnitudes and directions of regional metamorphic fluid flow in collisional orogens. *Journal of Petrology* 50: 1505–1531. (c) Close-up of peak (maximum) temperature mineral assemblages and time-integrated fluid flux contours in $\text{m}^3 \text{ m}^{-2}$ after 35 Ma of exhumation. G, garnet; B, biotite; Ch, chlorite; St, staurolite; Ky, kyanite; all mineral assemblages coexist with quartz, muscovite, and water. Model geometry differs slightly from part (a): initial thrust depth is 35 km, and initial Moho depth at $x = 0$ is 75 km. Modified from Lyubetskaya T and Ague JJ (2010) Modeling metamorphism in collisional orogens intruded by magmas: II. Fluid flow and implications for Barrovian and Buchan metamorphism, Scotland. *American Journal of Science* 310: 459–491. With permission from Yale University.

that permeability can be an order of magnitude or more greater parallel to layering than perpendicular to it (Figures 5 and 18; Ingebritsen and Manning, 1999). Moreover, barriers to flow, such as low-permeability metamorphic aquicludes (Ferry, 1987), can divert upward-migrating fluids horizontally at regional scales (Lyubetskaya and Ague, 2009). Although regional deep-crustal convection seems unlikely given the present knowledge, it has been postulated that smaller-scale, local

convection could develop (e.g., Etheridge et al., 1983, 1984; Yardley, 1986). Wing and Ferry (2002, 2007) used a method akin to those developed for tracing ocean circulation patterns (Lee and Veronis, 1989) to estimate regional time-integrated fluid fluxes and flow directions based on a three-dimensional inversion of reaction progress, $\delta^{18}\text{O}$, and $\delta^{13}\text{C}$ data for metamorphic rocks in Vermont, United States. Their results suggest that the fluid flow was highly complex locally and included

both upward and downward regimes. On the regional scale, however, flow was dominantly upward and parallel to regional lithologic layering.

A fundamental question regarding flow directions is whether they are in a direction of increasing temperature (up T) or decreasing temperature (down T). This distinction is important because the two flow regimes produce considerably different chemical and isotopic shifts in rocks (Section 4.6.8). For example, up- T flow can drive decarbonation reactions, produce sodic-calcic metasomatism, dissolve silica, and decrease rock $\delta^{18}\text{O}$. Down- T flow will promote carbonation, potassic metasomatism, silica precipitation, and increases in $\delta^{18}\text{O}$. In the absence of magmatism, upward flow will generally be down T (Figure 19(b)). Subhorizontal flow could potentially be either down T or up T , depending on regional thermal structure. However, numerical models indicate that, while subhorizontal flow is expected in the presence of appropriate permeability heterogeneities, it will generally be down T during prograde heating. Fluid production during devolatilization will act to increase fluid pressures. Consequently, as devolatilization proceeds in the hotter cores of orogens, it is unlikely that large fluxes of cooler fluids will flow sideways and up T into these regions of fluid production (Hanson, 1997; Lyubetskaya and Ague, 2009).

It is still possible, however, that large up- T fluxes may develop at regional scales. Magmas that are emplaced at mid- to deep-crustal levels can produce long-lived inverted geotherms. If devolatilization fluids generated deeper in the metamorphic pile flow upward into these perturbed thermal zones, then they will move up T beneath (and on the flanks of) the intrusions (Lyubetskaya and Ague, 2010). Another possible up- T flow scenario is if protracted underthrusting gives rise to long-lived inverted geotherms at the base of the overthrust plate or top of the underthrust plate. Deeply generated fluids would then flow upward and up T into the thrust zone (e.g., Selverstone et al., 1991). Clearly, much field, experimental,

and modeling work lies ahead to determine fluid flow directions in the deep crust.

4.6.9.2 Regional Fluid Fluxes

Middle- and lower-crustal fluid fluxes likely vary by several orders of magnitude in natural geologic environments. Time-integrated fluid fluxes for simple *single pass* flow constrained by the thickness of the metamorphic pile undergoing devolatilization are straightforward to quantify. Consider a crustal control volume having a uniform cross-sectional area = 1 m^2 , length = L_c , and constant, fluid-filled porosity. The mass of fluid produced by devolatilization per unit initial volume of rock (f_{mv}) is

$$f_{mv} = f_m \rho_s (1 - \phi) \quad [24]$$

in which ρ_s is the density of the solid (not including porosity) and f_m is the mass of fluid released per unit initial mass solid. If all the fluid produced flows unidirectionally out of the top of the column and if small volume changes due to devolatilization reactions are ignored, then the time-integrated fluid flux across the top surface of the column is

$$q_{\text{fl}} = \frac{f_{mv} L_c}{\rho_f} \quad [25]$$

in which ρ_f is the density of the fluid exiting the column. For example, a metasedimentary pile (or degassing magma) loses 2.25 wt% water ($f_m \sim 0.025$), and the densities of fluid and solid are 950 and 2800 kg m^{-3} , respectively. Taking a representative crustal-scale column 15 km long having $\phi = 0.001$, then q_{fl} is $\sim 1000 \text{ m}^3 \text{ m}^{-2}$ (Figure 20). These calculations are insensitive to reasonable variations in porosity. It is worth emphasizing that this large q_{fl} value means that a column of fluid 1 km long passes over each meter square of rock area at the top of the column, sufficient to displace an oxygen isotope front some 600 m (Section 4.6.7). Even the loss of just 1 wt%

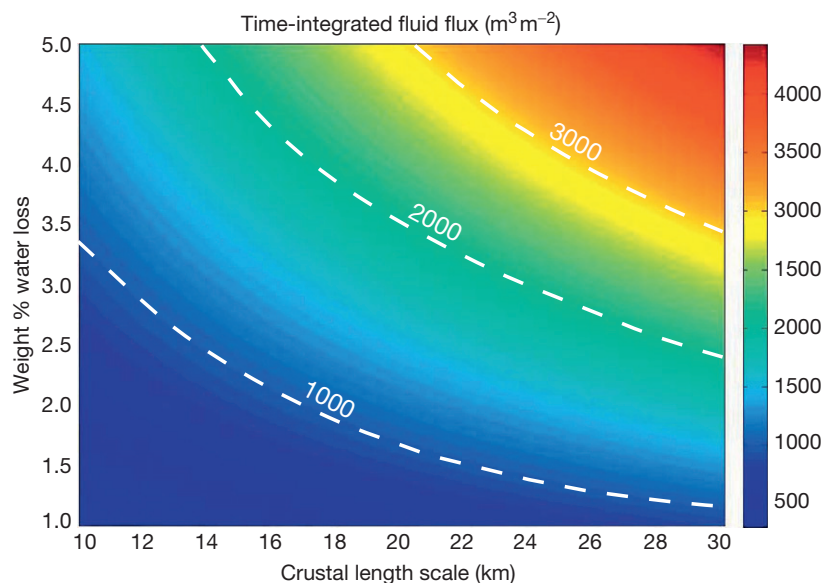


Figure 20 Time-integrated fluid fluxes calculated for top of vertical, dewatering crustal column. Crustal length scale on x -axis corresponds to L_c in eqn [25] and is the length of the dewatering column. The amount of water lost by the column is given on the y -axis. Processes that could generate larger fluxes include channelization and recirculation (see Figure 21).

water from a 10 km long column produces nearly $300 \text{ m}^3 \text{ m}^{-2}$; longer columns and larger amounts of devolatilization generate correspondingly larger fluxes (Figure 20). Small regional fluxes less than $\sim 100 \text{ m}^3 \text{ m}^{-2}$ would be expected only if the rocks involved in orogenesis were already *dry* to begin with (e.g., high-grade gneisses or metaigneous rocks).

These simple calculations lead to the inescapable conclusion that considerable fluid fluxes will accompany regional devolatilization in orogenic belts. Pervasive fluxes on the order of $500\text{--}1000 \text{ m}^3 \text{ m}^{-2}$ are clearly consistent with the range of estimates from natural settings shown in Figure 21. For example, carbonate-bearing metasedimentary rocks in the Acadian orogen of New England, United States, preserve a valuable record of fluid–rock interaction (Baumgartner and Ferry, 1991, Ferry, 1992, 1994a, 1994b; Léger and Ferry, 1993; Wing and Ferry, 2002, 2007). Estimated time-integrated fluid fluxes in the Waits River Formation, Vermont, increase from $\sim 10^2 \text{ m}^3 \text{ m}^{-2}$ in the greenschist facies to $\sim 7 \times 10^3 \text{ m}^3 \text{ m}^{-2}$ in the amphibolite facies (Figure 21), consistent with the ranges calculated in Figures 3 and 20. Fluid fluxes were sufficient to produce C and O isotopic shifts and variable degrees of alkali metasomatism.

This regional flow was part of a complex hydrologic system in which the prograde release of CO_2 and H_2O was critically dependent on local fluid–rock interactions between intercalated metacarbonate, metapelite, and metasandstone layers. As discussed earlier, infiltration of fluid with lower X_{CO_2} than the equilibrium value for a given rock can drive reaction (Figure 17(a)). For example, H_2O derived from dehydrating metapelites that infiltrates into metacarbonate layers across lithologic contacts or vein margins (selvages) by hydrodynamic dispersion (Ague, 2000; Ague and Rye, 1999; Hewitt, 1973) or by advection (Ague and Rye, 1999; Evans and Bickle, 1999) can drive substantial prograde CO_2 loss (Figure 17(a)). In this way, prograde dehydration and decarbonation are coupled. Field tests show that length scales for hydrodynamic dispersion transport across layers range from the decimeter scale to tens of meters (Ague, 2003; Bickle et al., 1997; Ferry, 2008; Penniston-Dorland and Ferry, 2006). Degassing magmas are another significant source of H_2O that can, at least in part, account for water-rich diopside zone conditions that drove prograde CO_2 loss (Figure 17(a); Ague, 2002; Ague and Rye, 1999; Léger and Ferry, 1993; Palin, 1992; Wing and Ferry, 2007).

Fluid fluxes will likely vary widely across metamorphic belts, even within the same facies or index mineral zone. Modeling predicts that time-integrated fluxes will tend to be higher through rocks in the upper parts of metamorphic sequences, as they overlie longer integrated length scales of devolatilization (Figure 19(c)). Large fluxes are predicted to develop at deeper levels as well, depending on many geologic factors, including regional thermal structure, extent of devolatilization, and flow focusing. For example, Figure 19(c) predicts that time-integrated fluid fluxes could vary from a few $100 \text{ m}^3 \text{ m}^{-2}$ to well over $1000 \text{ m}^3 \text{ m}^{-2}$, all within the kyanite zone of regional metamorphism. The most vigorous circulation in Figure 19 is generated by the topographically driven flow of surficial fluids in the higher-permeability, shallower parts of the crust ($< \sim 10\text{--}15 \text{ km}$), producing time-integrated fluxes of $\sim 10^4 \text{ m}^3 \text{ m}^{-2}$. Within this region, shallow fluids will

mix with deeper metamorphic *basement* fluids produced by devolatilization; this mixing may have important consequences for ore deposition. These results are, of course, specific to the model's initial and boundary conditions but still illustrate general levels of variability to be expected in collisional orogens.

4.6.9.3 Channelized Flow

Regional time-integrated fluid fluxes of $\sim 10^2\text{--}10^3 \text{ m}^3 \text{ m}^{-2}$ should be commonplace during crustal-scale devolatilization. Furthermore, a survey of the literature shows that structural features that focus flow, including veins, fold hinges, permeable layers, and ductile shear zones, may transfer significantly greater fluxes of fluid, ranging from $\sim 10^4 \text{ m}^3 \text{ m}^{-2}$ to in excess of $10^5 \text{ m}^3 \text{ m}^{-2}$ (Figure 21). These fluxes are large enough to cause significant isotopic shifts and mass transfer of rock-forming elements. If the focused flow conduits deprive other areas of the rock mass of fluid, then regionally averaged fluxes could, of course, be less than $\sim 10^4 \text{ m}^3 \text{ m}^{-2}$.

4.6.9.3.1 Fractures, veins, and shear zones

Rock failure caused by, for example, hydrofracture or tectonic stress, will create fractures that increase rock permeability (eqn [4]) and focus flow. Veins (mineralized fractures) can be present at all levels of the crust and in the high-pressure and ultrahigh-pressure rocks of subduction zones (see succeeding text). They are unambiguous indicators of mass transfer. The nature and scale of mass transfer, however, vary strongly, depending on the vein-forming process. Vein minerals may be precipitated from large-scale fluid flow through regional fracture systems, local diffusion of mass to (and from) fractures through an essentially stagnant pore fluid, and local-scale fluid flow from wall rocks to fractures (e.g., Ague, 1994b, 1997b; Ferry and Dipple, 1991; Fisher and Brantley, 1992; Oliver and Bons, 2001; Oliver et al., 1990; Walther and Orville, 1982; Whitney et al., 1996; Widmer and Thompson, 2001; Yardley, 1975, 1986; Yardley and Bottrell, 1992). The fluid fluxes required to precipitate veins by regional flow are large, but local formation by diffusional mass transfer may occur with little or no flow (Figure 22). Consequently, vein formation mechanisms must be assessed before any conclusions about fluid fluxes can be drawn.

Veins can make up a significant portion of outcrops. For example, in the chlorite through staurolite Barrovian zones north of Stonehaven, Scotland, veins occupy $\sim 1\text{--}18 \text{ vol}\%$ of the rock mass; $5\text{--}15\%$ is typical (Masters and Ague, 2005). The lowest values are measured in quartzofeldspathic layers, the highest in metapelitic ones. Significant fracturing and veining also occurred during Barrovian-style metamorphism of the Wepawaug Schist, Connecticut. Historically, it is interesting to note that these were probably the first metamorphic veins to be described in a North American scientific publication (Silliman, 1820). Here, vein abundance increases from a few $\text{vol}\%$ in the chlorite zone to $20\text{--}30\%$ in the amphibolite facies (Ague, 1994b). In their study of veining in metapelitic rocks of the Waits River Formation, Vermont, Penniston-Dorland and Ferry (2008) measured 4.5% veins in a chlorite zone outcrop and over 12% in a kyanite zone outcrop. In the Ottago Schist,

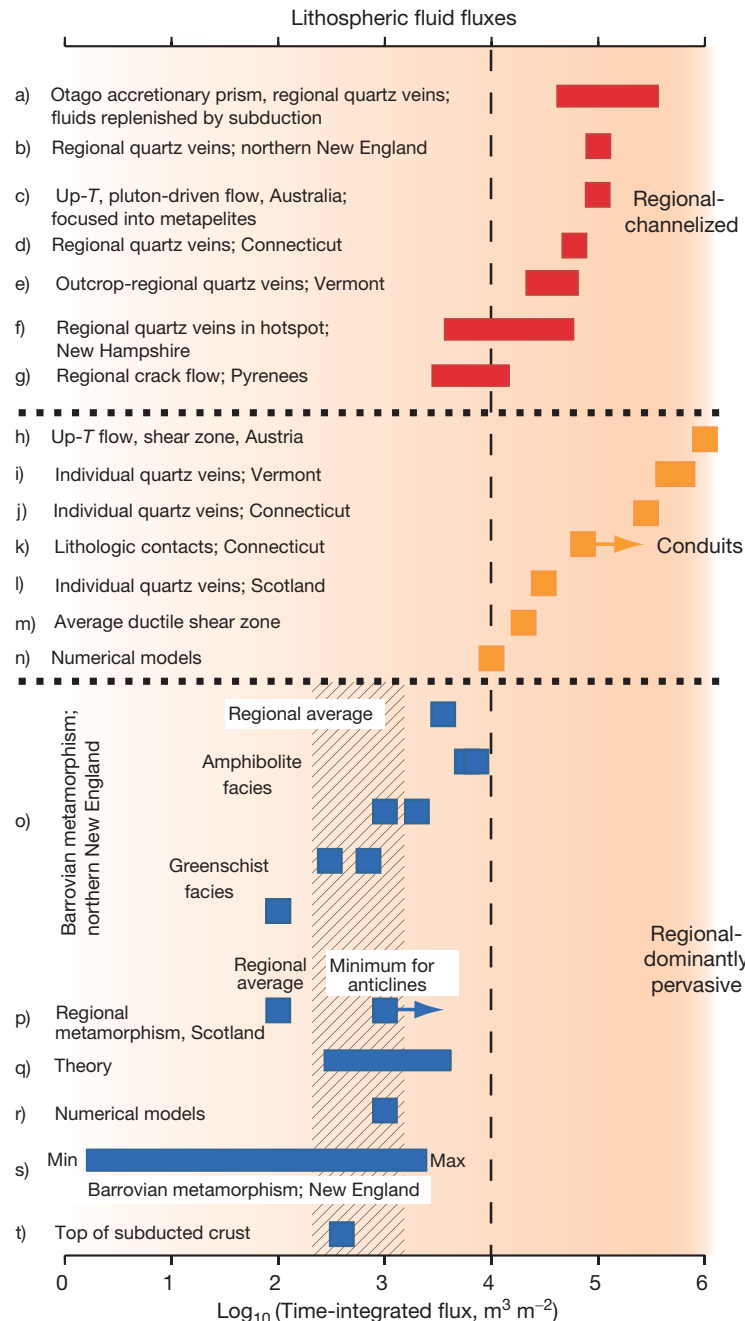


Figure 21 Selection of time-integrated fluid fluxes from the literature. The average regional, pervasive flow-dominated flux of $10^{2.7 \pm 0.5} \text{ m}^3_{(\text{fluid})} \text{ m}^{-2}_{(\text{rock})}$ (2σ) denoted with diagonal ruled bar (computed using geometric mean). Data sources as follows: (a) Breeding and Ague (2002); (b) Ferry (1992); (c) Ague (1994b); (d) Oliver et al. (1998); (e) Penniston-Dorland and Ferry (2008); (f) Chamberlain and Rumble (1989). Range computed using average flux of $1.5 \times 10^3 \text{ m}^3 \text{ m}^{-2} \text{ s}^{-1}$ for 10^5 and 10^6 years. (g) Bickle (1992); (h) Selverstone et al. (1991); (i) Penniston-Dorland and Ferry (2008); (j) Ague (1994b); (k) Ague (2003); (l) Ague (1997a); (m) Dipple and Ferry (1992a); (n) Lyubetskaya and Ague (2009); (o) Ferry (1992), Léger and Ferry (1993), and Wing and Ferry (2007); (p) Skelton et al. (1995); (q) Walther and Orville (1982) and Walther (1990). Range computed using total timescales of fluid flow of 10^6 and 10^7 years. (r) Hanson (1997) and Lyubetskaya and Ague (2009); (s) Evans and Bickle (1999); (t) Schmidt and Poli (see Chapter 4.19).

New Zealand, vein proportions increase from a few percent or less in the lowest-grade rocks to as much as 30% in the greenschist facies rocks (Breeding and Ague, 2002).

The source of vein mass is critical to evaluate in order to assess fluid fluxes, but relatively few studies have quantified the proportions of internally and externally derived vein mass.

Those that do commonly conclude that a significant proportion of the vein mass was externally derived and was precipitated from through-going fluids. For example, in the Wepawaug Schist, thin section, outcrop-scale, and regional-scale analyses indicate that $\sim 30\%$ of the mass in the average amphibolite facies quartz vein was externally derived; in some cases, the proportion

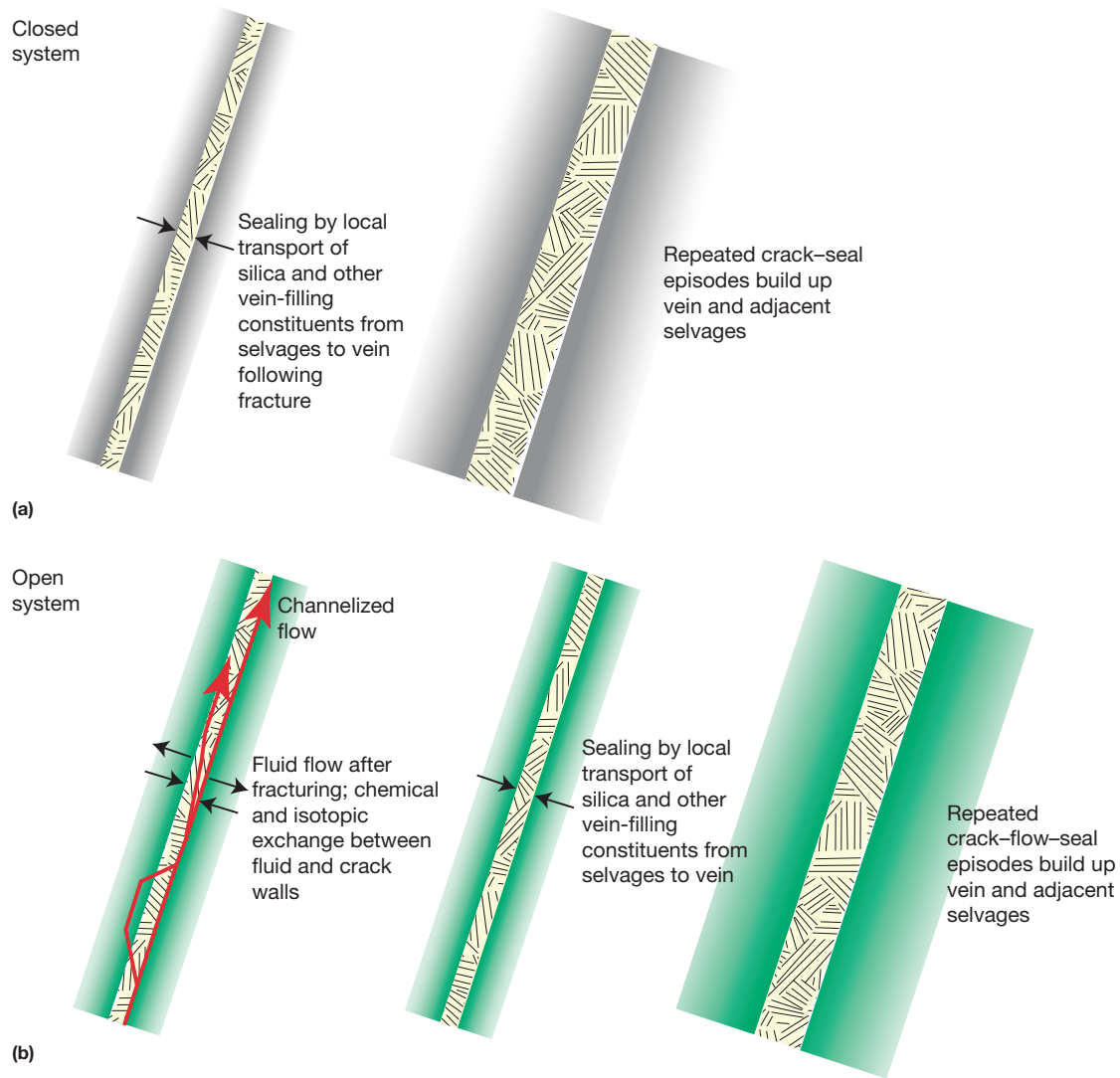


Figure 22 Cartoons illustrating some possible closed- and open-system vein-forming processes. (a) Closed-system vein formation. After fracturing, silica and other vein-forming constituents (e.g., CaCO_3) diffuse through a more or less static pore fluid to the fracture and precipitate. Repeated crack-seal events enlarge veins; adjacent selvages (gray shading) are depleted in vein-forming constituents. (b) Illustration of open-system *crack flow seal model* of vein formation derived for Wepawaug Schist, Connecticut, United States (modified from Ague JJ (1997) Compositional variations in metamorphosed sediments of the Littleton Formation, New Hampshire (Discussion). *American Journal of Science* 297: 440–449). In this scenario, fracturing increases permeability and facilitates channelized flow and chemical and isotopic reaction between infiltrating fluids and selvage zones adjacent to cracks (green shading). Sealing by local mass transfer depletes selvages in vein-forming constituents, like silica. Repeated crack-flow-seal episodes enlarge the veins and selvages.

is as high as $\sim 60\%$ (Ague, 1994b, 2011). The remainder was derived from silica-depleted selvage zones adjacent to the veins. Penniston-Dorland and Ferry (2008) found even larger proportions; their estimates for externally derived vein mass exceed 90%. If quartz precipitation occurred largely in response to decreases in pressure and temperature along regional flow paths, which seems likely, then the necessary time-integrated fluid fluxes are enormous (eqn [21]; e.g., Yardley, 1986; Walther, 1990; Ferry and Dipple, 1991). Estimated q_{H} values are $\sim 2.8 \times 10^5 \text{ m}^3 \text{ m}^{-2}$ for the average amphibolite facies vein in the Wepawaug (Ague, 1994b) and $4\text{--}9 \times 10^5 \text{ m}^3 \text{ m}^{-2}$ for the Waits River Formation veins (Penniston-Dorland and Ferry, 2008). Geochemical interactions between infiltrating fluids and adjacent wall rocks were

facilitated by diffusion with some contributions from advection, producing chemically and isotopically altered vein selvages (Figure 22(b)).

The presence of both internally and externally derived vein mass gives valuable clues regarding processes of vein formation. In the crack-seal vein formation model of Ramsay (1980), cracks open during deformation and then are sealed by mineral precipitation. The process is repeated many times to build up typical veins. Fluid inclusion evidence suggests that the initial fluid pressure drop upon fracturing can be as great as $\sim 0.1 \text{ GPa}$ in accretionary prism settings (Vrolijk, 1987); such large drops are likely to be highly transient and short-lived (Fisher and Brantley, 1992). For quartz veins that contain

both internally and externally derived mass, it is likely that deformation created fractures that were zones of elevated permeability and that channelized fluid flow. Some precipitation of silica (or other vein-forming constituents) occurred as the fluids flowed down P and T gradients in the fractures. This flow was accompanied and/or followed by fracture sealing due to local diffusional transport of silica from wall rocks to fractures, producing altered, silica-depleted selvages marginal to the veins. The chemical potential gradients necessary to drive diffusion could have arisen due to gradients in a number of variables, including strain energy, surface free energy, and fluid pressure (e.g., Elias and Hajash, 1992; Fisher and Brantley, 1992; Yardley, 1975). This *crack flow seal* process would be repeated many times to build up large quartz veins (Figure 22(b)). Crack-seal textures (Ramsay, 1980) are commonly preserved and attest to multiple episodes of fracture opening and healing (see Oliver and Bons, 2001; and references therein).

Not all veins are regional flow conduits (Figure 22(a)); some may represent essentially closed-system fracture infillings developed during deformation (e.g., Henry et al., 1996; Ramsay, 1980; Verlaquet et al., 2011; Yardley and Bottrell, 1992). In such cases, all vein mass must be derived from the local wall rocks. Nonetheless, to the author's knowledge, very few studies attempt to demonstrate this quantitatively using mass balance, even though some (e.g., Verlaquet et al., 2011) assume a closed-system behavior except for H_2O . Isotopic studies are, however, more numerous. For example, Yardley and Bottrell (1992) found that oxygen isotope ratios for quartz in veins and their enclosing wall rocks in the Connemara Schists (Ireland) were essentially identical, suggesting limited fluid-rock interaction and local derivation of vein mass.

An ambiguity, however, is that infiltrating fluids may have altered the isotopic ratios of wall rock quartz to the point that they were indistinguishable from the veins. This problem can be addressed by a study of isotopic zonation within refractory minerals, such as garnet (e.g., Page et al., 2010). If such crystals grow during infiltration, then they can provide an invaluable record of the isotopic evolution of the fluid, even when other minerals have largely equilibrated with vein fluids (see Chapter 4.7). For example, van Haren et al. (1996) found that garnet rims were as much as $\sim 2\%$ heavier than garnet cores in an alteration selvage adjacent to an amphibolite facies vein cutting metapelite. They concluded that the garnets record progressive increases in the $\delta^{18}O$ of the selvage resulting from isotopic exchange between the wall rock and large fluxes of regional devolatilization fluids that ascended through fractures (down- T flow will tend to partition the heavy oxygen into the rock). Garnets outside the selvages contain significantly less zonation, indicating smaller degrees of fluid-rock reaction away from the veins (e.g., Kohn et al., 1993).

Shear zones can be loci of extensive focused fluid flow, metasomatism, and mass transfer-related volume changes (e.g., Dipple and Ferry, 1992a; Dipple and Wintsch, 1990; Konrad-Schmolke et al., 2011; O'Hara, 1988; Ring, 1999; Selverstone et al., 1991). In their survey of ductile shear zones, Dipple and Ferry (1992a) concluded that time-integrated fluid fluxes of $\sim 2 \times 10^4 \text{ m}^3 \text{ m}^{-2}$ attended down- T flow, leading to considerable K gain and other major element metasomatism. Selverstone et al. (1991) document extreme metasomatism in a shear zone from the Tauern Window, Austria. Granodiorite

host rock was converted to highly aluminous schist as a result of fluid-rock interaction in the shear zone; time-integrated fluid fluxes were $\sim 10^6 \text{ m}^3 \text{ m}^{-2}$. In the Bergen Arcs, Norway, flow along shear zones, veins, and infiltration fronts facilitated conversion of metastable deep-crustal granulite facies rocks to eclogite facies assemblages (Figure 8; Austrheim, 1990).

4.6.9.3.2 Lithologic contacts and layer-parallel flow

Large time-integrated fluid fluxes are predicted and observed for regional devolatilization. Nonetheless, some rocks preserve evidence for considerably less advection. For example, Bickle et al. (1997) studied greenschist facies fluid infiltration from metapelitic rock into metacarbonate rock across lithologic contacts in the Waterville Formation, Maine. They estimated time-integrated fluid fluxes of only $\sim 3.2 \text{ m}^3 \text{ m}^{-2}$. Fluxes from metapelites into marbles recorded in the amphibolite facies on Naxos, Greece, were similarly small, ranging from 0.2 to $1.0 \text{ m}^3 \text{ m}^{-2}$ (Bickle and Baker, 1990). These small values can be reconciled with the expectation of larger regional devolatilization fluxes if the regional flow was predominantly layer parallel, such that cross-layer components were small. On Naxos, the marbles probably had very low permeability, resulting in the bulk of the flow being channelized into the metapelitic layers (e.g., Figure 5). Oliver et al. (1998) quantify fluxes for an example of regional focusing into metapelitic layers. Fluids flowed up- T over 20 km length scales in the vicinity of the Kanmantoo ore deposit, Australia, achieving large time-integrated fluid fluxes of $\sim 10^5 \text{ m}^3 \text{ m}^{-2}$, which led to substantial chemical and oxygen isotopic metasomatism. Although flow channelized along layers and lithologic contacts has been widely recognized in many studies (see review in Oliver, 1996), the number of quantitative estimates of time-integrated fluid fluxes for cross-layer and layer-parallel flow components remains surprisingly modest.

4.6.9.3.3 Flow channelization in subduction zones

Subduction zone fluids and mass transfer are very large topics that are examined in depth in Chapters 4.9, 4.19, and 4.20; nonetheless, it is useful to discuss some aspects of the fluid flow here. A basic constraint is that the time-integrated fluid flux at the top of the slab, assuming vertical flow, will be $\sim 3 \times 10^2 \text{ m}^3 \text{ m}^{-2}$ (Zack and John, 2007; see Chapter 4.19). This flux is considerable – sufficient to transport an oxygen isotopic front some 180 m – but is still smaller than expected for devolatilization in some other settings, such as collisional orogens (Figure 19(c)).

As seen in the previous examples, however, focusing of fluid will produce larger fluxes in and around flow conduits. Veins are one means to focus flow; they have been documented widely in diverse exhumed subduction complexes, including the Catalina Schist, California (Bebout and Barton, 1989), the Tianshan subduction complex, China (Gao et al., 2007; John et al., 2008), and Guatemala (Simons et al., 2010). The flow direction is also critical. A major, as yet unresolved question is, do fluids always flow vertically up out of the slab, or can they be channeled along the subduction zone décollement? If channeled, then larger fluxes could be focused along the slab-mantle interface. Studies of subduction zone mélanges are critical in this regard. These mélanges typically consist of metamorphosed igneous (predominantly mafic and ultramafic)

and/or sedimentary rocks set in a metasedimentary or ultramafic matrix. In many cases, field evidence indicates that they probably represent the interface between the downgoing lithosphere and the overlying mantle wedge (see [Chapter 4.20](#)). Consequently, mélanges will hold valuable clues about fluid flow in dynamic subduction environments.

In view of the critical role subduction plays in arc magmatism and global element cycling, the quantities and directions of fluid flow within subducted crust remain the subjects of vigorous investigation. Different workers, however, have come to markedly different conclusions regarding the nature and extent of subduction-related fluid flow. Field studies of stable isotope systematics (e.g., [Bebout and Barton, 1989, 1993](#)) and trace element mobility (e.g., [Cruz-Uribe et al., 2010; Sorensen and Grossman, 1989](#)) provide strong evidence for regional, kilometer-scale fluid migration during Mesozoic subduction in the Cordillera (CA, USA).

By contrast, diverse evidence from the Cycladic Archipelago (Greece) and the Alps indicates that subduction during Alpine orogenesis may have involved limited fluid flow and fluid-rock interaction (e.g., [Barnicoat and Cartwright, 1995; Bröcker et al., 1993; Ganor et al., 1996; Getty and Selverstone, 1994; Philippot and Selverstone, 1991; Putlitz et al., 2000](#)). For example, little evidence has been found for fluid-rock interactions during subduction on the Cycladic island of Naxos; the classic metamorphic sequence there formed during a later Barrovian-style overprint of original high-*P*, low-*T* assemblages ([Bickle and Baker, 1990; Rye et al., 1976](#)). [Putlitz et al. \(2000\)](#) found no evidence favoring the large-scale release or flow of fluids during high-*P*, low-*T* metamorphism of subducted oceanic crust based on O and H isotope studies of metabasalts and metagabbros in the Cyclades.

One possible explanation for the comparatively low fluid fluxes seen in these regions is channelization of fluids into high-permeability structures during Alpine orogenesis, which led to strong spatial heterogeneity of flow. Fractures are one candidate for such channels, although regionally extensive vein systems have yet to be documented. Veins are present, but were not necessarily conduits for large fluxes; in fact, [Philippot and Selverstone \(1991\)](#) documented local-scale heterogeneities in fluid composition recorded by eclogitic veins, which they interpreted to reflect limited fluid flow.

Another, perhaps more likely, scenario for the low fluid fluxes is channelization of fluids into mélangé zones. Strong metasomatic interactions between the rims of metamorphosed igneous and sedimentary rocks and the surrounding mélangé matrix occurred in mélangé zones in both the California and Alpine/Cycladic settings, unequivocally demonstrating the presence of fluids ([Bebout and Barton, 2002; Breeding et al., 2004b; Bröcker and Enders, 2001; Catlos and Sorensen, 2003; Dixon and Ridley, 1987; King et al., 2003; Miller et al., 2009; Putlitz et al., 2000](#)). Metasomatic rinds on mafic blocks in ultramafic matrix at Syros, Greece, show clear enrichments of lithium and boron related to fluid infiltration during exhumation ([Marschall et al., 2009](#)). Nonetheless, the time-integrated fluid fluxes recorded by the block interiors are relatively small, probably $<17 \text{ m}^3 \text{ m}^{-2}$ ([Ague, 2007](#)). However, the blocks are typically quite massive, in contrast to the highly foliated matrix. Thus, the blocks may have had much lower permeabilities than the matrix, such that the major flow was channelized into

the matrix and concentrated on block margins. Numerical simulations show that order of magnitude flux contrasts may develop over length scales as short as decimeters in mélangé zones with high permeability contrasts ([Figure 23](#)). Of course, mélangés undergo extensive deformation, but the general process of flow diversion around low-permeability blocks will hold true regardless.

If the flux out of the top of the downgoing lithospheric column ($\sim 3 \times 10^2 \text{ m}^3 \text{ m}^{-2}$) travels mostly upward, then it will enter the hanging wall of the subduction zone. As subduction-related fluids will be generated on timescales on the order of 10^7 – 10^8 years, the total flux into the hanging wall will be much larger than that emanating from any one point at the top of the subducted crust. [Peacock \(1990\)](#) estimates fluxes will range from $<10^{-4}$ to $10^{-3} \text{ m}^3 \text{ m}^{-2} \text{ year}^{-1}$ during subduction, depending on the nature of the devolatilization reactions proceeding as a function of depth. Taking a conservative value of $10^{-4} \text{ m}^3 \text{ m}^{-2} \text{ year}^{-1}$ and timescales of 10^7 and 10^8 years, the corresponding time-integrated fluid fluxes into the hanging wall are 10^3 – $10^4 \text{ m}^3 \text{ m}^{-2}$. Of course, the flux at any given point along the subduction zone will be a complex function of thermal history, reaction progress, reaction kinetics, and other geologic factors. Nonetheless, this flux is critical to consider when evaluating fluid flow into accretionary prisms, mantle metasomatism, and the genesis of arc magmas. For example, [Breeding and Ague \(2002\)](#) estimated large regional time-integrated fluid fluxes of $c. >10^4 \text{ m}^3 \text{ m}^{-2}$ for fracture-controlled flow into the Otago Schist accretionary prism, New Zealand, based on a mass balance analysis of silica addition to regional quartz vein sets. The fluid fluxes were large

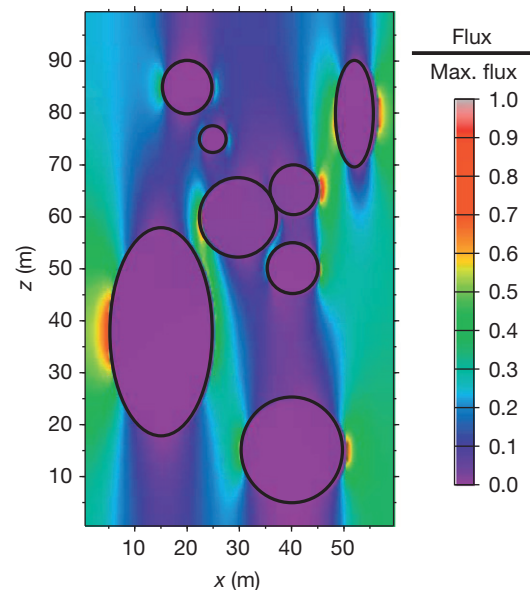


Figure 23 Numerical model of fluid flow in mélangé with large permeability contrasts. Mélangé blocks (circles and ellipses) have low permeability relative to matrix. Flow is diverted around blocks, leading to concentrated zones of high flux on block margins. Fluxes can vary by orders of magnitude over meter or even decimeter scales. General direction of flow is upward. Modified from [Ague JJ \(2007\) Models of permeability contrasts in subduction zone mélangé: Implications for gradients in fluid fluxes, Syros and Tinos Islands, Greece. *Chemical Geology* 239: 217–227.](#)

enough to produce Au mineralization in Otago and in accretionary environments elsewhere (e.g., [Craw and Norris, 1991](#); [Jia and Kerrich, 2000](#)) and to provide a mechanism for the long-term bulk silica enrichment of the continents.

The evolving picture of fluid flow in subducted lithosphere suggests that channelization of fluid is common, such that conduits experience high fluxes and the surroundings are impoverished in fluid (e.g., [Zack and John, 2007](#)). However, many fundamental questions persist. Indeed, the fact remains that very few field-based estimates of time-integrated fluid fluxes are available for subduction zones. It is essential to clarify the fluid flow picture, since subduction of sediment and hydrothermally altered oceanic crust and mantle is the primary means by which reactive volatiles, including H₂O and CO₂, are returned to the deep earth, ultimately giving rise to arc magma genesis at ~100–150 km depth.

4.6.9.4 Channelization and Fluid Fluxes at the Regional Scale

As shown in [Figure 21](#), the maximum large-scale fluxes are associated with areas of long-term regional flow channelization into fracture sets or with flow patterns generated around cooling intrusions. Fracture-controlled, outflow of fluids during regional metamorphism, metamorphic *hot spot* genesis (see [Section 4.6.9.6](#)), and devolatilization of subducted slabs beneath accretionary prisms can involve large-scale fluxes of $\sim 10^4$ to $>10^5$ m³ m⁻². Fluid flow toward cooling intrusions may also produce fluxes in this range, although examples to date are mostly from midcrustal levels (<~15 km depth). Large-scale focusing of flow is one way to produce regional time-integrated fluxes well in excess of 10^4 m³ m⁻². For example, areal focusing of devolatilization fluids derived from underlying crust by a factor of ~10–20 could have produced the large fluxes recorded by the regional vein systems of the Wepawaug Schist ([Ague, 1994b](#)). Subduction can also generate large time-integrated fluid fluxes in the hanging wall, as the supply of fluid is continually replenished as new oceanic crust and sediment is fed into the subduction zone and undergoes devolatilization during burial ([Nur and Walder, 1990](#)). In addition, large fluxes could potentially be achieved by convective recycling of fluids or by the long-term circulation of fluids derived from near surface reservoirs into the deep crust. These latter two possibilities seem unlikely for the deep crust, given current understanding, but future research may prove otherwise.

4.6.9.5 Mass Transport by Fluids

Fluid flow through rocks will transport volatile species (e.g., H₂O and CO₂) and *nonvolatile* rock-forming and trace elements. Volatiles have received a tremendous amount of attention, but the geochemical behavior of the nonvolatile elements is also crucial to understand. For example, Rb/Sr, Sm/Nd, and Lu/Hf isotopic dating of garnet is predicated on the immobility of these elements in crustal fluids. Fluid-driven, coupled dissolution–precipitation reactions and phosphorous mobility can cause major changes in the U–Th–Pb systematics of accessory minerals commonly used for dating, such as monazite ([Section 4.6.6.3](#)). The transport of rock-forming elements, such as alkali and alkaline earth metals and aluminum, can modify rock bulk chemistry and stabilize or destabilize key

metamorphic index minerals. In subduction zones, release of these and other elements (including silicon) during devolatilization can produce silicification of the mantle wedge (e.g., [Kesson and Ringwood, 1989](#)) and exert profound controls on arc magma chemistry ([Chapters 4.9, 4.19, and 4.20](#)). Fluid–rock reaction leads to chemical and isotopic modification of rocks and minerals, providing an invaluable record of fluid flow histories that permits quantification of fluid fluxes ([Sections 4.6–4.8](#)). Furthermore, element transfer by fluids deep in mountain belts must play a considerable role in large-scale geochemical cycling and ore deposition; interactions between deep and shallow fluids remain as an important research frontier.

It has long been understood that certain trace elements can be mobilized in crustal fluids. For example, the mobility of strontium has been quantitatively appreciated since the early days of Rb–Sr dating. Some soluble elements, like lithium, can be lost together with water and other volatiles during prograde heating ([Qiu et al., 2011](#); [Teng et al., 2007](#)). Owing to their low concentrations in rocks, trace elements will tend to be more easily mobilized by infiltrating fluids than major elements. This is not true of HFSE, like zirconium, however, which tend to have extremely low concentrations in fluids ([Section 4.6.5](#)). The received wisdom has been that most rock-forming elements and HFSE are largely inert during orogenesis, but research over the past few decades has shown that a more diverse spectrum of geochemical behavior is possible.

Some of the most well-established examples of fluid-driven, mid- to deep-crustal mass transfer are found in and around veins, shear zones, or lithologic contacts. As shown in [Figure 21](#), these features can act as flow conduits and carry large fluxes, which may exceed 10^4 m³ m⁻² on a time-integrated basis. The large fluxes, in turn, have the ability to transport more mass than is possible via *background* levels of regional devolatilization. Of course, if fluids are focused into conduits, then other areas of the rock mass will be correspondingly impoverished in fluid. As a consequence, the nature and extent of mass transfer can vary significantly, even at the outcrop scale ([Ague, 2007, 2011](#)). Another reason that conduits have received so much attention is a practical one. In order to quantify chemical and isotopic changes, one needs to compare the altered rock to less-altered or unaltered equivalents. These are relatively straightforward to identify in cases of focused flow (e.g., [Figure 8](#)) but are much more challenging to assess for pervasively altered systems in which little trace of the unmodified rock remains. Rocks of the Mt. Isa Inlier provide examples of massive metasomatism on the regional scale in the shallow crust ([Section 4.6.9.1.1](#)).

Mass transfer will depend on a host of geologic variables, including *P*, *T*, fluid composition, rock composition, fluid flux, fluid transport mechanism, and tectonic setting. Consequently, generalizations must be made with great caution. Nonetheless, some broad patterns are beginning to become clear. The relative ease of transport will scale roughly with the magnitudes of elemental concentrations and concentration gradients in lithospheric fluids ([Figure 24](#)). Many commonly cited types of nonvolatile element mass transfer involve the alkali and alkaline earth metals, principally potassium, sodium, and calcium; examples are known from the shallow crust to subduction zones (e.g., [Ague, 1991, 1994b, 1997a,](#)

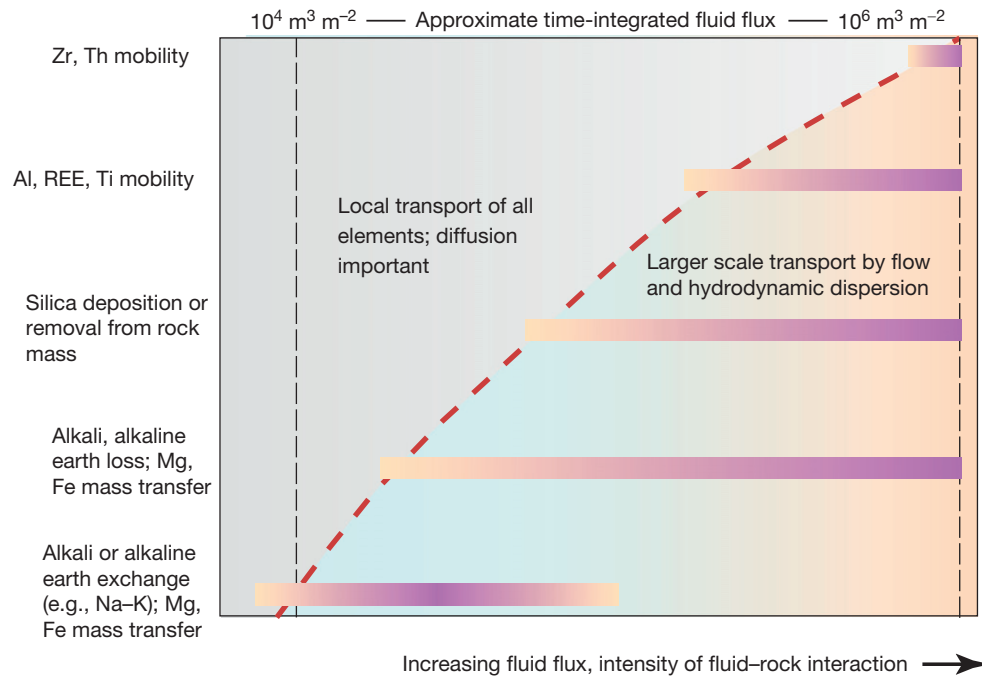


Figure 24 Nonvolatile element mass transfer scaling. Local transport, principally by diffusion, dominates to the left of the red dashed line. Larger-scale advective-dispersive transport becomes important to the right. Intensity of fluid-rock interaction increases to the right (e.g., larger fluid fluxes, more chemically aggressive fluids, and/or higher P - T conditions).

2011; Baumgartner and Olsen, 1995; Breeding et al., 2004b; Catlos and Sorensen, 2003; Dasgupta et al., 2009; Dipple and Ferry, 1992a; Dixon and Ridley, 1987; Ferry and Dipple, 1991; Harlov et al., 1998; Léger and Ferry, 1993; Meyer, 1965; Oliver et al., 1990, 1998; Penniston-Dorland and Ferry, 2008; Putnis and Austrheim, 2010; Rubenach, 2005; Selverstone et al., 1991; Shaw, 1956; Thompson, 1975; Tracy et al., 1983; Vidale, 1969; Yardley, 1986). This mobility is consistent with the fact that these elements typically have high concentrations in Cl-bearing fluids coexisting with mica- and/or feldspar-bearing mineral assemblages (e.g., Fyfe et al., 1978; Figure 6). As expected on geochemical grounds, trace element behavior typically follows that of the major elements; for example, strontium tends to follow calcium, whereas rubidium and barium tend to follow potassium.

At time-integrated fluid fluxes of $\sim 10^4 \text{ m}^3 \text{ m}^{-2}$, alkali exchanges, such as sodium-potassium, can produce important changes in rock chemistry. Dipple and Ferry (1992a) report potassium gains and sodium losses that drove mica growth as a result of down- T flow in shear zones. Gain of sodium and calcium and loss of potassium, coupled to Mg/Fe increases, destroyed muscovite and promoted garnet and plagioclase growth in altered zones (*selvages*) adjacent to veins cutting metaclastic rocks in Barrow's garnet zone, Scotland (Ague, 1997a; Masters and Ague, 2005). In addition, as expected from geochemical affinities, strontium was gained and rubidium was lost. The open-system mass transfer stabilized the index mineral garnet in a number of lithologies that originally had bulk compositions unsuitable for the growth of this key index mineral. Regional fluid transport took place through fractures (now veins), and mass transfer between the fractures and the selvages was largely by diffusion (Figure 22(b)).

Another, related, type of behavior involves loss of alkali and alkaline earth metals rather than simple exchanges such as sodium-potassium or potassium-sodium. Much remains to be learned, but it is likely that these mass losses require more chemically aggressive fluids (e.g., high chlorine content), larger fluid fluxes, and/or more extreme P - T conditions than simple exchange. Loss of these metals can produce highly peraluminous rock types in which aluminous minerals, such as staurolite and Al_2SiO_5 polymorphs, can crystallize. Moreover, the large fluxes involved, which can reach $\sim 10^6 \text{ m}^3 \text{ m}^{-2}$, can transport significant silica. Selverstone et al. (1991) describe silica depletions and variable alkali metal losses during up- T flow in a major shear zone in the Tauern Window, eastern Alps. Down- T flow in quartz veins precipitated silica and stripped alkalis from adjacent selvages, which strongly enhanced staurolite and kyanite growth in the Wepawaug Schist, Connecticut (Ague, 1994b, 2011). Overall, silica was deposited in veins by ascending, through-going fluids, but there was also substantial silica depletion from the selvages following the *crack flow seal* model described in Section 4.6.9.3.1. The alkali loss was due mainly to destruction of micas and plagioclase. Yardley (1986) documents retrograde alkali metasomatism and the resultant formation of aluminous mineral assemblages, including tourmaline, staurolite, garnet, and andalusite in Knockaunbaun, Ireland. Oliver et al. (1998) describe midcrustal amphibolite facies alkali and calcium loss and the growth of aluminous mineral assemblages in vein selvages related to regional fluid flow in the vicinity of the Kanmantoo ore deposit, Australia.

Major element mass transfer can be coupled to isotopic shifts that allow the fluid source to be traced. Tracy et al. (1983) found strong metasomatism, including the loss of nearly all potassium and sodium, in metacarbonate rock

adjacent to an amphibolite facies quartz vein. The infiltrating fluid had lower X_{CO_2} than fluid in equilibrium with the wall rock and, thus, drove extensive decarbonation of the selvage (e.g., [Figure 17\(a\)](#)). The $\delta^{18}\text{O}$ of the vein quartz (and selvage calcite) is lower than in metacarbonate rock beyond the selvage margins ([Tracy et al., 1983](#)), consistent with infiltration of external fluid derived from or equilibrated with syn-metamorphic intrusions or underlying mafic metavolcanic rocks ([Palin, 1992](#); [van Haren et al., 1996](#)).

At higher degrees of fluid–rock interaction or more extreme metamorphic conditions, elements typically considered to be inert can be mobilized at scales larger than hand samples ([Figure 24](#)). In spite of its low concentrations in typical chlorine-bearing aqueous fluids, the field occurrence of aluminosilicates and other aluminum-bearing minerals in veins clearly demonstrates some degree of aluminum mobility (e.g., [Austrheim, 1990](#); [Beitter et al., 2008](#); [Kerrick, 1990](#); [McLelland et al., 2002](#); [Nabelek, 1997](#); [Whitney and Dilek, 2000](#); [Widmer and Thompson, 2001](#)). What is less well documented is whether the mass transfer is local- or requires larger-scale fluid flow.

Evidence to date, although limited, demonstrates that both are possible. For example, [Widmer and Thompson \(2001\)](#) propose that disequilibrium overstepping of reactions in wall rocks could generate large chemical potential differences between the wall rocks and precipitation sites in veins. They argue that aluminum can be mobilized locally without significant fluid flow to form kyanite-bearing segregation veins in high- P (~ 2.5 GPa) environments. On the other hand, mass balance studies of veins cutting amphibolite facies metapelitic and metacarbonate rocks in Connecticut ([Ague, 2003, 2011](#)) and metapelites in the Shetland Islands, Scotland ([Buchholz and Ague, 2010](#)), demonstrate aluminum addition. The selvages surrounding kyanite-bearing quartz veins in the metapelitic examples underwent aluminum mass additions. Thus, the kyanite in the veins was not derived by local aluminum loss from the surroundings; precipitation from migrating fluids was required. Aluminum gains were accompanied by silica precipitation in veins and significant alkali losses; in the Connecticut example, the added aluminum, together with the loss of alkalis, helped to stabilize selvage kyanite and staurolite. The selvage alteration is more extensive around kyanite-bearing veins than around those that are composed mostly of quartz. In the Connecticut metacarbonate rocks, the added aluminum is manifested by crystallization of minerals, such as clinozoisite, zoisite, and hornblende in vein selvages and along other conduits, including lithologic contacts.

Complexing of aluminum with aqueous silica, alkalis, and/or halogens is probably important for enhancing aluminum concentrations and facilitating aluminum transport, particularly at scales larger than local vein–wall rock systems (e.g., [Diakonov et al., 1996](#); [Manning, 2006, 2007](#); [Manning et al., 2010](#); [Salvi et al., 1998](#); [Tagirov and Schott, 2001](#); [Walther, 2001](#); [Wohlert and Manning, 2009](#)). Of course, aluminum is strongly mobilized during partial melting; sillimanite-rich restites and other igneous phenomena are distinct from the fluid-driven mass transfer focused on herein.

HFSE, including REE, titanium, and zirconium, likely have very low concentrations in most lithospheric fluids. Nonetheless, there are a growing number of examples of HFSE transport

([Figure 24](#)). Most of these are from deep-crustal and subduction zone settings. For example, [Gao et al. \(2007\)](#) describe titanium–niobium–tantalum transport in fractures cutting eclogite facies rocks, Tianshan subduction complex, NW China. In the same orogenic belt, [John et al. \(2008\)](#) document LREE losses, lithium gains, and other metasomatic phenomena associated with eclogite facies veining that cuts blueschist, and [van der Straaten et al. \(2008\)](#) describe REE and uranium loss from eclogite that was rehydrated to form blueschist. [Rubatto et al. \(1999\)](#) and [Rubatto \(2002\)](#) interpret oscillatory-zoned zircon in a vein from an eclogitic mica schist in the Sesia-Lanzo zone to represent deposition from a fluid phase during prograde metamorphism. On the other hand, zirconium appears to be mostly inert during jadeitite formation in subduction zones ([Fu et al., 2010](#)). Thorium probably has very limited mobility in fluids (e.g., [Breeding et al., 2004b](#); [Hawkesworth et al., 1997](#); [Johnson and Plank, 1999](#)), but uranium can be transported, particularly in relatively oxidized fluids ([Hawkesworth et al., 1997](#)). It is probable that the high- P (and in some cases T) conditions encountered in subduction settings enhances complex formation and the solubility of refractory phases, such as rutile ([Antignano and Manning, 2008a](#); [Audétat and Keppler, 2005](#)). The wide variety of rock types juxtaposed in subduction channels, including metamorphosed ultramafic, mafic, and metasedimentary rocks, will lead to diverse metasomatic behaviors, as no single fluid will be in chemical equilibrium with all lithologies ([Chapter 4.20](#)). An important research problem is whether the HFSE transport is regional or if it occurs only at local scales; [Gao et al. \(2007\)](#) conclude that titanium–niobium–tantalum transport occurred over distances of at least 1 m. Given their low concentrations in fluids, mass transfer of HFSE, even at these scales, implies considerable fluid fluxes.

HFSE transport has been documented in other settings as well, including Barrovian metamorphism. For example, in the Wepawaug Schist of Connecticut, HREE addition to vein selvages is observed in both metacarbonate and metapelitic rocks. In one strongly HREE-enriched greenschist facies metacarbonate rock, the HREE are hosted in vein xenotime (see [Figure 6](#) in [Ague, 2003](#)). In amphibolite facies metapelitic selvages surrounding quartz–kyanite veins, the HREE are hosted by garnet, which grew extensively in the selvages as a result of fluid–rock interaction ([Figure 25\(a\)](#); [Ague, 2011](#)). Additions of other elements to the selvages, including iron, manganese, and yttrium, also reflect this widespread garnet growth ([Figure 26](#)). Middle REE were mobile as well, leading to significant changes in, for example, Sm/Nd ratios ([Figure 25\(b\)](#)). In these examples, geochemical profiles across vein–wall rock contacts demonstrate that the HREE were not derived locally and must have been deposited by migrating fluids. By contrast, zirconium and titanium were essentially immobile in most rocks ([Figure 26](#)), although local depletion of titanium to form rutile in veins was observed in isolated examples. Extremely aluminous kyanite-bearing rocks from Unst, Shetland Islands, Scotland, also record limited local titanium mobility and significant REE transport ([Buchholz and Ague, 2010](#)). Here, garnet is absent from most rocks, so the REE transport fingerprint is different; REE were gained in vein selvages, with light and middle REE showing the strongest mass additions. All these examples were metamorphosed at relatively high pressures (~ 0.7

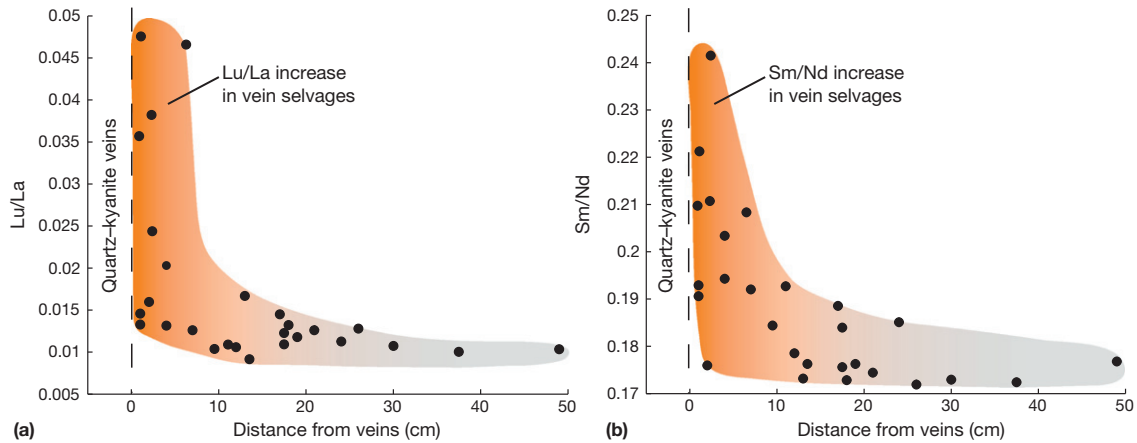


Figure 25 REE mass transfer by fluids. Geochemical profiles for rocks sampled on three separate traverses perpendicular to vein–wallrock contacts in two outcrops. Results for all three profiles are similar and are thus plotted together. Amphibolite facies metapelites, Wepawaug Schist, Connecticut, United States (Ague, 2011). (a) Lu/La ratio increases toward veins. (b) Sm/Nd ratio increases toward veins.

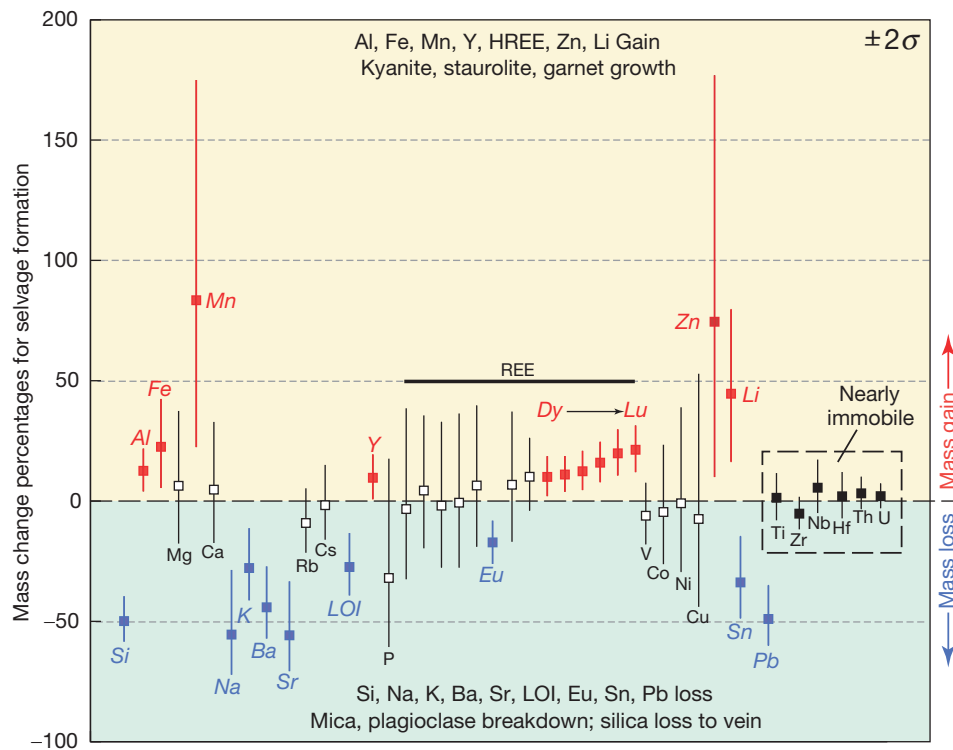


Figure 26 Mass changes for elements in geochemically altered selvages adjacent to amphibolite facies quartz–kyanite veins relative to little-altered schists distal to veins. Sample set described in Figure 25. Mass changes shown in red (gains) or blue (losses) statistically significant at 95% confidence level. Addition of aluminum and loss of alkalis and alkaline earths stabilized aluminous index minerals staurolite and kyanite and enhanced garnet growth. Continued growth of these minerals sequestered elements from passing fluids, leading to mass gains. Garnet incorporated iron, manganese, yttrium, and REE; staurolite incorporated iron, zinc, and lithium; staurolite, kyanite, and garnet incorporated aluminum. Breakdown of micas (mainly muscovite) led to losses of sodium, potassium, barium, LOI (loss on ignition, a proxy for volatile content), tin, and lead. Plagioclase breakdown resulted in losses of strontium, europium, and sodium. Silica lost locally due to transfer from selvages to adjacent veins (Figure 22). Mass balance demonstrates that 40–80% of the vein mass was derived locally; remainder was precipitated by through-going fluids. Modified from Ague JJ (2011) Extreme channelization of fluid and the problem of element mobility during Barrovian metamorphism. *American Mineralogist* 96: 333–352.

to >1.0 GPa) and, thus, complexing of HFSE with aluminum-silicon species in fluids may have enhanced refractory phase solubilities (e.g., Antignano and Manning, 2008a). Moreover, the common association of yttrium and/or phosphorus mass addition in these rocks with REE addition suggests REE transport as yttrium or phosphorus complexes (Ague, 2003, 2011; Bucholz and Ague, 2010).

Considerable confusion surrounding the scale of mass transfer has arisen in the literature, so scale issues are critical to discuss here. All elements can be mobilized on the scale of microns to thin sections during prograde or retrograde mineral reaction. Most can probably be mobile on the scale of several centimeter to decimeter scales as well, particularly in the presence of strong compositional contrasts between adjacent rock types that could be present, for example, along relic bedding planes in metasedimentary sequences or between blocks and matrix in mélangé (e.g., Ague, 2003; Bebout and Barton, 2002; Brady, 1977; Dixon and Ridley, 1987; Joesten and Fisher, 1988; King et al., 2003; Thompson, 1975; Vidale, 1969; Vidale and Hewitt, 1973). In these settings, metasomatic zonation across contacts is possible if fluids are present for sufficient durations and the chemical gradients in the fluids are large enough. For thin section- to roughly decimeter-scale transport, diffusion will dominate. To move nonvolatile element mass at scales of several meters to outcrop to regional scales, however, advective fluxes will be necessary in most cases. The scale of transport, regardless of transport process, will be linked to fluid-rock partitioning behavior (K_v ; Section 4.6.7); elements with large K_v will have larger characteristic transport distances than those with small K_v . Consequently, even though HFSE transport may have only occurred over a few meters in a particular outcrop, the fluid flux necessary would be large, given the likely exceedingly small K_v . A critical point to emphasize regarding vein selvages is that, although they may only be centimeter to meter scale in thickness (Figures 8 and 22), they can line flow conduit networks stretching over kilometer scales. Thus, selvages are critical loci of interaction between regionally migrating fluids and their enclosing wall rocks, facilitating ion exchange and modifying the composition of fluids substantially along lithospheric flow paths.

The focusing of fluids into conduits can lead to strong spatial heterogeneities in flow patterns. The isotopic and chemical metasomatism recorded around conduits provides a record of large fluid fluxes and focusing. On the other hand, channelization will deprive other parts of the rock mass of fluid. In these areas, fluxes will actually be lower than expected for regional devolatilization (Zack and John, 2007). In fact, flux variations of two orders of magnitude or more are possible even on meter or decimeter scales (Figure 23; Ague, 2007, 2011). As a consequence, the mass transfer effects of regional fluid flow can be highly heterogeneous, even at the outcrop scale. Rocks far removed from veins, shear zones, lithologic contacts, and other features that may focus flow will undergo the least chemical and isotopic modification during fluid transport. Therefore, they are the best targets for studies which seek to trace the geochemistry of rocks back to their low- T origins to elucidate, for example, original sedimentary depositional environments or biomarkers of early life. Moreover, low-flux and high-flux rocks in the same outcrop will undergo different mineral reaction histories and, thus, record different parts of P - T -

paths; this information will, in turn, provide multiple independent constraints on orogenic evolution.

Despite the near ubiquity of veins and other conduits in orogenic belts, the number of mass balance studies that quantify nonvolatile element mass transfer is surprisingly small. These data are necessary to integrate heterogeneous flux and mass transfer results from the outcrop scale to the regional scale.

4.6.9.6 Heat Transport by Fluids

Rocks conduct heat fairly readily, so fluid fluxes must be large, channelized, and/or transient for advection of heat to be important (cf. Bickle and McKenzie, 1987; Brady, 1988; Connolly and Thompson, 1989; England and Thompson, 1984; Gerya et al., 2002; Hoisch, 1991). For example, a series of ten granulite facies thermal anomalies or *hot spots* measuring 10–30 km² are spread out in a belt ~150 km long in part of the Acadian orogen, New Hampshire, United States (Chamberlain and Rumble, 1988). Chamberlain and Rumble (1988, 1989) proposed that the hot spot near the town of Bristol is an area where large volumes of ascending hot fluid were focused through a network of quartz veins, thereby perturbing regional thermal and oxygen isotope systematics. The large fluxes could have been achieved by focusing of fluids generated by metamorphic devolatilization or magmatic degassing into the comparatively small area of the hot spot (Brady, 1988; Chamberlain and Rumble, 1989), or by recycling fluids in a convective flow system (Chamberlain and Rumble, 1989). The timescale of flow must have been less than ~10⁶ years; otherwise, the surroundings would have heated up, destroying the steep thermal gradients observed in the field (Brady, 1988; Chamberlain and Rumble, 1989). Another alternative is that heat was transported vertically through the hot spots mostly by magmas rather than hot fluids, although no direct evidence for such magmas has been found.

Ferry (1992) and Ague (1994b) used the dimensionless thermal Peclet number (B) of Brady (1988) to assess whether or not the large fluxes needed to make regional quartz vein sets elsewhere in the Acadian orogen of New England may have also transported heat:

$$B = \frac{(q_{II}/\Delta t)L\rho_f C_{p,f}}{K_{T,r}} \quad [26]$$

in which L is the length scale, $\rho_f C_{p,f}$ is the product of the density and heat capacity of the fluid, $K_{T,r}$ is the thermal conductivity of the rock, and Δt is the total time of fluid flow. B estimates the relative importance of heat transfer by advection (numerator) and conduction (denominator). For example, a B of ~2.7 is obtained using the q_{II} for the higher grade parts of the Wepawaug Schist = $6 \times 10^4 \text{ m}^3 \text{ m}^{-2}$, a regional $L = 10 \text{ km}$, $\Delta t = 10^7$ years, $K_{T,r} = 2.5 \text{ W m}^{-1} \text{ K}^{-1}$, and $\rho_f C_{p,f} = 3.5 \times 10^6 \text{ J m}^{-3} \text{ K}^{-1}$ (Ague, 1994b). $B > \sim 2$ suggests a significant role for heat transport by fluid flow. Ferry (1992) came to a similar conclusion for rocks in northern New England.

These examples notwithstanding, there are relatively few documented cases of strong, fluid-driven heat transport at mid- or deep-crustal levels in orogenic belts. Modeling shows that for typical devolatilization fluxes and timescales, heat conduction will play a much larger role than fluid advection (e.g., Bickle and McKenzie, 1987; Brady, 1988; Connolly and

Thompson, 1989; Hanson, 1997). Even for a comparatively large q_{fl} value of $10^4 \text{ m}^3 \text{ m}^{-2}$, B is <1 for orogenic time (10^7 years) and length scales, and the associated temperature anomalies are only $\sim 5\text{--}15^\circ\text{C}$ (Lyubetskaya and Ague, 2009). It is reasonable to conclude that large, fluid-driven thermal anomalies will be limited to very high flux and/or very short timescale settings. An important research challenge is to determine how common such anomalies are in orogenic belts and assess their importance to lithospheric heat budgets.

4.6.9.7 Timescales of Fluid Flow

As discussed in Section 4.6.9.6 earlier, the timescale of fluid flow is critical to problems of advective heat transport by fluids. Timescales are also fundamental to fluid–rock reactions, as slow transport relative to reaction rates will favor local equilibrium, whereas fast transport and slow rates will lead to disequilibrium (Figure 15). Isotopic dating provides direct constraints on the timing and timescales of reaction. Furthermore, the preservation of isotopic or chemical disequilibrium in crystals or rocks yields important quantitative information about timescales if temperatures and rates of diffusion or recrystallization are known. For example, consider a mineral that fails to reach oxygen isotope equilibrium with an infiltrating fluid. If intracrystalline diffusion is the primary means by which the mineral interacts with the fluid, and the temperature of infiltration is known, then the maximum timescale over which the mineral and fluid were in contact can be estimated based on the degree of isotopic disequilibrium preserved in the mineral (e.g., Palin, 1992; van Haren et al., 1996; Young and Rumble, 1993). If complete equilibration is achieved, then only minimum timescales can be estimated. There are many other ways to use transport–reaction theory to estimate rates; Skelton (2011) provides a current example. Dating of the growth histories of porphyroblasts, such as garnet, does not, in and of itself, provide direct constraints on fluid presence or absence. However, most garnet-producing reactions liberate water, so the age ranges provide insights into the timescales of fluid presence in a dewatering rock mass.

The range of timescales relevant to fluid–rock processes in the crust spans at least six orders of magnitude (Figure 27). Some of the shortest timescales of fluid infiltration are found in and around veins, shear zones, and subduction zone mélange. Timescales are typically less than a few hundred thousand years; some studies calculate that individual events in some geological settings can be as short as 10–100 years! These results are consistent with highly pulsed, transient fluid or thermal regimes associated with deformation and may, in some cases, reflect hydrofracturing, rapid seismic moment release, or the passage of porosity waves. Some metacarbonate rocks also preserve evidence for short timescales of fluid–rock interaction. It is possible that extremely low rock permeabilities limited the amount of fluid infiltration and, thus, the timescales of reaction.

It is important to emphasize that the short timescales for veins and other settings shown in Figure 27 need not represent the total span of time over which fluid activity occurred. For example, say there were five pulses of fluid flow, each lasting 10^4 years, spaced 1 My apart. The total integrated timescale for direct fluid–rock interaction would be 50 000 years, but the

activity occurred over a ~ 4 Ma time interval. Most diffusion-based methods will estimate the 50 000 year integrated timescale; isotopic dating is needed to pin down the longer time interval (e.g., Camacho et al., 2005; Pollington and Baxter, 2010).

Available timescale estimates for regions that undergo large-scale, pulsed thermal events are on the order of a few hundred thousand to a few million years (e.g., (g), (h), (k), (m), and (n) in Figure 27). In a number of cases, direct links to advective emplacement of syn-metamorphic magmas can be made, but other heat sources, including heating from viscous deformation (e.g., shear zones) and fluid flow, may also be important. Timescales will reflect both rates of advection and of conduction away from advective heat sources.

In the Barrovian type locality, Scotland, Baxter et al. (2002) determined precise Sm/Nd ages for garnet growth which, when combined with the age data of Oliver et al. (2000), indicate a total time span of ~ 8 Ma for garnet crystallization ((h) in Figure 27). However, the difference in *peak* (maximum) T attainment between the garnet and sillimanite zones was only 2.8 ± 3.7 Ma (2σ ; statistically indistinguishable from 0). This short time span ($\sim 464\text{--}468$ Ma) is inconsistent with the larger intervals predicted by conductive thermal relaxation of variably overthickened crust (e.g., Thompson and England, 1984) and strongly suggests the involvement of an additional, advective component of heat transfer. Modeling of chemical diffusion in garnet and apatite indicates that the pulse or pulses of peak heating were of brief integrated duration, probably on the order of 10^6 years or less (Ague and Baxter, 2007; Vorhies and Ague, 2011). There could have been one large pulse of this duration or a series of shorter pulses spread out over a longer interval of time. Baxter et al. (2002) and Ague and Baxter (2007) concluded that considerable advective heat was supplied by syn-metamorphic magmas (e.g., the Newer Gabbros), although shear zones (Viète et al., 2011) and hydrothermal fluids, perhaps exsolved from the crystallizing intrusions, may have also played a role. The *total* timescale of Barrovian metamorphism was 10–15 Ma (e.g., Dewey, 2005), but pulsed heating to peak conditions, and the associated fluid release, was likely to have been more transient. It is worthwhile to note that Barrow himself first proposed (1893) that intrusions provided, at least in part, the heat required for metamorphism.

The longest timescales in Figure 27 ($> \sim 10^7$ year) are for extended periods of garnet growth; these timescales are comparable to those expected for large-scale orogenic events. It is not known if the garnets grew slowly and continuously over these time intervals or if growth occurred in a series of shorter pulses spread out over longer periods of time. Long-timescale growth and slow fluid release during the course of orogeny would be consistent with classical models of thermal relaxation of thickened crustal sections (e.g., England and Thompson, 1984). Even so, if devolatilization reactions are limited to narrow $P\text{--}T$ windows in a given bulk composition, then the duration of fluid generation and flow may be far less than that for the total orogeny. For example, Skelton (2011) concludes that fluid flow associated with regional greenschist facies metamorphism in the southwestern Scottish Highlands may have lasted only ~ 4000 years.

A growing body of evidence suggests that geologically brief pulses of fluid activity associated with deformation (e.g.,

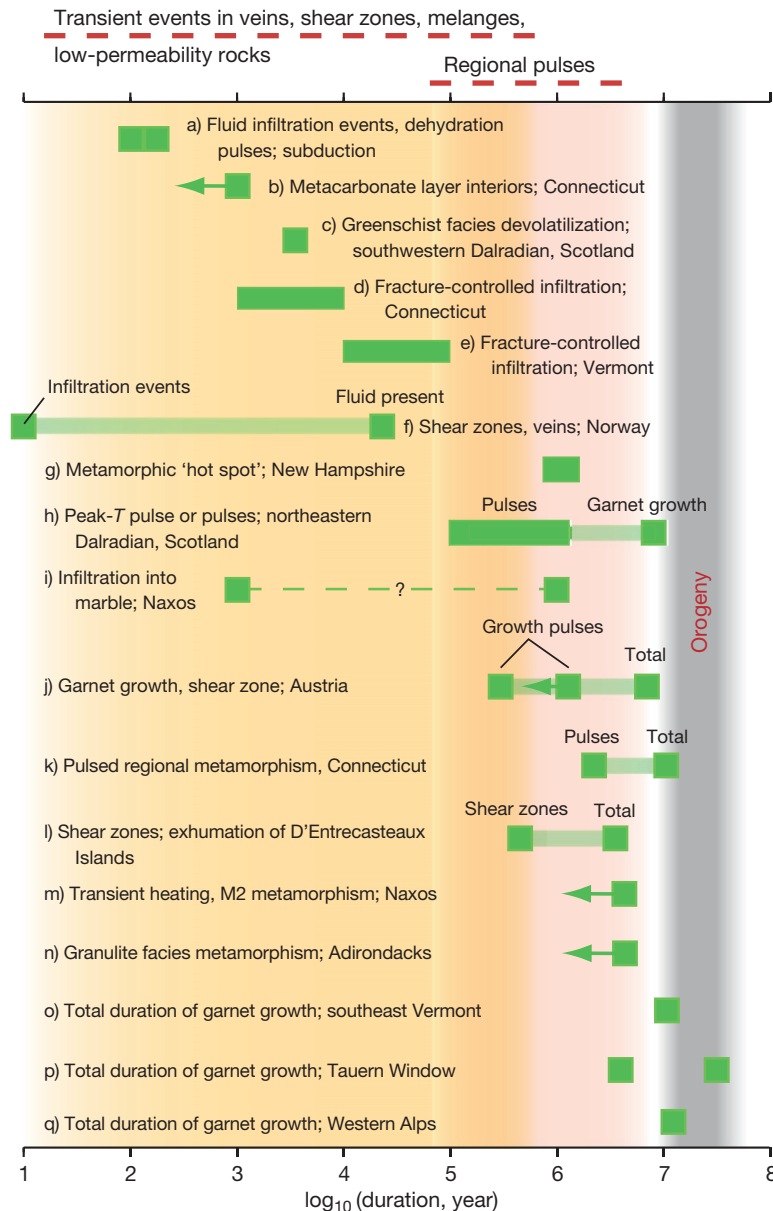


Figure 27 Selected published timescales relevant for fluid processes: (a) Penniston-Dorland et al. (2010) and John et al. (2012); (b) Palin (1992); (c) Skelton (2011); (d) van Haren et al. (1996); (e) Young and Rumble (1993); (f) Camacho et al. (2005). Total time span of orogenic activity ~ 13 Ma: (g) Chamberlain and Rumble (1989); (h) Baxter et al. (2002) for total garnet growth duration, and Ague and Baxter (2007) for thermal pulse activity; (i) Bickle and Baker (1990); (j) Pollington and Baxter (2010); (k) Lancaster et al. (2008); (l) Baldwin et al. (1993); (m) Wijbrans and McDougall (1985, 1988); (n) Page et al. (2010); (o) Christensen et al. (1989); (p) Christensen et al. (1994); (q) Lapen et al. (2003).

fracturing and shear zones) or advective thermal pulses can be part of much longer orogenic cycles lasting 10^7 years or more. If a thermal pulse is generated due to, for example, deep regional magma intrusion, then dehydration will be rapid, potentially generating high fluid pressures, hydrofracturing, transient fluid flow, and seismicity (e.g., Lyubetskaya and Ague, 2010). Determination of fluid–rock interaction timescales is an evolving research frontier that will advance along with continued improvements in isotopic dating techniques and new diffusion coefficient calibrations.

4.6.9.8 Fluids in the Granulite Facies

Phase relations and fluid inclusion evidence indicate greatly reduced water activity ($a_{\text{H}_2\text{O}}$) in the granulite facies (e.g., Aranovich and Newton, 1996, 1997, 1998; Crawford and Hollister, 1986; Frost and Frost, 1987; Lamb and Valley, 1984; Newton, 1995, and numerous references cited within these papers). Concentrated aqueous solutions of strong electrolytes, including (Na and K)Cl, would have low $a_{\text{H}_2\text{O}}$, as would CO_2 -rich fluids. If both chlorine and CO_2 contents are high, then it is

likely that immiscible CO₂-rich and chlorine-rich fluids would coexist at high *P* and *T* (Duan et al., 1995; Schmidt and Bodnar, 2000), consistent with fluid inclusion evidence for multiphase granulite facies fluids (Crawford and Hollister, 1986; Touret, 1985). The flow of dense, CO₂-rich fluid would be limited by the inability of CO₂ to wet grain boundaries effectively, unlike chlorine-rich brines (Watson and Brenan, 1987). Consequently, brines are probably more effective deep-crustal transport agents and have the potential to cause metasomatic effects, including alkali metasomatism and regional rubidium depletion owing to their high chlorine contents and alkali exchange capacities (e.g., Harlov et al., 1997; Smit and Van Reenen, 1997). Nonetheless, direct expulsion of CO₂ from crystallizing intrusions could lower *a*_{H₂O} dramatically, promote granulite facies metamorphism, and, in some cases, result in graphite precipitation (Farquhar and Chacko, 1991). A variety of mechanisms for generating low *a*_{H₂O} fluids have been proposed, including infiltration of connate brines or fluids equilibrated with metaevaporites, loss of H₂O to anatexis melts (e.g., Valley et al., 1990), which can leave behind residual fluids enriched in salts and CO₂ (Fyfe, 1973; Philippot, 1993), release of brines and CO₂ from deep-crustal intrusions (Hansen et al., 1995), and loss of H₂O to retrograde rehydration reactions (Mark et al., 1998).

4.6.10 Concluding Remarks

The concerted efforts of a diverse spectrum of Earth scientists have made it possible to estimate the amounts of fluid that flow through the continental lithosphere during mountain building and constrain the processes, timescales, and directions of fluid motion. Progress to date has been substantial, but many fundamental questions remain. For example, how deep do surficial waters penetrate into metamorphic belts? How do large fluid fluxes modify the chemical and isotopic composition of the crust and influence regional thermal structure? What are the directions and fluxes of fluid in deeply subducted crust and ultrahigh-pressure metamorphic rocks? What fraction of this deep fluid enters the mantle (see Chapter 3.11), and how does it influence the chemistry and isotopic systematics of mantle-derived melts? Time-integrated fluxes can be estimated, but over what timescales are the fluids evolved? Is the devolatilization slow and continuous, or rapid and pulsed? Rapid CO₂ release, for instance, may perturb the climate system toward higher global average temperatures (Kerrick and Caldeira, 1998), whereas long-term sequestering of CO₂ may lead to cooling (Selverstone and Gutzler, 1993). Emerging evidence indicates that rapid CO₂ release from both contact metamorphic (Svensen and Jamtveit, 2010) and regional metamorphic (Skelton, 2011) environments may play significant roles in global carbon cycling.

Acknowledgments

I would like to thank D.M. Rye, M.T. Brandon, B.J. Skinner, K. K. Turekian, J. Park, Z. Wang, E. F. Baxter, E.W. Bolton, C.M.

Breeding, C.E. Bucholz, C.J. Carson, J.O. Eckert, S. Emmanuel, A. Lüttge, T. Lyubetskaya, R.L. Masters, J.L.M. van Haren, S.H. Vorhies, and D.E. Wilbur for stimulating discussions and collaborations over the course of the past two decades at Yale. R.L. Rudnick and B.A. Wing provided thoughtful and constructive reviews. The support from Department of Energy grant DE-FG02-01ER15216 and National Science Foundation grants EAR-0105927, 0509934, 0744154, 0948092, and 1250269 is gratefully acknowledged.

References

- Abart R and Pozzorini D (2000) Implications of kinetically controlled mineral–fluid exchange on the geometry of stable isotope fronts. *European Journal of Mineralogy* 12: 1069–1082.
- Abart R and Sperb R (1997) Grain-scale stable isotope disequilibrium during fluid–rock interaction. 1: Series approximations for advective-dispersive transport and first-order kinetic mineral–fluid exchange. *American Journal of Science* 297: 679–706.
- Ague JJ (1991) Evidence for major mass transfer and volume strain during regional metamorphism of pelites. *Geology* 19: 855–858.
- Ague JJ (1994a) Mass transfer during Barrovian metamorphism of pelites, south-central Connecticut. I: Evidence for changes in composition and volume. *American Journal of Science* 294: 1061–1134.
- Ague JJ (1994b) Mass transfer during Barrovian metamorphism of pelites, south-central Connecticut. II: Channelized fluid flow and the growth of staurolite and kyanite. *American Journal of Science* 294: 1061–1134.
- Ague JJ (1995) Deep crustal growth of quartz, kyanite, and garnet into large aperture, fluid-filled fractures, north-eastern Connecticut, USA. *Journal of Metamorphic Geology* 13: 299–314.
- Ague JJ (1997a) Crustal mass transfer and index mineral growth in Barrow's garnet zone, northeast Scotland. *Geology* 25: 73–76.
- Ague JJ (1997b) Compositional variations in metamorphosed sediments of the Littleton Formation, New Hampshire (Discussion). *American Journal of Science* 297: 440–449.
- Ague JJ (1998) Simple models of coupled fluid infiltration and redox reactions in the crust. *Contributions to Mineralogy and Petrology* 132: 180–197.
- Ague JJ (2000) Release of CO₂ from carbonate rocks during regional metamorphism of lithologically heterogeneous crust. *Geology* 28: 1123–1126.
- Ague JJ (2002) Gradients in fluid composition across metacarbonate layers of the Wepawaug Schist, Connecticut, USA. *Contributions to Mineralogy and Petrology* 143: 38–55.
- Ague JJ (2003) Fluid infiltration and the transport of major, minor, and trace elements during regional metamorphism of carbonate rocks, Wepawaug Schist, Connecticut, USA. *American Journal of Science* 303: 753–816.
- Ague JJ (2007) Models of permeability contrasts in subduction zone mélange: Implications for gradients in fluid fluxes, Syros and Tinos Islands, Greece. *Chemical Geology* 239: 217–227.
- Ague JJ (2011) Extreme channelization of fluid and the problem of element mobility during Barrovian metamorphism. *American Mineralogist* 96: 333–352.
- Ague JJ and Baxter EF (2007) Brief thermal pulses during mountain building recorded by Sr diffusion in apatite and multicomponent diffusion in garnet. *Earth and Planetary Science Letters* 261: 500–516.
- Ague JJ, Baxter EF, and Eckert JO Jr. (2001) High *f*_{O₂} during sillimanite zone metamorphism of part of the Barrovian type locality, Glen Clova, Scotland. *Journal of Petrology* 42: 1301–1320.
- Ague JJ, Park JJ, and Rye DM (1998) Regional metamorphic dehydration and seismic hazard. *Geophysical Research Letters* 25: 4221–4224.
- Ague JJ and Rye DM (1999) Simple models of CO₂ release from metacarbonates with implications for interpretation of directions and magnitudes of fluid flow in the deep crust. *Journal of Petrology* 40: 1443–1462.
- Aharonov E, Whitehead JA, Kelemen PB, and Spiegelman M (1995) Channeling instability of upwelling melt in the mantle. *Journal of Geophysical Research* 100: 20433–20450.
- Anderson GM and Burnham CW (1965) The solubility of quartz in supercritical water. *American Journal of Science* 263: 494–511.
- Antignano A and Manning CE (2008a) Rutile solubility in H₂O, H₂O–SiO₂, and H₂O–NaAlSi₃O₈ fluids at 0.7–2.0 GPa and 700–1000 °C: Implications for mobility of nominally insoluble elements. *Chemical Geology* 255: 283–293.

- Antignano A and Manning CE (2008b) Fluorapatite solubility in H₂O and H₂O–NaCl at 700–900 °C 0.7–2.0 GPa. *Chemical Geology* 251: 112–119.
- Aranovich LY and Newton RC (1996) H₂O activity in concentrated NaCl solutions at high pressures and temperatures measured by the brucite-periclase equilibrium. *Contributions to Mineralogy and Petrology* 125: 200–212.
- Aranovich LY and Newton RC (1997) H₂O activity in concentrated KCl and KCl–NaCl solutions at high temperatures and pressures measured by the brucite-periclase equilibrium. *Contributions to Mineralogy and Petrology* 127: 261–271.
- Aranovich LY and Newton RC (1998) Reversed determination of the reaction: Phlogopite + quartz = enstatite + potassium feldspar + H₂O in the ranges 750–875 °C and 2–12 kbar at low H₂O activity with concentrated KCl solutions. *American Mineralogist* 127: 261–271.
- Aranovich LY and Newton RC (1999) Experimental determination of CO₂–H₂O activity–composition relations at 600–1000 °C and 6–14 kbar by reversed decarbonation and dehydration reactions. *American Mineralogist* 84: 1319–1332.
- Audétat A and Keppler H (2005) Solubility of rutile in subduction zone fluids, as determined by experiments in the hydrothermal diamond anvil cell. *Earth and Planetary Science Letters* 232: 393–402.
- Austrheim H (1987) Eclogitization of lower crustal granulites by fluid migration through shear zones. *Earth and Planetary Science Letters* 81: 221–232.
- Austrheim H (1990) The granulite–eclogite facies transition: A comparison of experimental work and a natural occurrence in the Bergen Arcs, western Norway. *Lithos* 25: 163–169.
- Ayers JC and Watson EB (1991) Solubility of apatite, monazite, zircon, and rutile in supercritical aqueous fluids with implications for subduction zone geochemistry. *Philosophical Transactions of the Royal Society of London Series A* 335: 365–375.
- Ayers JC and Watson EB (1993) Rutile solubility and mobility in supercritical aqueous fluids. *Contributions to Mineralogy and Petrology* 114: 321–330.
- Baker AJ (1990) Stable isotopic evidence for fluid–rock interactions in the Ivrea zone, Italy. *Journal of Petrology* 31: 243–260.
- Baker J and Spiegelman M (1995) Modelling an infiltration-driven geochemical front. *Earth and Planetary Science Letters* 136: 87–96.
- Balashov VN and Yardley BWD (1998) Modeling metamorphic fluid flow with reaction–compaction–permeability feedbacks. *American Journal of Science* 298: 441–470.
- Baldwin SL, Lister GS, Hill EJ, Foster DA, and McDougall I (1993) Thermochronologic constraints on the tectonic evolution of active metamorphic core complexes, D'Entrecasteaux Islands, Papua New Guinea. *Tectonics* 12: 611–628.
- Barnicoat AC and Cartwright I (1995) Focused fluid flow during subduction: Oxygen isotope data from high-pressure ophiolites of the western Alps. *Earth and Planetary Science Letters* 132: 53–61.
- Barrow G (1893) On an intrusion of muscovite–biotite gneiss in the south-eastern Highlands of Scotland, and its accompanying metamorphism. *Quarterly Journal of the Geological Society of London* 49: 330–354.
- Baumgartner LP and Ferry JM (1991) A model for coupled fluid-flow and mixed-volatile mineral reactions with applications to regional metamorphism. *Contributions to Mineralogy and Petrology* 106: 273–285.
- Baumgartner LP, Gerdes ML, Person MA, and Roselle GT (1997) Porosity and permeability of carbonate rocks during contact metamorphism. In: Jamveit B and Yardley BWD (eds.) *Fluid Flow and Transport in Rocks: Mechanisms and Effects*, pp. 83–98. London: Chapman and Hall.
- Baumgartner LP and Olsen SN (1995) A least-squares approach to mass transport calculations using the isocoen method. *Economic Geology* 90: 1261–1270.
- Baxter EF, Ague JJ, and DePaolo DJ (2002) Prograde temperature–time evolution in the Barrovian type-locality constrained by Sm/Nd garnet ages from Glen Clova, Scotland. *Journal of the Geological Society (London)* 159: 71–82.
- Baxter EF and DePaolo DJ (2000) Field measurement of slow metamorphic reaction rates at temperatures of 500° to 600 °C. *Science* 288: 1411–1414.
- Baxter EF and DePaolo DJ (2002a) Field measurement of high temperature bulk reaction rates I: Theory and technique. *American Journal of Science* 302: 442–464.
- Baxter EF and DePaolo DJ (2002b) Field measurement of high temperature bulk reaction rates II: Interpretation of results from a field site near Simplon Pass, Switzerland. *American Journal of Science* 302: 465–516.
- Bear J (1972) *Dynamics of Fluids in Porous Media*. New York: Dover.
- Bebout GE and Barton MD (1989) Fluid flow and metasomatism in a subduction zone hydrothermal system: Catalina Schist terrane, California. *Geology* 17: 976–980.
- Bebout GE and Barton MD (1993) Metasomatism during subduction: Products and possible path in the Catalina Schist, California. *Chemical Geology* 108: 61–91.
- Bebout GE and Barton MD (2002) Tectonic and metasomatic mixing in a high-T, subduction-zone mélange – Insights into the geochemical evolution of the slab–mantle interface. *Chemical Geology* 187: 79–106.
- Becker H, Jochum HP, and Carlson RW (1999) Constraints from high-pressure veins in eclogites on the composition of hydrous fluids in subduction zones. *Chemical Geology* 160: 291–308.
- Beitter T, Wagner T, and Markl G (2008) Formation of kyanite–quartz veins of the Alpe Sponda, Central Alps, Switzerland: Implications for Al transport during regional metamorphism. *Contributions to Mineralogy and Petrology* 156: 689–707.
- Berner RA (1980) *Early Diagenesis: A Theoretical Approach*. Princeton, New Jersey: Princeton University Press.
- Bickle MJ (1992) Transport mechanisms by fluid flow in metamorphic rocks: Oxygen and strontium decoupling in the Trois Seigneurs Massif – A consequence of kinetic dispersion? *American Journal of Science* 292: 289–316.
- Bickle MJ and Baker J (1990) Advective–diffusive transport of isotopic fronts: An example from Naxos, Greece. *Earth and Planetary Science Letters* 97: 78–93.
- Bickle MJ, Chapman HJ, Ferry JM, Rumble D III, and Fallick AE (1997) Fluid flow and diffusion in the Waterville Limestone, south-central Maine: Constraints from strontium, oxygen, and carbon isotope profiles. *Journal of Petrology* 38: 1489–1512.
- Bickle MJ and McKenzie D (1987) The transport of heat and matter by fluids during metamorphism. *Contributions to Mineralogy and Petrology* 95: 384–392.
- Blattner P and Lassey KR (1989) Stable isotope exchange fronts, Damköhler numbers and fluid to rock ratios. *Chemical Geology* 78: 381–392.
- Blencoe JG, Seitz JC, and Anovitz LM (1999) The CO₂–H₂O system II. Calculated thermodynamic mixing properties for 400 °C, 0–400 MPa. *Geochimica et Cosmochimica Acta* 63: 2393–2408.
- Bolton EW, Lasaga AC, and Rye DM (1999) Long-term flow/chemistry feedback in a porous medium with heterogeneous permeability: Kinetic control of dissolution and precipitation. *American Journal of Science* 299: 1–68.
- Boucher DF and Alves GE (1959) Dimensionless numbers for fluid mechanics, heat transfer, mass transfer, and chemical reaction. *Chemical Engineering Progress* 55: 55–64.
- Bouihol P, Connolly JAD, and Burg J (2011) Geological evidence and modeling of melt migration by porosity waves in the sub-arc mantle of Kohistan (Pakistan). *Geology* 39: 1091–1094.
- Bowman JR, Willett SD, and Cook SJ (1994) Oxygen isotopic transport and exchange during fluid flow: One-dimensional models and applications. *American Journal of Science* 294: 1–55.
- Brace WF (1980) Permeability of crystalline and argillaceous rocks. *International Journal of Rock Mechanics and Mining Sciences and Geomechanics Abstracts* 17: 241–251.
- Brace WF (1984) Permeability of crystalline rocks: New in situ measurements. *Journal of Geophysical Research* 89: 4327–4330.
- Brady JB (1977) Metasomatic zones in metamorphic rocks. *Geochimica et Cosmochimica Acta* 41: 113–125.
- Brady JB (1988) The role of volatiles in the thermal history of metamorphic terranes. *Journal of Petrology* 29: 1187–1213.
- Breeding CM and Ague JJ (2002) Slab-derived fluids and quartz-vein formation in an accretionary prism, Otago Schist, New Zealand. *Geology* 30: 499–502.
- Breeding CM, Ague JJ, Bröcker M, and Bolton EW (2003) Blueschist preservation in a retrograded HP–LT terrane, Tinos, Greece: Implications for fluid flow paths in subduction zones. *Geochemistry, Geophysics, and Geosystems* 4: 9002. <http://dx.doi.org/10.1029/2002GC000380>, 11 p.
- Breeding CM, Ague JJ, and Bröcker M (2004a) Fluid–metasedimentary rock interactions and the chemical composition of arc magmas. *Geology* 32: 1041–1044.
- Breeding CM, Ague JJ, Grove M, and Rupke AL (2004b) Isotopic and chemical alteration of zircon by metamorphic fluids: U–Pb age depth-profiling of zircon crystals from Barrow's garnet zone, northeast Scotland. *American Mineralogist* 89: 1067–1077.
- Brimhall GH (1979) Lithologic determination of mass transfer mechanisms of multiple-stage porphyry copper mineralization at Butte, Montana: Vein formation by hypogene leaching and enrichment of potassium silicate protore. *Economic Geology* 74: 556–589.
- Bröcker M and Enders M (2001) Unusual bulk-rock compositions in eclogite-facies rocks from Syros and Tinos (Cyclades, Greece): Implications for U–Pb zircon geochronology. *Chemical Geology* 175: 581–603.
- Bröcker M, Kreuzer H, Matthews A, and Okrusch M (1993) ⁴⁰Ar/³⁹Ar and oxygen isotope studies of polymetamorphism from Tinos Island, Cycladic blueschist belt, Greece. *Journal of Metamorphic Geology* 11: 223–240.
- Bucholz CE and Ague JJ (2010) Fluid flow and Al transport during quartz–kyanite vein formation, Unst, Shetland Islands, Scotland. *Journal of Metamorphic Geology* 28: 19–39.
- Bureau H and Keppler H (1999) Complete miscibility between silicate melts and hydrous fluids in the upper mantle: Experimental evidence and geochemical implications. *Earth and Planetary Science Letters* 165: 187–196.

- Camacho A, Lee JKW, Hensen BJ, and Braun J (2005) Short-lived orogenic cycles and the eclogitization of cold crust by spasmodic hot fluids. *Nature* 435: 1191–1196.
- Carlson WD (1989) The significance of intergranular diffusion to the mechanisms and kinetics of porphyroblast crystallization. *Contributions to Mineralogy and Petrology* 103: 1–24.
- Carlson WD (2010) Dependence of reaction kinetics on H₂O activity as inferred from rates of intergranular diffusion of aluminum. *Journal of Metamorphic Geology* 28: 735–752.
- Carpenter RA (1974) Pyrrhotite isograd in southeastern Tennessee and southwestern North Carolina. *Geological Society of America Bulletin* 85: 451–456.
- Carson CJ, Ague JJ, Grove M, Coath CD, and Harrison TM (2002) U–Pb isotopic behavior of zircon during upper-amphibolite facies fluid infiltration in the Napier Complex, east Antarctica. *Earth and Planetary Science Letters* 199: 287–310.
- Cartwright I and Oliver NHS (1994) Fluid flow during contact metamorphism at Mary Kathleen, Queensland, Australia. *Journal of Petrology* 35: 1493–1521.
- Cartwright I, Vry J, and Sandiford M (1995) Changes in stable isotope ratios of metapelites and marbles during regional metamorphism, Mount Lofty Ranges, South Australia: Implications for crustal scale fluid flow. *Contributions to Mineralogy and Petrology* 120: 292–310.
- Carlos EJ, Gilley LD, and Harrison TM (2002) Interpretation of monazite ages obtained via in situ analysis. *Chemical Geology* 88: 193–215.
- Carlos EJ and Sorensen SS (2003) Phengite-based chronology of K- and Ba-rich fluid flow in two paleosubduction zones. *Science* 299: 92–95.
- Chamberlain CP and Conrad ME (1991) The relative permeabilities of quartzites and schists during active metamorphism at midcrustal levels. *Geophysical Research Letters* 18: 959–962.
- Chamberlain CP and Rumble D (1988) Thermal anomalies in a regional metamorphic terrane: An isotopic study of the role of fluids. *Journal of Petrology* 29: 1215–1232.
- Chamberlain CP and Rumble D (1989) The influence of fluids on the thermal history of a metamorphic terrain: New Hampshire, USA. In: Daly JS, Cliff RA, and Yardley BWD (eds.) *Evolution of Metamorphic Belts*, vol. 43, pp. 203–213. London: Geological Society Special Publication.
- Chernoff CB and Carlson WD (1997) Disequilibrium for Ca during growth of pelitic garnet. *Journal of Metamorphic Geology* 15: 421–438.
- Christensen JN, Rosenfeld JL, and DePaolo DJ (1989) Rates of tectonometamorphic processes from rubidium and strontium isotopes in garnet. *Science* 224: 1465–1469.
- Christensen JN, Selverstone J, Rosenfeld J, and DePaolo DJ (1994) Correlation by Rb–Sr geochronology of garnet growth histories from different structural levels within the Tauern Window, Eastern Alps. *Contributions to Mineralogy and Petrology* 118: 1–12.
- Coleman RG and Lee DE (1963) Glaucophane-bearing metamorphic rock types of the Cazadero area, California. *Journal of Petrology* 4: 260–301.
- Connolly JAD (1990) Multivariable phase diagrams: An algorithm based on generalized thermodynamics. *American Journal of Science* 290: 666–718.
- Connolly JAD (1995) Phase diagram methods for graphitic rocks and application to the system C–O–H–FeO–TiO₂–SiO₂. *Contributions to Mineralogy and Petrology* 119: 94–116.
- Connolly JAD (1997) Devolatilization-generated fluid pressure and deformation-propagated fluid flow during prograde regional metamorphism. *Journal of Geophysical Research* 102: 18149–18173.
- Connolly JAD (2010) The mechanics of metamorphic fluid expulsion. *Elements* 6: 165–172.
- Connolly JAD and Podladchikov YY (1998) Compaction-driven fluid flow in viscoelastic rock. *Geodinamica Acta* 11: 55–84.
- Connolly JAD and Podladchikov YY (2007) Decompaction weakening and channeling instability in ductile porous media: Implications for asthenospheric melt segregation. *Journal of Geophysical Research* 112: B10205. <http://dx.doi.org/10.1029/2005JB004213>.
- Connolly J and Thompson A (1989) Fluid and enthalpy production during regional metamorphism. *Contributions to Mineralogy and Petrology* 102: 347–366.
- Cook SJ, Bowman JR, and Forster CB (1997) Contact metamorphism surrounding the Alta Stock; finite element model simulation of heat- and ¹⁸O/¹⁶O mass-transport during prograde metamorphism. *American Journal of Science* 297: 1–55.
- Cox SF (2007) Structural and isotopic constraints on fluid flow regimes and fluid pathways during upper crustal deformation: An example from the Taemas area of the Lachlan Orogen, SE Australia. *Journal of Geophysical Research* 112: B08208. <http://dx.doi.org/10.1029/2006JB004734>.
- Cox SF and Etheridge MA (1989) Coupled grain-scale dilatancy and mass transfer during deformation at high pressures: Examples from Mt. Lyell, Tasmania. *Journal of Structural Geology* 11: 147–162.
- Craw D and Norris RJ (1991) Metamorphogenic Au–W veins and regional tectonics: Mineralisation throughout the uplift history of the Haast Schist, New Zealand. *New Zealand Journal of Geology and Geophysics* 34: 373–383.
- Crawford ML and Hollister LS (1986) Metamorphic fluids, the evidence from fluid inclusions. In: Walther JV and Wood BJ (eds.) *Fluid–rock interactions during metamorphism*, pp. 1–35. New York: Springer-Verlag.
- Cruz-Uribe AM, Zack T, Feineman MD, and Barth MG (2010) *Trace Element Mobility During Rutile Replacement by Titanite: Open vs. Closed System Examples from the Franciscan Complex, CA*. Washington, DC: American Geophysical Union, Abstract V31D-06.
- Dasgupta S, Chakraborty S, and Neogi S (2009) Petrology of an inverted Barrovian sequence of metapelites in Sikkim Himalaya, India: Constraints on the tectonics of inversion. *American Journal of Science* 309: 43–84.
- David C, Wong T, Zhu W, and Zhang J (1994) Laboratory measurement of compaction-induced permeability change in porous rock: Implications for the generation and maintenance of pore pressure excess in the crust. *Pure and Applied Geophysics* 143: 425–456.
- Davis TL and Namson JS (1994) A balanced cross-section of the 1994 Northridge earthquake, southern California. *Nature* 372: 167–169.
- de Capitani C and Petrakakis K (2010) The computation of equilibrium assemblage diagrams with Theriak/Domino software. *American Mineralogist* 95: 1006–1016.
- DeGroot SR and Mazur P (1969) *Non-equilibrium Thermodynamics*. Amsterdam: North Holland Publications.
- DePaolo DJ and Getty SR (1996) Models of isotope exchange in reactive fluid–rock systems: Implications for geochronology in metamorphic rocks. *Geochimica et Cosmochimica Acta* 60: 3933–3947.
- Dewey JF (2005) Orogeny can be very short. *Proceedings of the National Academy of Sciences* 102: 15286–15293.
- Diakonov I, Pokrovski G, Schott J, Castet S, and Gout R (1996) An experimental and computational study of sodium–aluminum complexing in crustal fluids. *Geochimica et Cosmochimica Acta* 60: 197–211.
- Dipple GM and Ferry JM (1992a) Metasomatism and fluid flow in ductile fault zones. *Contributions to Mineralogy and Petrology* 112: 149–164.
- Dipple GM and Ferry JM (1992b) Fluid flow and stable isotopic alteration in rocks at elevated temperatures with applications to metamorphism. *Geochimica et Cosmochimica Acta* 56: 3539–3550.
- Dipple GM and Wintsch RP (1990) Identification of the scales of differential element mobility in a ductile fault zone. *Journal of Metamorphic Geology* 8: 645–661.
- Dixon JE and Ridley JR (1987) Syros. In: Helgeson HC (ed.) *Chemical Transport in Metasomatic Processes*, pp. 489–501. Boston: Reidel.
- Dohmen R and Chakraborty S (2003) Mechanism and kinetics of element and isotopic exchange mediated by a fluid phase. *American Mineralogist* 88: 1251–1270.
- Dolejš D and Manning CE (2010) Thermodynamic model for mineral solubility in aqueous fluids: Theory, calibration and application to model fluid-flow systems. *Geofluids* 10: 20–40.
- Duan Z, Moller N, and Weare JH (1995) Equation of state for the NaCl–H₂O–CO₂ system: Prediction of phase equilibria and volumetric properties. *Geochimica et Cosmochimica Acta* 59: 2869–2882.
- Dumond P, McLean N, Williams ML, Jercinovic MJ, and Bowring SA (2008) High-resolution dating of granite petrogenesis and deformation in a lower crustal shear zone: Athabasca granulite terrane, western Canadian Shield. *Chemical Geology* 254: 175–196.
- Elias BP and Hajash A Jr. (1992) Changes in quartz solubility and porosity due to effective stress: An experimental investigation of pressure solution. *Geology* 20: 451–454.
- England PC and Thompson AB (1984) Pressure–temperature–time paths of regional metamorphism. I. Heat transfer during the evolution of regions of thickened continental crust. *Journal of Petrology* 25: 894–928.
- Ernst WG and Banno S (1991) Neoblastic jadeitic pyroxene in Franciscan metagreywackes from Pacheco Pass, central Diablo Range, California, and implications for the inferred metamorphic P–T trajectory. *New Zealand Journal of Geology and Geophysics* 34: 285–292.
- Etheridge MA (1983) Differential stress magnitudes during regional deformation and metamorphism: Upper bound imposed by tensile fracturing. *Geology* 11: 213–234.
- Etheridge MA, Wall VJ, Cox SF, and Vernon RH (1984) High fluid pressures during regional metamorphism and deformation. *Journal of Geophysical Research* 89: 4344–4358.
- Etheridge MA, Wall VJ, and Vernon RH (1983) The role of the fluid phase during regional metamorphism and deformation. *Journal of Metamorphic Geology* 1: 205–226.
- Evans KA and Bickle MJ (1999) Determination of time-integrated metamorphic fluid fluxes from the reaction progress of multivariant assemblages. *Contributions to Mineralogy and Petrology* 134: 277–293.
- Farquhar J and Chacko T (1991) Isotopic evidence for involvement of CO₂-bearing magmas in granulite formation. *Nature* 354: 60–63.

- Feehan JG and Brandon MT (1999) Contribution of ductile flow to exhumation of low-temperature, high-pressure metamorphic rocks: San Juan-Cascade nappes, NW Washington State. *Journal of Geophysical Research* 104: 10883–10902.
- Ferry JM (1983) On the control of temperature, fluid composition, and reaction progress during metamorphism. *American Journal of Science* 283-A: 201–232.
- Ferry JM (1987) Metamorphic hydrology at 13-km depth and 400–500 °C. *American Mineralogist* 72: 39–58.
- Ferry JM (1992) Regional metamorphism of the Waits River Formation, eastern Vermont: Delineation of a new type of giant metamorphic hydrothermal system. *Journal of Petrology* 33: 45–94.
- Ferry JM (1994a) Overview of the petrologic record of fluid flow during regional metamorphism in northern New England. *American Journal of Science* 294: 905–988.
- Ferry JM (1994b) A historical review of metamorphic fluid flow. *Journal of Geophysical Research* 99: 15487–15498.
- Ferry JM (1996) Prograde and retrograde fluid flow during contact metamorphism of siliceous carbonate rocks from the Ballachulish aureole, Scotland. *Contributions to Mineralogy and Petrology* 124: 235–254.
- Ferry JM (2008) The role of volatile transport by diffusion and dispersion in driving biotite-forming reactions during regional metamorphism of the Gile Mountain Formation, Vermont. *American Mineralogist* 92: 1288–1302.
- Ferry JM and Baumgartner LP (1987) Thermodynamic models of molecular fluids at the elevated pressures and temperatures of crustal metamorphism. In: Carmichael ISE and Eugster HP (eds.) *Thermodynamic Modeling of Geological Materials: Minerals, Fluids, and Melts. Reviews in Mineralogy*, vol. 17, pp. 323–365. Freiburg, Germany: Mineralogical Society of America.
- Ferry JM and Dipple GM (1991) Fluid flow, mineral reactions, and metasomatism. *Geology* 19: 211–214.
- Ferry JM and Gerdes ML (1998) Chemically reactive fluid flow during metamorphism. *Annual Review of Earth and Planetary Sciences* 26: 255–287.
- Ferry JM and Gottschalk M (2009) The effect of fluid salinity on infiltration-driven contact metamorphism of carbonate rocks. *Contributions to Mineralogy and Petrology* 158: 619–636.
- Ferry JM, Ushikubo T, Kita NT, and Valley JW (2010) Assessment of grain-scale homogeneity and equilibration of carbon and oxygen isotope compositions of minerals in carbonate-bearing metamorphic rocks by ion microprobe. *Geochimica et Cosmochimica Acta* 74: 6517–6540.
- Fisher DM and Brantley SL (1992) Models of quartz overgrowth and vein formation: Deformation and episodic fluid flow in an ancient subduction zone. *Journal of Geophysical Research* 97: 20043–20061.
- Fisher GW and Elliott D (1973) Criteria for quasi-steady diffusion and local equilibrium in metamorphism. In: Hoffman AW, Gilotti BJ, Yoder HS Jr., and Yund RA (eds.) *Geochemical Transport and Kinetics. Carnegie Institution of Washington Publication* 634, pp. 231–241. Washington, DC: Carnegie Institution of Washington.
- Fletcher RC and Hofmann AW (1973) Simple models of diffusion and combined diffusion–infiltration metasomatism. In: Gilotti BJ, Yoder HS Jr., and Yund RA (eds.) *Geochemical Transport and Kinetics. Carnegie Institution of Washington Publication* 634, pp. 243–259. Washington, DC: Carnegie Institution of Washington.
- Freeze RA and Cherry JA (1979) *Groundwater*. New York: Prentice-Hall.
- French BM (1966) Some geological implications of equilibrium between graphite and a C–O–H gas phase at high temperatures and pressures. *Reviews of Geophysics* 4: 223–253.
- Friedl JJ and Combarous MA (1971) Dispersion in porous media. In: Chow VT (ed.) *Advances in Hydroscience*, vol. 7, pp. 170–282. New York: Academic Press.
- Frost BR and Frost CD (1987) CO₂, melts and granulite metamorphism. *Nature* 327: 503–506.
- Fu B, Valley JW, Kita NT, et al. (2010) Multiple origins of zircons in jadeitite. *Contributions to Mineralogy and Petrology* 159: 769–780.
- Fyfe WS (1973) The granulite facies, partial melting and the Archean crust. *Philosophical Transactions of the Royal Society of London Series A* 273: 457–461.
- Fyfe WS, Price NJ, and Thompson AB (1978) *Fluids in the Earth's crust*. Amsterdam: Elsevier.
- Ganor JA, Matthews A, and Paldor N (1989) Constraints on effective diffusivity during oxygen isotope exchange at a marble–schist contact, Sifnos (Cyclades), Greece. *Earth and Planetary Science Letters* 94: 208–216.
- Ganor J, Matthews A, Schliestedt M, and Garfunkel Z (1996) Oxygen isotope heterogeneities of metamorphic rocks: An original tectonostratigraphic signature, or an imprint of exotic fluids? A case study of Sifnos and Tinos Islands (Greece). *European Journal of Mineralogy* 8: 719–731.
- Gao J, John T, Klemd R, and Xiong X (2007) Mobilization of Ti–Nb–Ta during subduction: Evidence from rutile-bearing dehydration segregations and veins hosted in eclogite, Tianshan, NW China. *Geochimica et Cosmochimica Acta* 71: 4974–4996.
- Garven G and Freeze AR (1984a) Theoretical analysis of the role of groundwater flow in the genesis of stratabound ore deposits. 1. Mathematical and numerical model. *American Journal of Science* 284: 1085–1124.
- Garven G and Freeze AR (1984b) Theoretical analysis of the role of groundwater flow in the genesis of stratabound ore deposits. 2. Quantitative results. *American Journal of Science* 284: 1125–1174.
- Gerya TV, Perchuk LL, Maresch WV, Willner AP, Van Reenen DD, and Smit CA (2002) Thermal regime and gravitational instability of multi-layered continental crust: Implications for the buoyant exhumation of high-grade metamorphic rocks. *European Journal of Mineralogy* 14: 687–699.
- Getty S and Selverstone J (1994) Stable isotope and trace element evidence for restricted fluid migration in 2 GPa eclogites. *Journal of Metamorphic Geology* 12: 747–760.
- Gieré R (1990) Hydrothermal mobility of Ti, Zr, and REE: Examples from the Bergell and Adamello contact aureoles (Italy). *Terra Nova* 2: 60–67.
- Gieré R (1993) Transport and deposition of REE in H₂S-rich fluids – Evidence from accessory mineral assemblages. *Chemical Geology* 110: 251–268.
- Gieré R and Williams CT (1992) REE-bearing minerals in a Ti-rich vein from the Adamello contact aureole (Italy). *Contributions to Mineralogy and Petrology* 112: 83–100.
- Giorgetti G, Tropper P, Essene EJ, and Peacor DR (2000) Characterization of non-equilibrium and equilibrium occurrences of paragonite/muscovite intergrowths in an eclogite from the Sesia-Lanzo Zone (Western Alps, Italy). *Contributions to Mineralogy and Petrology* 138: 326–336.
- Graf DL, Anderson DE, and Woodhouse JE (1983) Ionic diffusion in naturally-occurring aqueous solutions: Transition-state models that use either empirical expressions or statistically-derived relationships to predict mutual diffusion coefficients in the concentrated-solution regions of 8 binary systems. *Geochimica et Cosmochimica Acta* 47: 1985–1998.
- Graham CM, Valley JW, Eiler JM, and Wada H (1998) Timescales and mechanisms of fluid infiltration in a marble: An ion microprobe study. *Contributions to Mineralogy and Petrology* 132: 371–389.
- Grant JA (1986) The isocon diagram—a simple solution to Gresens' equation for metasomatic alteration. *Economic Geology* 81: 1976–1982.
- Grauch RI (1989) Rare earth elements in metamorphic rocks. In: Lipin BR and McKay GA (eds.) *Geochemistry and Mineralogy of Rare Earth Elements. Reviews in Mineralogy*, vol. 21, pp. 147–167. Washington, DC: Mineralogical Society of America.
- Greenwood HJ (1975) Buffering of pore fluids by metamorphic reactions. *American Journal of Science* 275: 573–593.
- Gresens RL (1967) Composition–volume relations of metasomatism. *Chemical Geology* 2: 47–65.
- Guenther RB and Lee JW (1988) *Partial Differential Equations of Mathematical Physics and Integral Equations*. Englewood Cliffs, NJ: Prentice-Hall.
- Haar C, Gallagher JS, and Kell GS (1984) *NBS/NRC Steam Tables*. Washington, DC: Hemisphere.
- Hansen EC, Newton RC, Janardhan AS, and Lindenberg S (1995) Differentiation of Late Archean crust in the Eastern Dharwar Craton, South India. *Journal of Geology* 103: 629–651.
- Hanson RB (1997) Hydrodynamics of regional metamorphism due to continental collision. *Economic Geology* 92: 880–891.
- Harlov DE, Hansen EC, and Bigler C (1998) Petrologic evidence for K-feldspar metasomatism in granulite facies rocks. *Chemical Geology* 151: 373–376.
- Harlov DE, Newton RC, Hansen EC, and Janardhan AS (1997) Oxide and sulfide minerals in highly oxidized, Rb-depleted, Archean granulites of the Shevaroy Hills massif, South India: Oxidation states and the role of metamorphic fluids. *Journal of Metamorphic Geology* 15: 701–717.
- Harlov DE, Wirth W, and Förster H-J (2005) An experimental study of dissolution–reprecipitation in fluorapatite: Fluid infiltration and the formation of monazite. *Contributions to Mineralogy and Petrology* 150: 268–286.
- Hauzenberger CA, Baumgartner LP, and Pak TM (2001) Experimental study on the solubility of the “model”-pelite mineral assemblage albite + K-feldspar + andalusite + quartz in supercritical chloride-rich aqueous solutions at 0.2 GPa and 600 °C. *Geochimica et Cosmochimica Acta* 65: 4493–4507.
- Hawkesworth CJ, Turner SP, McDermott F, Peate DW, and van Calsteren P (1997) U–Th isotopes in arc magmas: Implications for element transfer from the subducted crust. *Science* 276: 551–555.
- Heaman LM, Creaser RA, and Cookenboo HO (2002) Extreme enrichment of high field strength elements in Jericho eclogite xenoliths: A cryptic record of Paleoproterozoic subduction, partial melting, and metasomatism beneath the Slave craton, Canada. *Geology* 30: 507–510.
- Heinrich W, Churakov SS, and Gottschalk M (2004) Mineral–fluid equilibria in the system CaO–MgO–SiO₂–H₂O–CO₂–NaCl and the record of reactive fluid flow in contact metamorphic aureoles. *Contributions to Mineralogy and Petrology* 148: 131–149.

- Helgeson HC (1979) Mass transfer among minerals and hydrothermal solutions. In: Barnes HL (ed.) *Geochemistry of Hydrothermal Ore Deposits*, pp. 568–610. New York: John Wiley and Sons.
- Henry C, Burkhard M, and Goffé B (1996) Evolution of synmetamorphic veins and their wallrocks through a Western Alps transect: No evidence for large-scale fluid flow. Stable isotope, major- and trace-element systematics. *Chemical Geology* 127: 81–109.
- Hewitt DA (1973) The metamorphism of micaceous limestones from south-central Connecticut. *American Journal of Science* 273-A: 444–469.
- Himmelberg GR and Coleman RG (1968) Chemistry of primary minerals and rocks from the Red Mountain-Del Puerto ultramafic mass, California. *United States Geological Survey Professional Paper* 600-C, C18–C26.
- Hiraga T, Nishikawa O, Nagase T, and Akizuki M (2001) Morphology of intergranular pores and wetting angles in pelitic schists studied by transmission electron microscopy. *Contributions to Mineralogy and Petrology* 141: 613–622.
- Hoisch TD (1991) The thermal effects of pervasive and channelized fluid flow in the deep crust. *Journal of Geology* 99: 69–80.
- Holland TJB and Powell R (1991) A compensated Redlich–Kwong equation for volumes and fugacities of CO₂ and H₂O in the range 1 bar to 50 kbar and 100–1600 °C. *Contributions to Mineralogy and Petrology* 109: 265–273.
- Holland TJB and Powell R (1998) An internally consistent data set for phases of petrological interest. *Journal of Metamorphic Geology* 16: 309–343.
- Holland TJB and Powell R (2003) Activity–composition relations for phases in petrological calculations: An asymmetric multicomponent formulation. *Contributions to Mineralogy and Petrology* 145: 492–501.
- Hollister LS and Crawford ML (1981) *Fluid Inclusions: Applications to Petrology. Short Course Handbook*, vol. 6, 304 p. Calgary: Mineralogical Association of Canada.
- Hubbert MK and Willis DG (1957) Mechanics of hydraulic fracturing. *Transactions. American Institute of Mining, Metallurgical and Petroleum Engineers* 210: 153–168.
- Huenges E, Erzinger J, Kuck J, Engeser B, and Kessels W (1997) The permeable crust: Geohydraulic properties down to 9101 m depth. *Journal of Geophysical Research* 102: 18255–18265.
- Ingebritsen SE and Manning CE (1999) Geological implications of a permeability–depth curve for the continental crust. *Geology* 27: 1107–1110.
- Ingebritsen SE and Manning CE (2010) Permeability of the continental crust: Dynamic variations inferred from seismicity and metamorphism. *Geofluids* 10: 193–205.
- Jacobs GK and Kerrick DM (1981) Methane: An equation of state with application to the ternary system H₂O–CO₂–CH₄. *Geochimica et Cosmochimica Acta* 45: 607–614.
- Jamtveit B and Andersen TB (1992) Morphological instabilities during rapid growth of metamorphic garnets. *Physics and Chemistry of Minerals* 19: 176–184.
- Jamtveit B, Malthe-Sørenssen A, and Kostenko O (2008) Reaction enhanced permeability during retrogressive metamorphism. *Earth and Planetary Science Letters* 267: 620–627.
- Jia Y and Kerrick R (2000) Giant quartz vein systems in accretionary orogenic belts: The evidence for a metamorphic fluid origin from δ¹⁵N and δ¹³C studies. *Earth and Planetary Science Letters* 184: 211–224.
- Jiang SY, Wang RC, Xu XS, and Zhao KD (2005) Mobility of high field strength elements (HFSE) in magmatic-, metamorphic-, and submarine hydrothermal systems. *Physics and Chemistry of the Earth* 30: 1020–1029.
- Joesten RL and Fisher G (1988) Kinetics of diffusion-controlled mineral growth in the Christmas Mountains (Texas) contact aureole. *Geological Society of America Bulletin* 100: 714–732.
- John T, Gussone N, Podladchikov YY, et al. (2012) Volcanic arcs fed by rapid pulsed fluid flow through subducting slabs. *Nature Geoscience* 5: 489–492.
- John T, Klemd R, Gao J, and Garbe-Schönberg C-D (2008) Trace-element mobilization in slabs due to non steady-state fluid–rock interaction: Constraints from an eclogite facies transport vein in blueschist (Tianshan, China). *Lithos* 103: 1–24.
- Johnson MC and Plank T (1999) Dehydration and melting experiments constrain the fate of subducted sediments. *Geochemistry, Geophysics and Geosystems* 1, 1999GC000014.
- Kelemen PB and Matter J (2008) In situ carbonation of peridotite for CO₂ storage. *Proceedings of the National Academy of Sciences* 105: 17295–17300.
- Kennedy GC (1950) A portion of the system silica–water. *Economic Geology* 45: 629–653.
- Kerrick DM (1990) *The Al₂SiO₅ Polymorphs. Reviews in Mineralogy*, vol. 22, pp. 311–352. Washington, DC: Mineralogical Society of America.
- Kerrick DM and Caldeira K (1998) Metamorphic CO₂ degassing from orogenic belts. *Chemical Geology* 145: 213–232.
- Kerrick DM and Jacobs GK (1981) A modified Redlich–Kwong equation for H₂O, CO₂, and H₂O–CO₂ mixtures at elevated temperatures and pressures. *American Journal of Science* 281: 735–767.
- Kesson SE and Ringwood AE (1989) Slab–mantle interactions: 1. Sheared and refertilised garnet peridotite xenoliths – Samples of Wadati-Benioff zones? *Chemical Geology* 78: 83–96.
- King RL, Kohn MJ, and Eiler JM (2003) Constraints on the petrologic structure of the subduction zone slab–mantle interface from Franciscan Complex exotic ultramafic blocks. *Geological Society of America Bulletin* 115: 1097–1109.
- Kirschner DL, Sharp ZD, and Teyssier C (1993) Vein growth mechanisms and fluid sources revealed by oxygen isotope laser microprobe. *Geology* 21: 85–88.
- Kohn MJ, Valley JW, Eisenheimer D, and Spicuzza MJ (1993) Oxygen isotope zoning in garnet and staurolite: Evidence for closed system mineral growth during regional metamorphism. *American Mineralogist* 78: 988–1001.
- Konrad-Scholke M, Zack T, O'Brien PJ, and Barth M (2011) Fluid migration above a subducted slab — thermodynamic and trace element modelling of fluid–rock interaction in partially overprinted eclogite-facies rocks (Sesia Zone, Western Alps). *Earth and Planetary Science Letters* 311: 287–298.
- Koons PO and Craw D (1991) Evolution of fluid driving forces and composition within collisional orogens. *Geophysical Research Letters* 18: 935–938.
- Labotka TC, Cole DR, Fayek M, Riciputi LR, and Stadermann FJ (2004) Coupled cation and oxygen-isotope exchange between alkali feldspar and aqueous chloride solution. *American Mineralogist* 89: 1822–1825.
- Lamb W and Valley JW (1984) Metamorphism of reduced granulites in a low-CO₂ vapour-free environment. *Nature* 312: 56–58.
- Lancaster PJ, Baxter EF, Ague JJ, Breeding CM, and Owens TL (2008) Synchronous peak Barrovian metamorphism driven by syn-orogenic magmatism and fluid flow in southern Connecticut, USA. *Journal of Metamorphic Geology* 26: 527–538.
- Lapen TJ, Johnson CM, Baumgartner LP, Mahlen NJ, Beard BL, and Amato JM (2003) Burial rates during prograde metamorphism of an ultra-high-pressure terrane: An example from Lago di Cignana, western Alps, Italy. *Earth and Planetary Science Letters* 215: 57–72.
- Lasaga AC and Rye DM (1993) Fluid flow and chemical reaction kinetics in metamorphic systems. *American Journal of Science* 293: 361–404.
- Lassey KR and Blattner P (1988) Kinetically controlled oxygen isotope exchange between fluid and rock in one-dimensional advective flow. *Geochimica et Cosmochimica Acta* 52: 2169–2175.
- Lee JH and Veronis G (1989) Determining velocities and mixing coefficients from tracers. *Journal of Physical Oceanography* 19: 487–500.
- Lees JL and Lindley GT (1994) Three dimensional attenuation tomography at Loma Prieta: Inversion of t* for Q. *Journal of Geophysical Research* 99: 6843–6863.
- Léger A and Ferry JM (1993) Fluid infiltration and regional metamorphism of the Waits River Formation, northeast Vermont, USA. *Journal of Metamorphic Geology* 11: 3–29.
- Lewis S, Holness M, and Graham C (1998) Ion microprobe study of marble from Naxos Greece: Grain-scale fluid pathways and stable isotope equilibration during metamorphism. *Geology* 26: 935–938.
- Liang Y, Richter FM, and Watson EB (1996) Diffusion in silicate melts: II. Multicomponent diffusion in CaO–Al₂O₃–SiO₂ at 1500 °C and 1 GPa. *Geochimica et Cosmochimica Acta* 60: 5021–5035.
- Liu X-M, Rudnick RL, Hier-Majumder S, and Sirbescu M-LC (2010) Processes controlling lithium isotopic distribution in contact aureoles: A case study of the Florence County pegmatites, Wisconsin. *Geochemistry, Geophysics, and Geosystems* 11: Q08014. <http://dx.doi.org/10.1029/2010GC003063>.
- Lüttge A, Bolton EW, and Rye DM (2004) A kinetic model of metamorphism: An application to siliceous dolomites. *Contributions to Mineralogy and Petrology* 146: 546–565.
- Lyubetskaya T and Ague JJ (2009) Modeling the magnitudes and directions of regional metamorphic fluid flow in collisional orogens. *Journal of Petrology* 50: 1505–1531.
- Lyubetskaya T and Ague JJ (2010) Modeling metamorphism in collisional orogens intruded by magmas: II. Fluid flow and implications for Barrovian and Buchan metamorphism, Scotland. *American Journal of Science* 310: 459–491.
- Mäder UK and Berman RG (1991) An equation of state for carbon dioxide at high pressure and temperature. *American Mineralogist* 76: 1547–1559.
- Manning CE (1994) The solubility of quartz in the lower crust and upper mantle. *Geochimica et Cosmochimica Acta* 58: 4831–4839.
- Manning CE (2006) Mobilizing aluminum in crustal and mantle fluid. *Journal of Geochemical Exploration* 89: 251–253.
- Manning CE (2007) Solubility of corundum + kyanite in H₂O at 700 °C and 10 kbar: Evidence for Al–Si complexing at high pressure and temperature. *Geofluids* 7: 258–269.
- Manning CE, Antignano A, and Lin HA (2010) Premelting polymerization of crustal and mantle fluids, as indicated by the solubility of albite + paragonite + quartz in H₂O at 1 GPa and 350–620 °C. *Earth and Planetary Science Letters* 292: 325–336.
- Manning CE and Ingebritsen SE (1999) Permeability of the continental crust: Implications of geothermal data and metamorphic systems. *Reviews of Geophysics* 37: 127–150.

- Markl G, Ferry J, and Bucher K (1998) Formation of saline brines and salt in the lower crust by hydration reactions in partially retrogressed granulites from the Lofoten Islands, Norway. *American Journal of Science* 298: 705–757.
- Marschall HR, Altherr R, Gmeling K, and Kasztovszky Z (2009) Lithium, boron and chlorine as tracers for metasomatism in high-pressure metamorphic rocks: A case study from Syros (Greece). *Mineralogy and Petrology* 95: 291–302.
- Martin A, Gehrels GE, and DeCelles PG (2007) The tectonic significance of (U, Th)/Pb ages of monazite inclusions in garnet from the Himalaya of central Nepal. *Chemical Geology* 244: 1–24.
- Masters RL and Ague JJ (2005) Regional-scale fluid flow and element mobility in Barrow's metamorphic zones, Stonehaven, Scotland. *Contributions to Mineralogy and Petrology* 150: 1–18.
- McLelland J, Morrison J, Selleck B, Cunningham B, Olson C, and Schmidt K (2002) Hydrothermal alteration of late- to post-tectonic Lyon Mountain granitic gneiss, Adirondack Mountains, New York: Origin of quartz-sillimanite segregations, quartz-albite lithologies, and associated Kiruna-type low-Ti–Fe-oxide deposits. *Journal of Metamorphic Geology* 20: 175–190.
- Meyer C (1965) An early potassic type of alteration at Butte, Montana. *American Mineralogist* 50: 1717–1722.
- Miller DP, Marschall HR, and Schumacher JC (2009) Metasomatic formation and petrology of blueschist-facies hybrid rocks from Syros (Greece): Implications for reactions at the slab–mantle interface. *Lithos* 107: 53–67.
- Mohr DW and Newton RC (1983) Kyanite–staurolite metamorphism in sulfidic schists of the Anakeesta Formation, Great Smoky Mountains, North Carolina. *American Journal of Science* 283: 97–134.
- Müller T, Baumgartner LP, Foster CT Jr., and Vennemann TW (2004) Metastable prograde reactions in contact aureoles. *Geology* 32: 821–824.
- Nabelek PI (1997) Quartz–sillimanite leucosomes in high-grade schists, Black Hills, South Dakota: A perspective on the mobility of Al in high-grade metamorphic rocks. *Geology* 25: 995–998.
- Nabelek PI (2009) Numerical simulation of kinetically-controlled calc–silicate reactions and fluid flow with transient permeability around crystallizing plutons. *American Journal of Science* 309: 517–548.
- Nagel T, de Capitani C, and Frey M (2002) Isograds and P – T evolution in the eastern Lepontine Alps (Graubünden, Switzerland). *Journal of Metamorphic Geology* 20: 309–324.
- Nakamura M and Watson EB (2001) Experimental study of aqueous fluid infiltration into quartzite: Implications for the kinetics of fluid redistribution and grain growth driven by interfacial energy reduction. *Geofluids* 1: 73–89.
- Newton RC (1995) Simple-system mineral reactions and high-grade metamorphic fluids. *European Journal of Mineralogy* 7: 861–881.
- Newton RC and Manning CE (2000a) Quartz solubility in H_2O – $NaCl$ and H_2O – CO_2 solutions at deep crust–upper mantle pressures and temperatures: 2–15 kbar and 500–900 °C. *Geochimica et Cosmochimica Acta* 64: 2993–3005.
- Newton RC and Manning CE (2000b) Metasomatic phase relations in the system CaO – MgO – SiO_2 – H_2O – $NaCl$ at high temperatures and pressures. *International Geology Review* 42: 152–162.
- Niedermeier DRD, Putnis A, Geisler T, Golla-Schindler U, and Putnis CV (2009) The mechanism of cation and oxygen isotope exchange in alkali feldspars under hydrothermal conditions. *Contributions to Mineralogy and Petrology* 157: 65–76.
- Norton D and Dutrow BL (2001) Complex behavior of magma–hydrothermal processes: Role of supercritical fluid. *Geochimica et Cosmochimica Acta* 65: 4009–4017.
- Norton D and Knapp R (1977) Transport phenomena in hydrothermal systems: The nature of porosity. *American Journal of Science* 277: 913–936.
- Norton D and Knight J (1977) Transport phenomena in hydrothermal systems: Cooling plutons. *American Journal of Science* 277: 937–981.
- Norton D and Taylor HP Jr. (1979) Quantitative simulation of the hydrothermal systems of crystallizing magmas on the basis of transport theory and oxygen isotope data: An analysis of the Skaergaard intrusion. *Journal of Petrology* 20: 421–486.
- Nur A and Walder J (1990) Time-dependent hydraulics of the Earth's crust. In: Powley DE (ed.) *The Role of Fluids in Crustal Processes*, pp. 113–127. Washington, DC: National Academy Press.
- Oelkers EH and Helgeson HC (1988) Calculation of the thermodynamic and transport properties of aqueous species at high pressures and temperatures: Aqueous tracer diffusion coefficients of ions to 1000 °C and 5 kb. *Geochimica et Cosmochimica Acta* 52: 63–85.
- O'Hara KD (1988) Fluid flow and volume loss during mylonitization: An origin for phyllonite in an overthrust setting. *Tectonophysics* 156: 21–34.
- O'Neill JR and Taylor HP (1967) The oxygen isotope and exchange chemistry of feldspars. *American Mineralogist* 52: 1414–1437.
- Ogata A (1964) Mathematics of dispersion with linear absorption isotherm. *United States Geological Survey Professional Paper* 441-H.
- Ohl M, Halliday AN, and Peacor DR (1994) Mobility and fractionation of rare earth elements in argillaceous sediments: Implications for dating diagenesis and low-grade metamorphism. *Geochimica et Cosmochimica Acta* 58: 289–312.
- Oliver NHS (1996) Review and classification of structural controls on fluid flow during regional metamorphism. *Journal of Metamorphic Geology* 14: 477–492.
- Oliver NHS and Bons PD (2001) Mechanisms of fluid flow and fluid–rock interaction in fossil metamorphic hydrothermal systems inferred from vein–wallrock patterns, geometry and microstructure. *Geofluids* 1: 137–162.
- Oliver NHS, Butera K, Rubenach MJ, et al. (2008) The protracted hydrothermal evolution of the Mount Isa Eastern Succession: A review and tectonic implications. *Precambrian Research* 163: 108–130.
- Oliver GJH, Chen F, Buchwaldt R, and Hegner E (2000) Fast tectonometamorphism and exhumation in the type area of the Barrovian and Buchan zones. *Geology* 28: 459–462.
- Oliver NHS, Dipple GM, Cartwright I, and Schiller J (1998) Fluid flow and metasomatism in the genesis of the amphibolite-facies, pelite-hosted Kanmantoo copper deposit, south Australia. *American Journal of Science* 298: 181–218.
- Oliver NHS, Valenta RK, and Wall VJ (1990) The effect of heterogeneous stress and strain on metamorphic fluid flow, Mary Kathleen, Australia, and a model for large scale fluid circulation. *Journal of Metamorphic Geology* 8: 311–332.
- Olson P and Christensen U (1986) Solitary wave propagation in a fluid conduit within a viscous matrix. *Journal of Geophysical Research* 91: 6367–6374.
- Orville PM (1962) Alkali metasomatism and the feldspars. *Norsk Geologisk Tidsskrift* 42: 283–316.
- Oxtoby DW, Gillis HP, and Nachtrieb NH (1999) *Principles of Modern Chemistry*, 4th edn. New York: Saunders College.
- Page FZ, Kita NT, and Valley JW (2010) Ion microprobe analysis of oxygen isotopes in garnets of complex chemistry. *Chemical Geology* 270: 9–19.
- Palin JM (1992) *Stable Isotope Studies of Regional Metamorphism in the Wepawaug Schist, Connecticut*. PhD Thesis, Yale University.
- Pan Y and Fleet ME (1996) Rare earth element mobility during prograde granulite facies metamorphism: Significance of fluorine. *Mineralogy and Petrology* 123: 251–262.
- Passchier CW and Trouw RAJ (1996) *Microtectonics*. Berlin: Springer-Verlag.
- Pattison DRM (2006) The fate of graphite in prograde metamorphism of pelites: An example from the Ballachulish aureole, Scotland. *Lithos* 88: 85–99.
- Pattison DRM, de Capitani C, and Gaides F (2011) Petrological consequences of variations in metamorphic reaction affinity. *Journal of Metamorphic Geology* 29: 953–977.
- Pattison DRM and Tinkham DT (2009) Interplay between equilibrium and kinetics in prograde metamorphism of pelites: An example from the Nelson aureole, British Columbia. *Journal of Metamorphic Geology* 27: 249–279.
- Peacock SM (1983) Numerical constraints on rates of metamorphism, fluid production, and fluid flux during regional metamorphism. *Geological Society of America Bulletin* 101: 476–485.
- Peacock SM (1990) Fluid processes in subduction zones. *Science* 248: 329–337.
- Penniston-Dorland SC and Ferry JM (2006) Development of spatial variations in reaction progress during regional metamorphism of micaceous carbonate rocks, northern New England. *American Journal of Science* 306: 475–524.
- Penniston-Dorland SC and Ferry JM (2008) Element mobility and scale of mass transport in the formation of quartz veins during regional metamorphism of the Waits River Formation, east-central Vermont. *American Mineralogist* 93: 7–21.
- Penniston-Dorland SC, Sorensen SS, Ash RD, and Khadke SV (2010) Lithium isotopes as a tracer of fluids in a subduction zone mélange: Franciscan Complex, CA. *Earth and Planetary Science Letters* 292: 181–190.
- Person M and Baumgartner L (1995) New evidence for long-distance fluid migration within the Earth's crust. *Reviews of Geophysics* (Part 2, Supplement) S 33: 1083–1091.
- Philippot P (1993) Fluid–melt–rock interaction in mafic eclogites and coesite-bearing metasediments: Constraints on volatile recycling during subduction. *Chemical Geology* 108: 93–112.
- Philippot P and Selverstone J (1991) Trace-element-rich brines in eclogitic veins: Implications for fluid composition and transport during subduction. *Contributions to Mineralogy and Petrology* 106: 417–430.
- Philippot AR and Ague JJ (2009) *Principles of Igneous and Metamorphic Petrology*, 2nd edn., Cambridge: Cambridge University Press.
- Poage MC, Chamberlain CP, and Craw D (2000) Massif-wide metamorphism and fluid evolution at Nanga Parbat, northern Pakistan. *American Journal of Science* 300: 463–482.
- Podladchikov Y, John T, Beinlich A, and Klemd R (2009) Channeled Fluid Flow Through Slabs: Reactive Porosity Waves. Fall Meeting, Abstract V13D-2066, American Geophysical Union: Washington, DC.

- Pokrovskii VA and Helgeson HC (1995) Thermodynamic properties of aqueous species and the solubilities of minerals at high pressures and temperatures: The system $\text{Al}_2\text{O}_3\text{-H}_2\text{O-NaCl}$. *American Journal of Science* 295: 1255–1342.
- Pollington AD and Baxter EF (2010) High resolution Sm–Nd garnet geochronology reveals the uneven pace of tectonometamorphic processes. *Earth and Planetary Science Letters* 293: 63–71.
- Powell R, Holland TJB, and Worley B (1998) Calculating phase diagrams involving solid solutions via non-linear equations, with examples using THERMOCALC. *Journal of Metamorphic Geology* 16: 577–588.
- Priestley K, Jackson J, and McKenzie D (2008) Lithospheric structure and deep earthquakes beneath India, the Himalaya, and southern Tibet. *Geophysical Journal International* 172: 345–362.
- Putlitz B, Matthews A, and Valley JW (2000) Oxygen and hydrogen isotope study of high-pressure metagabbros and metabasalts (Cyclades, Greece): Implications for the subduction of oceanic crust. *Contributions to Mineralogy and Petrology* 138: 114–126.
- Putnis A (2002) Mineral replacement reactions; from macroscopic observations to microscopic mechanisms. *Mineralogical Magazine* 66: 689–708.
- Putnis A and Austrheim H (2010) Fluid induced processes: Metasomatism and metamorphism. *Geofluids* 10: 254–269.
- Putnis A and Holland TJB (1986) Sector trilling in cordierite and equilibrium overstepping in metamorphism. *Contributions to Mineralogy and Petrology* 93: 265–272.
- Putnis A and John T (2010) Replacement processes in the Earth's crust. *Elements* 6: 159–164.
- Qiu L, Rudnick RL, Ague JJ, and McDonough WF (2011) A Li isotopic study of sub-greenschist to greenschist facies metamorphism in an accretionary prism, New Zealand. *Earth and Planetary Science Letters* 310: 213–221.
- Ramsay J (1980) The crack–seal mechanism of rock deformation. *Nature* 284: 135–139.
- Richter FM and McKenzie D (1984) Dynamical models for melt segregation from a deformable matrix. *Journal of Geology* 92: 729–740.
- Ridley J and Thompson AB (1986) The role of mineral kinetics in the development of metamorphic microtextures. In: Walther JV and Wood BJ (eds.) *Fluid–rock interactions during metamorphism*, pp. 154–193. New York: Springer-Verlag.
- Ring U (1999) Volume loss, fluid flow, and coaxial versus noncoaxial deformation in retrograde, amphibolite facies shear zones, northern Malawi, east-central Africa. *Geological Society of America Bulletin* 111: 123–142.
- Roedder E (1984) Fluid inclusions. *MSA Reviews* 12: 644.
- Rubatto D (2002) Zircon trace element geochemistry: Partitioning with garnet and the link between U–Pb ages and metamorphism. *Chemical Geology* 184: 123–138.
- Rubatto D, Gebauer D, and Compagnoni R (1999) Dating of eclogite-facies zircons: The age of Alpine metamorphism in the Sesia–Lanzo Zone (Western Alps). *Earth and Planetary Science Letters* 167: 141–158.
- Rubatto D and Hermann J (2003) Zircon formation during fluid circulation in eclogites (Monviso, Western Alps): Implications for Zr and Hf budget in subduction zones. *Geochimica et Cosmochimica Acta* 67: 2173–2187.
- Rubenach MJ (2005) Relative timing of albittization and chlorine enrichment in biotite in Proterozoic schists, Snake Creek Anticline, Mt. Isa Inlier, northeastern Australia. *The Canadian Mineralogist* 43: 349–372.
- Rubenach MJ and Lewthwaite KA (2002) Metasomatic albitites and related biotite-rich schists from a low-pressure metamorphic terrane, Snake Creek Anticline, Mount Isa Inlier, north-eastern Australia: Microstructures and P–T–d paths. *Journal of Metamorphic Geology* 20: 191–202.
- Rubie DC (1998) Disequilibrium during metamorphism: The role of nucleation kinetics. In: Treloar PJ and O'Brien PJ (eds.) *What Drives Metamorphism and Metamorphic Reactions?* pp. 199–214. Geological Society: London Special Publications 138.
- Rudnick RL and Fountain DM (1995) Nature and composition of the continental crust: A lower crustal perspective. *Reviews of Geophysics* 33: 267–309.
- Rumble D III (1989) Evidences for fluid flow during regional metamorphism. *European Journal of Mineralogy* 1: 731–737.
- Rumble D III, Oliver NHS, Ferry JM, and Hoering TC (1991) Carbon and oxygen isotope geochemistry of chlorite-zone rocks of the Waterville Limestone, Maine, USA. *American Mineralogist* 76: 857–866.
- Rumble D III and Spear FS (1983) Oxygen isotope equilibration and permeability enhancement during regional metamorphism. *Journal of the Geological Society (London)* 140: 619–628.
- Rutter EH (1995) Experimental study of the influence of stress, temperature, and strain on the dynamic recrystallization of Carrara marble. *Journal of Geophysical Research* 100: 24651–24663.
- Rye DM and Bradbury HJ (1988) Fluid flow in the crust: An example from a Pyrenean thrust ramp. *American Journal of Science* 288: 197–235.
- Rye DM and Rye RO (1974) Homestake gold mine, South Dakota: I. Stable isotope studies. *Economic Geology* 69: 293–317.
- Rye RO, Schuiling RD, Rye DM, and Jansen JBH (1976) Carbon, hydrogen and oxygen isotope studies of the regional metamorphic complex at Naxos, Greece. *Geochimica et Cosmochimica Acta* 40: 1031–1049.
- Salvi S, Pokrovskii GS, and Schott J (1998) Experimental investigation of aluminum–silica aqueous complexing at 300°C. *Chemical Geology* 151: 51–67.
- Sanchez-Navas A (1999) Sequential kinetics of a muscovite-out reaction: A natural example. *American Mineralogist* 84: 1270–1286.
- Schmidt C and Bodnar RJ (2000) Synthetic fluid inclusions: XVI. PVTX properties in the system $\text{H}_2\text{O-NaCl-CO}_2$ at elevated temperatures, pressures, and salinities. *Geochimica et Cosmochimica Acta* 64: 3853–3869.
- Scholz CH (1990) *The Mechanics of Earthquakes and Faulting*. New York: Cambridge University Press.
- Schramke JA, Kerrick DM, and Lasaga AC (1987) The reaction muscovite + quartz = andalusite + K-feldspar + water. Part I. Growth kinetics and mechanism. *American Journal of Science* 287: 517–559.
- Scott DR and Stevenson DJ (1984) Magma solitons. *Geophysical Research Letters* 11: 1161–1164.
- Scott DR, Stevenson DJ, and Whitehead J (1986) Observations of solitary waves in a viscously deformable pipe. *Nature* 319: 759–761.
- Selverstone J and Gutzler DS (1993) Post-125 Ma carbon storage associated with continent–continent collision. *Geology* 21: 885–888.
- Selverstone J, Morteani G, and Staude JM (1991) Fluid channeling during ductile shearing: Transformation of granodiorite into aluminous schist in the Tauern Window, eastern Alps. *Journal of Metamorphic Geology* 9: 419–431.
- Shaw DM (1956) Geochemistry of pelitic rocks. Part III: Major elements and general geochemistry. *Geological Society of America Bulletin* 67: 919–934.
- Shewmon PG (1969) *Transformations in Metals*. New York: McGraw-Hill.
- Shi P and Saxena SK (1992) Thermodynamic modeling of the C–H–O–S fluid system. *American Mineralogist* 77: 1038–1049.
- Shmulovich K, Graham C, and Yardley BWD (2001) Quartz, albite, and diopside solubilities in $\text{H}_2\text{O-CO}_2$ fluids at 0.5–0.9 GPa. *Contributions to Mineralogy and Petrology* 141: 95–108.
- Shock EL, Sassani DC, Willis M, and Sverjensky DA (1997) Inorganic species in geologic fluids: Correlations among standard molal thermodynamic properties of aqueous ions and hydroxide complexes. *Geochimica et Cosmochimica Acta* 61: 907–950.
- Sibson RH (1983) Continental fault structure and the shallow earthquake source. *Journal of the Geological Society (London)* 140: 741–767.
- Sibson RH (1992) Implications of fault-valve behaviour for rupture nucleation and recurrence. *Tectonophysics* 211: 283–293.
- Sibson RH, McMoore J, and Rankin RH (1975) Seismic pumping—a hydrothermal fluid transport mechanism. *Journal of the Geological Society (London)* 131: 653–659.
- Silliman B (1820) Sketches of a tour in the counties of New-Haven and Litchfield in Connecticut, with notices of the geology, mineralogy and scenery, &c. *American Journal of Science* 2: 201–235.
- Simons KK, Harlow GE, Brueckner HK, et al. (2010) Lithium isotopes in Guatemalan and Franciscan HP–LT rocks: Insights into the role of sediment-derived fluids during subduction. *Geochimica et Cosmochimica Acta* 74: 3621–3641.
- Skelton ADL (2011) Flux rates for water and carbon during greenschist facies metamorphism. *Geology* 39: 43–46.
- Skelton ADL, Graham CM, and Bickle MJ (1995) Lithological and structural controls on regional 3-D fluid flow patterns during greenschist facies metamorphism of the Dalradian of the SW Scottish Highlands. *Journal of Petrology* 36: 563–586.
- Skelton ADL, Valley JW, Graham CM, Bickle MJ, and Fallick AE (2000) The correlation of reaction and isotope fronts and the mechanism of metamorphic fluid flow. *Contributions to Mineralogy and Petrology* 138: 364–375.
- Skippen GB and Marshall DD (1991) The metamorphism of granulites and devolatilization of the lithosphere. *The Canadian Mineralogist* 29: 693–705.
- Smit CA and Van Reenen DD (1997) Deep crustal shear zones, high-grade tectonites, and associated metasomatic alteration in the Limpopo Belt, South Africa: Implications for deep crustal processes. *Journal of Geology* 105: 37–58.
- Smith MP and Yardley BWD (1999) Fluid evolution during metamorphism of the Otago Schist, New Zealand: (I) evidence from fluid inclusions. *Journal of Metamorphic Geology* 17: 173–186.
- Sorensen SS and Grossman JN (1989) Enrichment of trace elements in garnet–amphibolites from a paleo-subduction zone: Catalina Schist, Southern California. *Geochimica et Cosmochimica Acta* 53: 3155–3177.
- Spear FS (1993) *Metamorphic Phase Equilibria and Pressure–Temperature–Time Paths*. Washington, DC: Mineralogical Society of America.
- Spiegelman M and Kelemen PB (2003) Extreme chemical variability as a consequence of channelized melt transport. *Geochemistry, Geophysics and Geosystems* 4: 1055. <http://dx.doi.org/10.1029/2002GC000336>.

- Steeffel CI and Lasaga AC (1994) A coupled model for transport of multiple chemical species and kinetic precipitation/dissolution reactions with application to reactive flow in single phase hydrothermal systems. *American Journal of Science* 294: 529–592.
- Steeffel CI and van Cappellen P (1990) A new kinetic approach to modeling water–rock interaction: The role of nucleation, precursors, and Ostwald ripening. *Geochimica et Cosmochimica Acta* 54: 2657–2677.
- Sternner SM and Pitzer KS (1994) An equation of state for carbon dioxide valid from zero to extreme pressures. *Contributions to Mineralogy and Petrology* 117: 362–374.
- Steyrer HP and Sturm R (2002) Stability of zircon in a low-grade ultramylonite and its utility for chemical mass balancing: The shear zone at Miéville, Switzerland. *Chemical Geology* 187: 1–19.
- Stober I and Bucher K (2004) Fluid sinks within the Earth's crust. *Geofluids* 4: 143–151.
- Svensen H and Jamveit B (2010) Metamorphic fluids and global environmental changes. *Elements* 6: 179–182.
- Sverjensky DA (1987) Calculation of the thermodynamic properties of aqueous species and the solubilities of minerals in supercritical electrolyte solutions. In: Carmichael ISE and Eugster HP (eds.) *Thermodynamic Modeling of Geological Materials. Reviews in Mineralogy*, vol. 17, pp. 177–209. Washington, DC: Mineralogical Society of America.
- Sverjensky DA, Shock EL, and Helgeson HC (1997) Prediction of the thermodynamic properties of aqueous metal complexes to 1000 °C and 5 kb. *Geochimica et Cosmochimica Acta* 61: 1359–1412.
- Tagirov B and Schott J (2001) Aluminum speciation in crustal fluids revisited. *Geochimica et Cosmochimica Acta* 65: 3965–3992.
- Templeton AS, Chamberlain CP, Koons PO, and Craw D (1998) Stable isotopic evidence for mixing between metamorphic fluids and surface-derived waters during recent uplift of the southern Alps, New Zealand. *Earth and Planetary Science Letters* 154: 73–92.
- Teng F-Z, McDonough WF, Rudnick RL, and Walker RJ (2006) Diffusion-driven extreme lithium isotopic fractionation in country rocks of the Tin Mountain pegmatite. *Earth and Planetary Science Letters* 243: 701–710.
- Teng F-Z, McDonough WF, Rudnick RL, and Wing BA (2007) Limited lithium isotopic fractionation during progressive metamorphic dehydration in metapelites: A case study from the Onawa contact aureole, Maine. *Chemical Geology* 239: 1–12.
- Thomas R, Webster JD, and Heinrich W (2000) Melt inclusions in pegmatite quartz: Complete miscibility between silicate melts and hydrous fluids at low pressure. *Contributions to Mineralogy and Petrology* 139: 394–401.
- Thompson AB (1975) Calc-silicate diffusion zones between marble and pelitic schist. *Journal of Petrology* 16: 314–346.
- Thompson AB (1983) Fluid absent metamorphism. *Journal of the Geological Society (London)* 140: 533–547.
- Thompson JB Jr. (1987) A simple thermodynamic model for grain interfaces: Some insights on nucleation, rock textures, and metamorphic differentiation. In: Helgeson HC (ed.) *Chemical Transport in Metasomatic Processes*, pp. 169–188. Boston: Reidel.
- Thompson AB (2010) Perspectives on metamorphic processes and fluids. *Elements* 6: 142–143.
- Thompson AB and England PC (1984) Pressure–temperature–time paths of regional metamorphism II, their inference and interpretation using mineral assemblages in metamorphic rocks. *Journal of Petrology* 25: 929–955.
- Touret JR (1985) Fluid regime in Southern Norway: The record of fluid inclusions. In: Tobi AC and Touret JRL (eds.) *The Deep Proterozoic Crust in the North Atlantic Provinces*, pp. 517–549. Dordrecht: Reidel.
- Tracy RJ, Rye DM, Hewitt DA, and Schiffries CM (1983) Petrologic and stable-isotopic studies of fluid–rock interactions, south-central Connecticut I. The role of infiltration in producing reaction assemblages in impure marbles. *American Journal of Science* 283A: 589–616.
- Valley JW, Bohlen SW, Essene EJ, and Lamb W (1990) Metamorphism in the Adirondacks: II. The role of fluids. *Journal of Petrology* 31: 555–596.
- van der Straaten F, Schenk V, John T, and Gao J (2008) Blueschist-facies rehydration of eclogites (Tian Shan, NW-China): Implications for fluid–rock interaction in the subduction channel. *Chemical Geology* 255: 195–219.
- van Haren JLM, Ague JJ, and Rye DM (1996) Oxygen isotope record of fluid infiltration and mass transfer during regional metamorphism of pelitic schist, Connecticut, USA. *Geochimica et Cosmochimica Acta* 60: 3487–3504.
- Verlaquet A, Goffé B, Brunet F, et al. (2011) Metamorphic veining and mass transfer in a chemically closed system: A case study in Alpine metabauxites (western Vanoise). *Journal of Metamorphic Geology* 29: 275–300.
- Vidale R (1969) Metasomatism in a chemical gradient and the formation of calc-silicate bands. *American Journal of Science* 267: 857–874.
- Vidale R and Hewitt DA (1973) "Mobile" components in the formation of calc-silicate bands. *American Mineralogist* 58: 991–997.
- Viète DR, Hermann J, Lister G, and Stenhouse I (2011) The nature and origin of the Barrovian metamorphism, Scotland: Diffusion length scales in garnet and inferred thermal time scales. *Journal of the Geological Society, London* 168: 115–132.
- Villa I (2006) From nanometer to megameter: Isotopes, atomic-scale processes, and continent-scale tectonic models. *Lithos* 87: 155–173.
- Vorhies SH and Ague JJ (2011) Pressure–temperature evolution of the Barrovian zones, Scotland. *Journal of the Geological Society (London)* 168: 1147–1166.
- Vrolijk P (1987) Tectonically driven fluid flow in the Kodiak accretionary complex, Alaska. *Geology* 15: 466–469.
- Vry J, Powell R, Golden KM, and Petersen K (2009) The role of exhumation in metamorphic dehydration and fluid production. *Nature Geoscience* 3: 31–35.
- Walder J and Nur A (1984) Porosity reduction and crustal pore pressure development. *Journal of Geophysical Research* 89: 11539–11548.
- Wallmann K (2001a) The geological water cycle and the evolution of marine $\delta^{18}\text{O}$ values. *Geochimica et Cosmochimica Acta* 65: 2469–2485.
- Wallmann K (2001b) Controls on the Cretaceous and Cenozoic evolution of seawater composition, atmospheric CO_2 and climate. *Geochimica et Cosmochimica Acta* 65: 3005–3025.
- Walther JV (1990) Fluid dynamics during progressive regional metamorphism. In: Bredehoeft JD and Norton DL (eds.) *The Role of Fluids in Crustal Processes*, pp. 64–71. Washington, DC: National Academy Press.
- Walther JV (1996) Fluid production and isograd reactions at contacts of carbonate-rich and carbonate-poor layers during progressive metamorphism. *Journal of Metamorphic Geology* 14: 351–360.
- Walther JV (2001) Experimental determination and analysis of the solubility of corundum in 0.1 and 0.5 m NaCl solutions between 400 and 600 °C from 0.5 to 2.0 kbar. *Geochimica et Cosmochimica Acta* 65: 2843–2851.
- Walther JV and Orville PM (1982) Volatile production and transport in regional metamorphism. *Contributions to Mineralogy and Petrology* 79: 252–257.
- Walther JV and Orville PM (1983) The extraction-quench technique for determination of the thermodynamic properties of solute complexes. Application to quartz solubility in fluid mixtures. *American Mineralogist* 68: 731–741.
- Waters DJ and Lovegrove DP (2002) Assessing the extent of disequilibrium and overstepping of prograde metamorphic reactions in metapelites from the Bushveld Complex aureole, South Africa. *Journal of Metamorphic Geology* 20: 135–149.
- Watson EB and Baxter EF (2007) Diffusion in solid-Earth systems. *Earth and Planetary Science Letters* 253: 307–327.
- Watson EB and Brenan JM (1987) Fluids in the lithosphere: 1. Experimentally determined wetting characteristics of CO_2 – H_2O fluids and their implications for fluid transport, host-rock physical properties, and fluid inclusion formation. *Earth and Planetary Science Letters* 85: 497–515.
- Wedepohl KH (1995) The composition of the continental crust. *Geochimica et Cosmochimica Acta* 59: 1217–1232.
- Weill DF and Fyfe WS (1964) The solubility of quartz in H_2O in the range 1000–4000 bars and 400–550 °C. *Geochimica et Cosmochimica Acta* 28: 1243–1255.
- White FM (1979) *Fluid Mechanics*. New York: McGraw-Hill.
- Whitney DL and Dilek Y (2000) Andalusite–sillimanite–quartz veins as indicators of low-pressure–high-temperature deformation during late-stage unroofing of a metamorphic core complex, Turkey. *Journal of Metamorphic Geology* 18: 59–66.
- Whitney DL, Mechem TA, Dilek Y, and Kuehner SM (1996) Modification of garnet by fluid infiltration during regional metamorphism in garnet through sillimanite zone rocks, Dutchess County, New York. *American Mineralogist* 81: 696–705.
- Whitney DL and Olmsted JF (1998) Rare earth element metasomatism in hydrothermal systems: The Willsboro–Lewis wollastonite ores, New York, USA. *Geochimica et Cosmochimica Acta* 62: 2965–2977.
- Wickham SM and Taylor HP Jr. (1990) Hydrothermal systems associated with regional metamorphism and crustal anatexis: Examples from the Pyrenees, France. In: Bredehoeft JD and Norton DL (eds.) *The Role of Fluids in Crustal Processes*, pp. 96–112. Washington, DC: National Academy Press.
- Widmer T and Thompson AB (2001) Local origin of high pressure vein material in eclogite facies rocks of the Zermatt-Saas zone, Switzerland. *American Journal of Science* 301: 627–656.
- Wijbrans JR and McDougall I (1985) $^{40}\text{Ar}/^{39}\text{Ar}$ dating of white micas from an Alpine high pressure metamorphic belt on Naxos (Greece): The resetting of the argon isotopic system. *Contributions to Mineralogy and Petrology* 93: 187–194.
- Wijbrans JR and McDougall I (1988) Metamorphic evolution of the Attic Cycladic Metamorphic Belt on Naxos (Cyclades, Greece) utilizing $^{40}\text{Ar}/^{39}\text{Ar}$ age spectrum measurements. *Journal of Metamorphic Geology* 6: 571–594.
- Wilbur DE and Ague JJ (2006) Chemical disequilibrium during garnet growth: Monte Carlo simulations of natural crystal morphologies. *Geology* 34: 689–692.
- Wilke M, Schmidt C, Dubrill J, et al. (2012) Zircon solubility and zirconium complexation in $\text{H}_2\text{O}+\text{Na}_2\text{O}+\text{SiO}_2+/-\text{Al}_2\text{O}_3$ fluids at high pressure and temperature. *Earth and Planetary Science Letters* 349–350: 15–25.

- Williams IS, Buick IS, and Cartwright I (1996) An extended episode of early Mesoproterozoic metamorphic fluid flow in the Reynolds Range, central Australia. *Journal of Metamorphic Geology* 14: 29–47.
- Wing BA and Ferry JM (2002) Three-dimensional geometry of metamorphic fluid flow during Barrovian regional metamorphism from an inversion of combined petrologic and stable isotopic data. *Geology* 30: 639–643.
- Wing BA and Ferry JM (2007) Magnitude and geometry of reactive fluid flow from direct inversion of spatial patterns of geochemical alteration. *American Journal of Science* 307: 793–832.
- Wohlert A and Manning CE (2009) Solubility of corundum in aqueous KOH solutions at 700 °C and 1 GPa. *Chemical Geology* 262: 310–317.
- Wong T, Ko S, and Olgaard DL (1997) Generation and maintenance of pore pressure excess in a dehydrating system 2. Theoretical analysis. *Journal of Geophysical Research* 102: 841–852.
- Wong T and Zhu W (1999) Brittle faulting and permeability evolution: Hydromechanical measurement, microstructural observation, and network modeling. In: Haneberg WC, Mozley PS, Moore JC, and Goodwin LB (eds.) *Faults and Subsurface Fluid Flow in the Shallow Crust. Geophysical Monograph* 113, pp. 83–99. Washington, DC: American Geophysical Union.
- Xie Z and Walther JV (1993) Quartz solubilities in NaCl solutions with and without wollastonite at elevated temperatures and pressures. *Geochimica et Cosmochimica Acta* 57: 1947–1955.
- Yakovlev LYe (1993) The role of metamorphism of the basaltic basement of sedimentary basins in crustal evolution. *International Geology Review* 35: 27–47.
- Yardley BWD (1975) On some quartz-plagioclase veins in the Connemara Schists, Ireland. *Geological Magazine* 112: 183–190.
- Yardley BWD (1986) Fluid migration and veining in the Connemara Schists, Ireland. In: Walther JV and Wood BJ (eds.) *Fluid–Rock Interactions During Metamorphism*, pp. 109–131. New York: Springer-Verlag.
- Yardley BWD (1997) The evolution of fluids through the metamorphic cycle. In: Jamtveit B and Yardley BWD (eds.) *Fluid Flow and Transport in Rocks*, pp. 139–147. London: Chapman and Hall.
- Yardley BWD (2009) On the role of water in the evolution of the continental crust. *Journal of the Geological Society (London)* 166: 585–600.
- Yardley BWD and Bottrell SH (1992) Silica mobility and fluid movement during metamorphism of the Connemara schists, Ireland. *Journal of Metamorphic Geology* 10: 453–464.
- Yeats RS, Sieh K, and Allen CR (1997) *The Geology of Earthquakes*. USA: Oxford.
- Young ED (1995) Fluid flow in metamorphic environments. *Reviews of Geophysics, (Part 1, Supplement S)* 33: 41–52.
- Young ED and Rumble D III (1993) The origin of correlated variations in in-situ ¹⁸O/¹⁶O and elemental concentrations in metamorphic garnet from southeastern Vermont, USA. *Geochimica et Cosmochimica Acta* 57: 2585–2597.
- Zack T and John T (2007) An evaluation of reactive fluid flow and trace element mobility in subducting slabs. *Chemical Geology* 239: 199–216.
- Zhang SQ, FitzGerald JD, and Cox SF (2000) Reaction-enhanced permeability during decarbonation of calcite + quartz → wollastonite + carbon dioxide. *Geology* 28: 911–914.
- Zhang CF, Tullis TJ, and Scruggs VJ (2001) Implications of permeability and its anisotropy in a mica gouge for pore pressures in fault zones. *Tectonophysics* 335: 37–50.
- Zhao DH, Kanamori H, Negishi H, and Weins D (1996) Tomography of the source area of the 1995 Kobe earthquake: Evidence for fluids at the hypocenter? *Science* 274: 1891–1894.